

DEVELOPMENT AND ANALYSIS OF
HYBRID SOLAR DRYER WITH
BIOMASS BACKUP HEATER

YUSHEILA BT MD YUNUS

MASTERS OF SCIENCE
MECHANICAL ENGINEERING

UNIVERSITI TEKNOLOGI PETRONAS

AUGUST 2011

STATUS OF THESIS

Title of thesis

DEVELOPMENT AND ANALYSIS OF HYBRID SOLAR DRYER WITH BIOMASS BACKUP HEATER

I, YUSHEILA BT MD YUNUS

hereby allow my thesis to be placed at the Information Resource Center (IRC) of Universiti Teknologi PETRONAS (UTP) with the following conditions:

1. The thesis becomes the property of UTP
2. The IRC of UTP may make copies of the thesis for academic purposes only.
3. This thesis is classified as

Confidential

Non-confidential

If this thesis is confidential, please state the reason:

The contents of the thesis will remain confidential for _____ years.

Remarks on disclosure:

Endorsed by

Signature of Author

Signature of Supervisor

Permanent address:

Name of Supervisor

2, JALAN SN 1/2,
TAMAN SRI NEGERI,
70400, SEREMBAN,
NEGERI SEMBILAN.

ASSOC. PROF. DR. HUSSAIN
AL-KAYIEM

Date: _____

Date: _____

UNIVERSITI TEKNOLOGI PETRONAS
DEVELOPMENT AND ANALYSIS OF HYBRID SOLAR DRYER WITH
BIOMASS BACKUP HEATER

by

YUSHEILA BT MD YUNUS

The undersigned certify that they have read, and recommend to the Postgraduate Studies Programme for acceptance this thesis for the fulfilment of the requirements for the degree stated.

Signature:

Main Supervisor:

ASSOC. PROF. DR. HUSSAIN AL-KAYIEM

Signature:

Head of Department:

ASSOC. PROF. DR. AHMAD MAJDI ABDUL
RANI

Date:

DEVELOPMENT AND ANALYSIS OF HYBRID SOLAR DRYER WITH
BIOMASS BACKUP HEATER

By

YUSHEILA BT MD YUNUS

A Thesis

Submitted to the Postgraduate Studies Programme
as a Requirement for the Degree of

MASTERS OF SCIENCE

MECHANICAL ENGINEERING DEPARTMENT

UNIVERSITI TEKNOLOGI PETRONAS

BANDAR SRI ISKANDAR

PERAK

AUGUST 2011

DECLARATION OF THESIS

Title of thesis DEVELOPMENT AND ANALYSIS OF HYBRID SOLAR DRYER WITH BIOMASS BACKUP HEATER

I, YUSHEILA BT MD YUNUS

hereby declare that the thesis is based on my original work except for quotations and citations which have been duly acknowledged. I also declare that it has not been previously or concurrently submitted for any other degree at UTP or other institutions.

Witnessed by

Signature of Author

Signature of Supervisor

Permanent address:

Name of Supervisor

2, JALAN SN 1/2,
TAMAN SRI NEGERI,
70400 SEREMBAN,
NEGERI SEMBILAN.

ASSOC. PROF. DR HUSSAIN
AL-KAYIEM

Date: _____

Date: _____

ACKNOWLEDGEMENT

Alhamdulillah praises to The Almighty Allah for blessing me with the strength and health towards completing this project. It is a pleasure to thank the many people who made this thesis possible.

First and foremost, I would like to say a million of thankfulness to my supervisor, Assoc. Prof. Dr. Hussain H. Al-Kayiem who has been very supportive from the beginning to the end of the project. His guidance, attention and advice are very much appreciated. My heartfelt gratitude also goes out to the lecturers of Mechanical Engineering Department especially Ir Dr Masri Baharom for their willingness to share knowledge. Their suggestions, enthusiastic support, knowledge and constructive criticisms helped me greatly in understanding the project.

I also wanted to acknowledge Universiti Teknologi PETRONAS (UTP) and the postgraduate office staffs for providing the facilities and guidelines to ensure each project successful. Not forgotten to Mechanical Engineering Department technicians, especially Mr. Zailan Alang Ahmad who constantly gives a brilliant ideas and guidance in the experimental work of this study.

My utmost appreciation goes to my family and my beloved ones, who inspired, encouraged with never ending prayers and fully supported me for every trial that come to my way. Their advices will always be remembered and become the motivation in continuing the journey of my life. I would like to express my most sincere gratitude to all my friends whom immensely helped me by giving me encouragement and wonderful friendship. The love, support and precious time together has made this journey more meaningful.

DEDICATION

To my beloved parents,

Md Yunus Kitam & Azora Ambrose Abdul Molok

To my thoughtful siblings, sister and brother in law,

Mohd Yuzri & Roslina, Yuzrina & Mohammad Zamri

To my supportive supervisor,

AP Dr. Hussain Al-Kayiem

To my gracious aunt & coolest friends,

Zainon Kitam & UTPians

To special person in my life,

Rusdee Azeem Muhamad Rusli

ABSTRACT

The application of solar drying, especially in the agricultural areas, has been proven to be practical, economical, and environmental friendly. However, the drying process is limited only on a sunny environment and often interrupted during the cloudy or rainy days and also at night. A hybrid dryer with thermal backup technique has been adopted to overcome the limitation of solar dryer. The combination of the systems is expected to create 24 hours a day of non-interrupted drying process.

The study on the drying system was carried out by three analysis techniques; analytical, experimental and numerical. The conceptual design of the experimental model was based on analytical modeling of the drying process using solar, or the backing up heat source, or both of them simultaneously. The work was extended to involve numerical simulation of the fluid flow inside the developed hybrid dryer by employing CFD technique using FLUENT[®] software under different operational modes. Chillies and empty fruit bunch (EFB) as food and waste product respectively has been selected for the materials to be dried. They were dried under different modes, which were 'only solar', 'thermal backup alone' and 'solar-thermal backup' (hybrid). Open sun drying was also conducted and considered as a reference for comparison.

It was found that the fastest drying process was in the hybrid drying mode. Moisture content of chillies and EFB were reduced from 80% to 5% and 75% to 6% within 2.33 and 1.33 days of drying, respectively. The hybrid drying efficiencies of chillies and EFB were considerably high as compared to only solar and thermal alone mode which were 6.85% and 11% respectively. The experimental measurements have shown good agreement with the simulated results, with maximum percent of error of 15%. Hybrid mode was the most appropriate mode for drying application since it meets the required drying temperature. Also, it was capable to reduce the drying period considerably. The simulation results were validated by comparing with the experimental measurements.

ABSTRAK

Penggunaan alat pengering secara solar terutama di dalam pertanian telah dibuktikan sangat praktikal, ekonomikal dan mesra alam sekitar. Bagaimanapun, proses pengeringan hanya terhad pada persekitaran panas dan sering terganggu semasa hari hujan atau mendung dan pada waktu malam. Pengering hibrid dengan kaedah bantuan terma telah digunakan untuk mengatasi had pengering solar. Gabungan kedua-dua sistem akan mewujudkan proses pengeringan seharian selama 24 jam tanpa gangguan.

Kajian sistem pengeringan telah dijalankan melalui tiga teknik analisis; data analisis, eksperimen dan pengiraan. Pengajian konseptual model adalah berdasarkan analisis dalam proses pengeringan solar, bantuan haba, atau secara serentak. Kerja dilanjutkan dengan simulasi aliran bendalir di dalam pengering hibrid secara CFD menggunakan perisian FLUENT[®] dalam kaedah operasi berlainan. Cili dan tandan kosong (EFB) masing-masing sebagai makanan dan hasil sisa telah dipilih untuk dikeringkan. Ia telah dikeringkan di bawah kaedah yang berlainan, iaitu secara 'hanya solar', 'bantuan terma sahaja' dan 'bantuan terma dan solar' (hibrid). Pengeringan solar secara terbuka juga telah dijalankan dan diambil sebagai rujukan untuk perbandingan.

Proses pengeringan telah di dapati paling cepat berada dalam kaedah pengeringan hibrid. Kandungan lembapan cili dan EFB masing-masing telah dikurangkan dari 80% untuk 5% dan 75% untuk 6% selama 2.33 dan 1.33 hari pengeringan. Kecekapan pengeringan hibrid untuk cili dan EFB adalah sangat tinggi berbanding dengan kaedah hanya solar dan bantuan terma sahaja yang mana masing-masing ialah 6.85% dan 11%. Keputusan ukuran-ukuran eksperimen telah menunjukkan keputusan yang baik dengan keputusan simulasi, dengan maksimum peratus ralat 15%. Kaedah hibrid adalah kaedah yang paling sesuai di dalam penggunaan pengeringan kerana ia memenuhi suhu pengeringan yang diperlukan. Ia juga mampu mengurangkan tempoh pengeringan dengan cepat. Keputusan simulasi telah disahkan melalui perbandingan dengan keputusan eksperimen.

In compliance with the terms of the Copyright Act 1987 and the IP Policy of the university, the copyright of this thesis has been reassigned by the author to the legal entity of the university,

Institute of Technology PETRONAS Sdn Bhd.

Due acknowledgement shall always be made of the use of any material contained in, or derived from, this thesis.

© Yusheila Bt Md Yunus, 2011
Institute of Technology PETRONAS Sdn Bhd
All rights reserved.

TABLE OF CONTENTS

STATUS OF THESIS	I
APPROVAL PAGE	II
TITLE PAGE	III
DECLARATION OF THESIS	IV
ACKNOWLEDGEMENT	V
DEDICATION	VI
ABSTRACT	VII
ABSTRAK	VIII
COPYRIGHT PAGE	IX
TABLE OF CONTENTS	X
LIST OF FIGURES	XV
LIST OF TABLES	XVIII
LIST OF ABBREVIATIONS	XX
NOMENCLATURE	XXI
GREEK SYMBOLS	XXIV
CHAPTER 1	1
INTRODUCTION	1
1.1 BACKGROUND	1
1.1.1 Drying of Food Product	2
1.1.2 Drying of Biomass Products	3
1.2 PROBLEM STATEMENT	4
1.3 RESEARCH OBJECTIVES	6
1.4 SCOPE OF WORK	6
1.4.1 Analytical modeling and analysis	6
1.4.2 Experimental modeling with measurement	7
1.4.3 Computational simulation and analysis	7
1.4.4 Comparison of the results	7
1.5 ORGANIZATION OF THE THESIS	7

CHAPTER 2	9
LITERATURE REVIEW	9
2.1 CHAPTER OVERVIEW	9
2.2 DRYING PROCESS	9
2.3 FACTORS INFLUENCING THE DRYING RATE	9
2.3.1 Moisture Content of Solids	10
2.3.2 Types of Materials	11
2.3.3 Drying Temperature	12
2.4 DRYING MECHANISM	12
2.5 DRYING OF FOOD PRODUCTS	13
2.6 DRYING OF BIOMASS PRODUCT.....	14
2.6.1 Empty Fruit Bunch (EFB).....	15
2.7 DRYING PRINCIPLE AND QUALITY CHANGES	15
2.8 TRADITIONAL DRYING METHOD (DIRECT OPEN SUN DRYING)	17
2.9 SOLAR DRYING	19
2.9.1 Solar Dryer Classification.....	20
2.10 SOLAR DRYING OVERVIEW	21
2.10.1 Direct Solar Dryer	22
2.10.2 Indirect Solar Dryer	24
2.10.3 Mixed Mode Solar Dryer	27
2.11 OVERVIEW ON THE SUPPORTING ELEMENTS OF SOLAR DRYER.....	30
2.11.1 Solar Collectors in the Solar Dryers	30
2.11.2 Thermal Backup for Hybrid Drying	32
2.12 OVERVIEW OF GAS TO GAS HEAT EXCHANGER DESIGN	37
2.13 CHAPTER SUMMARY	39
CHAPTER 3	41
METHODOLOGY AND DESIGN APPROACH.....	41
3.1 CHAPTER OVERVIEW	41
3.2 OPERATIONAL PRINCIPLES OF THE MIXED MODE AND HYBRID SOLAR DRYER	41
3.3 GEOMETRICAL DESIGN PROCEDURE OF THE DRYER	43
3.3.1 Conceptual Design	43
3.3.2 Dryer Material Selection.....	45
3.3.3 Design Calculation.....	47

3.4 DESIGN OF THE THERMAL BACKUP UNIT (TBU).....	51
3.4.1 Conceptual Design of the TBU.....	53
3.4.2 Material Selection	56
3.4.3 Design Calculation.....	57
3.5 CHAPTER SUMMARY	71
CHAPTER 4	73
EXPERIMENTAL VERIFICATION	73
4.1 CHAPTER OVERVIEW	73
4.2 EXPERIMENTAL PROCEDURE AND MEASURING INSTRUMENTATION.....	73
4.3 THERMAL BACKUP UNIT EXPERIMENTS.....	76
4.3.1 Solid Biomass as Burning Fuel.....	77
4.3.2 Results of Rice Husk.....	78
4.3.3 Results of EFB	80
4.3.4 Results of Wood chips	81
4.3.5 Verification of TBU Design.....	82
4.4 NO-LOAD DRYER EXPERIMENT	82
4.4.1 Experimental Analysis of Solar Collector Performance.....	83
4.4.2 Experimental Analysis of Dryer under Solar Mode.....	84
4.4.3 Experimental Analysis of Dryer under Thermal Backup Mode	86
4.4.4 Experimental Analysis of Dryer under Hybrid Mode.....	88
4.5 LOADING EXPERIMENT	90
4.5.1 Experiments of Chillies Drying	90
4.5.2 Experiments of EFB.....	95
4.6 THERMAL ANALYSIS OF THE SOLAR COLLECTOR	99
4.7 ANALYSIS OF THE PERFORMANCES OF SOLAR DRYER AND TBU	101
4.7.1 The Efficiency of Solar Collector	101
4.7.2 The Drying Efficiency, η_d	102
4.8 CHAPTER SUMMARY	105
CHAPTER 5	107
NUMERICAL SIMULATION	107
5.1 CHAPTER OVERVIEW	107
5.2 OVERVIEW OF PREVIOUS ATTEMPTS ON DRYER SIMULATION	107
5.3 MODELING AND SIMULATION OF THE HYBRID DRYER	109

5.3.1 Computational Model	110
5.3.2 Computational Grid	110
5.3.3 Governing Equations of the Thermo Fluid Process	111
5.3.4 Irradiation Model	113
5.3.5 Turbulence Modeling.....	114
5.4 SIMULATION PROCEDURE	116
5.4.1 Boundary Conditions	116
5.4.2 Numerical Solution Procedure	119
5.5 SIMULATION RESULTS AND DISCUSSION.....	120
5.5.1 Simulation under Solar Mode	120
5.5.2 Simulation under Thermal Backup Mode – Hot Air and Flue Mode	122
5.5.3 Simulation under Hybrid Modes-Hot Air and Flue with Solar Mode	125
5.6 CHAPTER SUMMARY	127
CHAPTER 6	129
CONCLUSIONS AND RECOMMENDATIONS	129
6.1 CONCLUSION.....	129
6.1.1 Thermal-Backup Unit	130
6.1.2 No-load Experiment.....	130
6.1.3 Loading Experiments	131
6.1.4 The Efficiencies of Drying Systems	131
6.1.5 Simulation	132
6.2 RECOMMENDATIONS	132
6.2.1 Thermal Backup Unit.....	132
6.2.2 Mixed Mode Solar Dryer	133
6.2.3 Hybrid Drying System	134
6.2.4 The Efficiencies of Drying Systems	134
6.2.5 Simulation	135
6.3 SUGGESTION FOR FURTHER STUDIES	135
REFERENCES	137
LIST OF PUBLICATIONS & ACHIEVEMENTS.....	144
APPENDIX A.....	145
APPENDIX B.....	146
APPENDIX C.....	147

APPENDIX E.....	148
APPENDIX G.....	149
APPENDIX I.....	150
APPENDIX K.....	151
APPENDIX L.....	152
APPENDIX M.....	153
APPENDIX N.....	154

LIST OF FIGURES

Figure 1.1: The statistical data of imported chillies from year 1998 to 2007 [5]	2
Figure 2.1: Moisture sorption isotherm [23].....	11
Figure 2.2: Typical rate-of-drying curve, constant drying conditions. [22]	13
Figure 2.3: Direct open sun drying of fish in East of Malaysia.....	17
Figure 2.4: Direct solar dryer	22
Figure 2.5: Indirect solar dryer	25
Figure 2.6: Mixed mode solar dryer	28
Figure 2.7: Hybrid dryer (a combination of thermal and solar drying method)	33
Figure 3.1: The drying flow of hybrid solar dryer with biomass backup.	42
Figure 3.2: Sketching of the roof	44
Figure 3.3: Sketching of the floor	44
Figure 3.4: Sketching of the racks	45
Figure 3.5: The parameter assumption of solar dryer	48
Figure 3.6: Schematic of solar dryer with full dimensions (in mm).....	51
Figure 3.7: The process of heat supply flow diagram.....	53
Figure 3.8: The gas-to-gas heat exchanger design and its component	54
Figure 3.9: The flow path of the heat inside the biomass burner.....	55
Figure 3.10: The overall cross sectional unit design and boundary conditions (unit shown are not in scale)	58
Figure 3.11: Flue heat flow through the heat exchanger	59
Figure 3.12: Heat transfer network from flue to air side	62
Figure 3.13: Algorithm of the flue side analysis.....	66
Figure 3.14: Algorithm of the air side analysis.....	67
Figure 3.15: Characteristic length, L_c versus number of iteration	68
Figure 3.16: The sketch length of the heat exchanger inside the TBU (unit shown are not in scale).....	70
Figure 3.17: Sketch of the components of the TBU	70
Figure 4.1: Experimental program.....	74

Figure 4.2: Experimental Set-up of Hybrid Mode Solar Dryer	75
Figure 4.3: Experimental set-up of the TBU	77
Figure 4.4: Hot air outlet temperature obtained from burning of rice husk.....	79
Figure 4.5: Hot air outlet temperature obtained from burning of EFB	80
Figure 4.6: Hot air outlet temperature obtained from burning of wood chips	81
Figure 4.7: Transient measured values of temperature at collector, ambient, outlet air of dryer and solar irradiation	84
Figure 4.8: The average temperature of dryer under solar mode.....	85
Figure 4.9: Irradiation entering and escaping surface.....	86
Figure 4.10: The average measured temperature of dryer under clean hot air thermal backup mode.....	87
Figure 4.11: The average measured temperature of dryer under flue thermal backup mode	87
Figure 4.12: The average measured temperature of dryer under solar with clean hot air thermal backup mode.....	88
Figure 4.13: Variation of measured temperatures inside the dryer for solar with flue thermal backup mode.....	89
Figure 4.14: Drying of chillies under solar mode only	91
Figure 4.15: Drying of chillies under clean hot air thermal backup mode	92
Figure 4.16: Drying of chillies under hybrid mode	93
Figure 4.17: The overall comparison of chillies drying under different modes	94
Figure 4.18: Drying of EFB under only solar mode only	95
Figure 4.19: Drying of EFB under direct thermal backup mode	97
Figure 4.20: Drying of EFB under hybrid mode.....	98
Figure 4.21: The overall comparison of EFB drying under different modes.....	99
Figure 4.22: Transient behavior of the collector efficiency.....	102
Figure 4.23: Comparison of drying efficiencies at different modes	103
Figure 5.1: Labeled GAMBIT [®] solar dryer model	110
Figure 5.2: Mesh on solar dryer model	111
Figure 5.3: Laminar to Turbulent Transition.	115
Figure 5.4: Velocity vector of fluid flow under solar mode	121
Figure 5.5: Temperature contours under solar mode	122
Figure 5.6: Velocity vectors of fluid flow under separated hot air and flue mode	123

Figure 5.7: Temperature contours under separated hot air and flue mode	124
Figure 5.8: Velocity vectors of fluid flow under hybrid mode	125
Figure 5.9: Temperature contours under hybrid mode	126
Figure 6.1: Sketch of the proposed design of solar dryer	135

LIST OF TABLES

Table 2.1: Quality changes in foods during drying. [34].....	16
Table 2.2: Summary of experiment conducted by previous researchers on open sun drying method.....	19
Table 2.3: Summary of dryer design shape and material used by previous researchers in direct dryer fabrication	24
Table 2.4: Summary of indirect dryer design conducted by previous researchers	27
Table 2.5: Summary of mixed mode solar drying studies done by previous researchers	30
Table 2.6: Distribution of pyrolysis products for dry wood under combustion conditions [75].....	33
Table 2.7: Summary on the usage of biomass burner as a backup heater of solar dryer by previous researchers	36
Table 2.8: Summary of the studies on gas-to-gas heat exchanger by previous researchers	38
Table 3.1: Thermo-physical properties of candidate metals used for collector plate. Reproduced from [84]	46
Table 3.2: Properties of absorber materials. Reproduced from [85].....	46
Table 3.3: Thermal and optical properties of cover plate materials.	47
Table 3.4: Boundary conditions as used in the design.....	49
Table 3.5: Design calculation results	51
Table 3.6: Decision Matrix Table of Gas-to-gas Heat Exchanger.....	56
Table 3.7: Boundary condition of the TBU unit.....	65
Table 3.8: Result of the TBU design calculation.....	69
Table 4.1: The details of parameter measured	75
Table 4.2: Calorific value of the biomass fuel [96-98].....	78
Table 4.3: The percentage difference between mathematical calculation and experimental result	82
Table 4.4: Summary of chillies drying periods under solar mode.....	92

Table 4.5: Summary of chillies drying periods under clean hot air thermal backup mode	93
Table 4.6: Summary of chillies drying periods under hybrid mode	94
Table 4.7: Summary of EFB drying periods under solar mode	96
Table 4.8: Summary of EFB drying periods under flue thermal backup mode.....	97
Table 4.9: Summary of EFB drying periods under hybrid mode	98
Table 4.10: The external free convection flows on the upper and bottom surface of solar collector	101
Table 4.11: The drying efficiencies and enhancement index of chillies.....	104
Table 4.12: The drying efficiencies and enhancement index of EFB	104
Table 5.1: Summary of simulation studies conducted by previous researchers	109
Table 5.2: Models selection according to drying modes	116
Table 5.3: Parameters used in the numerical simulation	117
Table 5.4: Boundary conditions with P1 model (Involved with Solar mode)	118
Table 5.5: Boundary conditions without P1 model (Biomass mode only)	118
Table 5.6: Percentage difference between the experimental and simulation result under solar mode	122
Table 5.7: Percentage difference comparison between the experimental and simulation result under separated hot air and flue mode	124
Table 5.8: Percentage difference comparison between the experimental and simulation result under indirect with solar and direct with solar mode	126

LIST OF ABBREVIATIONS

CFD	Computational Fluid Dynamic
FASC	First American Scientific Corporation
FRIM	Forest Research Institute
EFB	Empty Fruit Bunch
EIB	Energy Information Bureau of Malaysia
G-to-G HEX	Gas-to-gas Heat Exchanger
MARDI	Malaysian Agricultural Research and Development Institute
MATLAB	Matrix Laboratory
TBU	Thermal Backup Unit
UKM	Universiti Kebangsaan Malaysia
USM	Universiti Sains Malaysia

NOMENCLATURE

Symbol	Nomenclature	Unit
A	Air side thermal area	m^2
A_c	Area of the solar collector	m^2
A_f	Flue side thermal area	m^2
$A_{fins\ in}$	Area of fins inside heat exchanger	m^2
$A_{fins\ o}$	Area of fins outside heat exchanger	m^2
A_s	Plate surface area	m^2
A_{win}	Inner wall area of heat exchanger	m^2
A_{wo}	Outer wall area of heat exchanger	m^2
c_p	Specific heat capacity of air	$J/kg \cdot K$
c_{pf}	Specific heat capacity of flue	$J/kg \cdot K$
D	Diameter	m
D_h	Hydraulic diameter	m
D_1	Cylinder diameter	m
D_2	G-to-G HEX diameter	m
E	Total useful energy	kJ
g	Gravity acceleration	m/s^2
Gr	Grashof number	-
H	Pressure head	m
h_{air}	Convection heat transfer coefficient of air	$W/m^2 \cdot K$
h_{bottom}	Bottom heat loss	$W/m^2 \cdot K$
h_f	Final enthalpy of drying air	kJ/kg
h_{fg}	Latent heat of evaporation	$kJ/kg\ H_2O$
h_{flue}	Convection heat transfer coefficient of flue	$W/m^2 \cdot K$
h_i	Initial enthalpy of drying air	kJ/kg
h_{top}	Top heat loss	$W/m^2 \cdot K$
I	Solar irradiation	W/m^2

ΣI_c	Total irradiation on the collector	MJ/m ²
k	Thermal conductivity	W/m·K
k_f	Thermal conductivity of flue	W/m·K
k_{wall}	Thermal conductivity of burner wall	W/m·K
L	Length	m
L_c	Characteristic length	m
L'_c	New characteristic length	m
L_f	Length of outer fins	m
L_t	Entry length	m
M	Mass of water evaporated	kg
\dot{m}	Mass flow rate	kg/s
\dot{m}_{ad}	Mass flow rate of air in dryer	kg/hr
m_{dr}	Average drying rate	kg H ₂ O/hr
M_f	Final moisture content (wet bulb)	%
\dot{m}_f	Mass flow rate of flue	kg/s
M_i	Initial moisture content (wet bulb)	%
m_p	Loading rate	kg
m_{pi}	Initial mass of dried product	kg
m_w	Mass of water evaporated	kg
n	Number of moles of a substance	-
Nu	Nusselt number	-
p	Absolute pressure	N/m ²
P	Perimeter	m
ΔP	Air pressure difference	Pa
Pr	Prandtl number	-
q	Heat	Watt
Q_d	Quantity of heat required for drying	kJ
Q_{TBU}	Heat supplied from the thermal backup unit	Watt
R	Ideal gas constant	kJ/kg·K
r_1	Outlet radius of cylinder	m
r_2	Inner radius of cylinder	m
®	Registered trademark symbol	-

Ra	Rayleigh number	-
Re	Reynolds number	-
RH_I	Relative humidity of air near collector	%
t	Drying time	s
T	Temperature	K
T_I	Near collector air temperature	K
T_{ab}	Absorber surface temperature	K
T_{amb}	Surrounding/Ambient temperature	K
TBU	Thermal Backup Unit	-
\bar{T}_{air}	Mean air temperature	K
T_{ao}	Outlet hot air temperature	K
T_c	Surface temperature of collector	K
$T_{chamber}$	Drying chamber temperature	K
t_d	Drying time	hr
ΔT_d	Temperature difference inside dryer	K
ΔT_f	Temperature difference in the burner flue side	K
T_{fi}	Inlet flue temperature	K
\bar{T}_{flue}	Mean flue temperature	K
T_{fo}	Outlet flue temperature	K
T_{ib}	Temperature supplied from burner	K
T_{od}	Dryer outlet temperature	K
T_{pr}	Product temperature	K
T_{wi}	Inside wall temperature	K
T_{wo}	Wall temperature in the air flow zone	K
V	Volume	m^3
\dot{V}	Volumetric flow rate	m^3/s
\dot{V}_a	Volumetric flow rate	m^3/hr
V_d	Air velocity in the air flow zone obtained from dryer	m/s
V_f	Flue velocity	m/s
$\{u, v, w\}$	Fluid flow velocity components	m/s
$\{x, y, z\}$	Cartesian coordinates	-

GREEK SYMBOLS

Symbol	Nomenclature	Unit
α	Absorption coefficient	-
β	expansion coefficient	K^{-1}
η_c	Collector efficiency	%
η_d	Drying efficiency	%
ρ	Density	kg/m^3
ρ_{air}	Density of air	kg/m^3
ρ_f	Density of flue	kg/m^3
μ	Dynamic viscosity	$N \cdot s/m^2$
μ_f	Dynamic viscosity of flue	$N \cdot s/m^2$
μ_s	Surface dynamic viscosity	$N \cdot s/m^2$
ν	Kinematic viscosity	m^2/s
ω_f	Final humidity ratio of drying air	$kg\ H_2O/kg$
ω_i	Initial humidity ratio of drying air	$kg\ H_2O/kg$
σ_s	Scattering coefficient	-
λ	Latent heat of vaporization of water	$MJ/kg \cdot H_2O$

CHAPTER 1 INTRODUCTION

1.1 Background

During history, people have dried multiple types of product inclusive of herbs, fishes, meats, fruits and vegetables to store them for use at a later time. The application of solar thermal systems for drying has shown to be practical, economical and environmental friendly especially in isolated area where solar energy is the only heat source. Even though the conventional fuel operated driers are more efficient, however it is beyond the reach of rural people. High prices and shortages of fossil fuels have increased the emphasis on the usage of alternative renewable energy resources.

Traditional drying which is open air sun drying is the common method that has been applied since time immemorial. It is also the common practice in Malaysia to dry crops such as chillies, cocoa beans, fish and many others. This method use and depend solely on the sun's heat. The products are spread on open surface and it is exposed directly to sun rays allowing products to be dried by irradiation from the sun. For fish drying along the shores of Peninsular Malaysia, the product is protected by covering with matting or plastic sheets when rain falls [1]. It was the cheapest and most adapted applied method but this type of drying consuming a large area, requires excessive manual labor and often results in food contamination by windblown dust and dirt, damage by birds or rodent, nutritional degradation, irregular quality and always depending on the weather condition. In addition, direct sunlight destroys some of the most fragile vitamins and enzymes and the food loses color [2].

The usage of solar dryer has been widely applied to overcome the traditional open sun drying method. The purpose of solar dryer is to supply the product with more heat than is available under ambient conditions, thereby increasing sufficiently the vapor pressure of the moisture held within the crop and decreasing significantly the relative

humidity of the drying air and thereby increasing its moisture carrying capacity and ensuring sufficiently low equilibrium moisture content [3]. Solar dryer consists of two types which are high temperature and low temperature dryers. High temperature dryers require higher cost and operate very fast. Low temperature drying systems took a longer time to dry, requires lower cost and suitable for the usage of remote area farmer. Solar drying is an efficient alternative for drying process especially in areas of tropical climate like Malaysia. Two types of product have been selected to be dried in this project which is chillies under food category and empty fruit bunch fiber (EFB), from palm waste category.

1.1.1 Drying of Food Product

Food scientist have found that by reducing moisture content of food to between 10 and 20%, bacteria, yeast, mold and enzymes are prevented from spoiling it. Solar drying technology application are varies from small, dessert or remote communities up to more sophisticated industrial installations. A. Samsudin from the Malaysian Agricultural Research and Development Institute (MARDI) stated that Malaysia imported most of the dried chillies from other Asian countries especially India to satisfy the local market [4]. The percentage increases especially during the period before a festive.

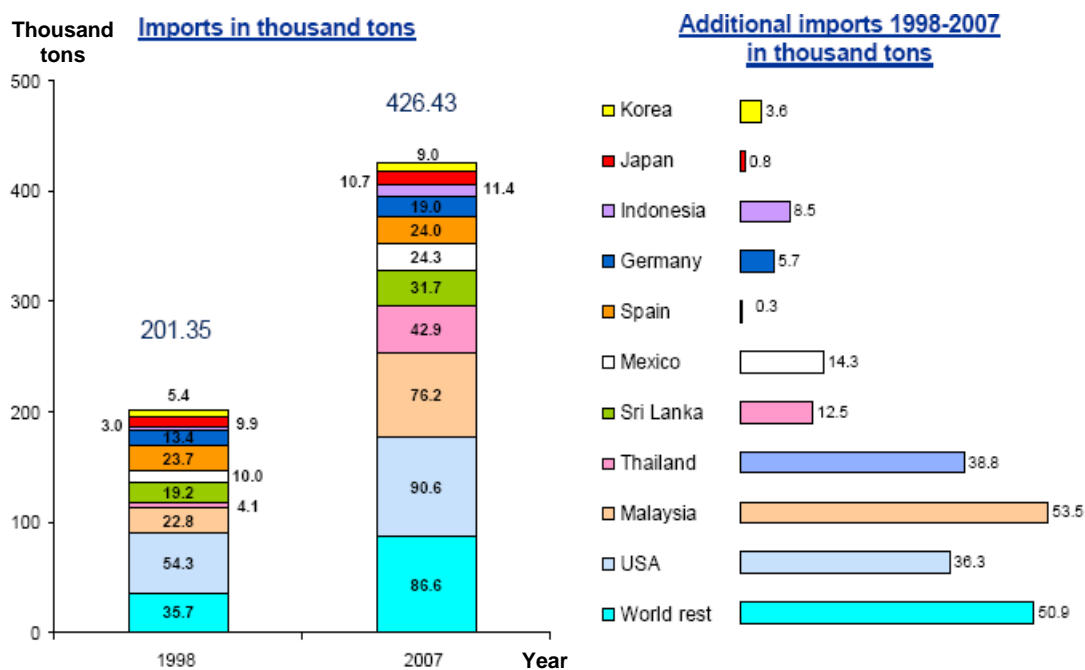


Figure 1.1: The statistical data of imported chillies from year 1998 to 2007 [5]

A review by Center for Agricultural Policy with Prosperity Initiative as shown in Figure 1.1 indicates that Malaysia have driven the growth in imported chillies accounted for more than 50% between the year of 1998 and 2007. Accordingly, various types of solar dryers have been designed to improve solar drying capabilities such as solar greenhouse dryers, solar cabinet dryers, forced convection dryers and many others. Most of the developed dryer is focusing on crops and foods product.

The Energy Information Bureau of Malaysia (EIB) reported that MARDI has carried out several tests to solar dry food products, such as coffee and cocoa beans, noodles and paddy. The Forest Research Institute (FRIM) also applied solar dryers for bamboo and Universiti Sains Malaysia (USM) conducted solar drying for rubber and desalination of potable water. A commercial size solar assisted dryer at Universiti Kebangsaan Malaysia (UKM) tested on chillies, peppers and green tea showing that solar energy can contribute up to 70% of overall energy requirements [6].

1.1.2 Drying of Biomass Products

Malaysia's palm-oil industry currently operates more than 300 palm oil mills that process palm oil from 2.5 million hectares of oil palm estates throughout the country and produce more than a million metric tons of EFB as waste material every year [7]. The EFB fibers could be processed into various dimensional grades to suit specific applications in mattress and cushion manufacture, soil stabilization/compaction for erosion control, landscaping and horticulture, ceramic and brick manufacture and flat fiber board manufacture. The EFB were found to be very wet in its raw state and it would be an excellent for power boilers after dried. Among EFB fibers drying technologies that has been applied are conventional rotary drum dryer with a flue gas drying medium from a diesel burner and superheated steam [8]. FASC Malaysia has installed a KDS machine in the 14 MWe TSH Biomass Power Plant in Kunak, Malaysia, for the purpose of drying EFB [9]. The rising utilization and highly depending on electricity to dry EFB fibers is expected to be reduced by using solar energy as the source of heat. However, one major problem which exists with these solar dryers is its capability to dry products only with the existence of solar energy

enabling it to be operated only on hot days. This causes inconsistency in drying and a decrease in the production scale.

The other alternative renewable energy which is able to be utilized in drying application is biomass. Currently, the usage of biomass, as a fuel of burner is relatively synonym in the drying industry. This burner extends the drying process during the cloudy or rainy days (backup heater) and even during the day and night. Several researchers have studied about the solar dryer with biomass burner. Biomass may be obtained from forests, woods and agricultural lands and commonly burned using inefficient technologies in most developing countries. Malaysia is one of the countries which took advantage of its enormous output of biomass from oil palm residues and wood wastes. At present, biomass fuels account for about 16% of the energy consumption in the country, of which 51% is from palm oil biomass and 22% from wood waste [6].

In addition, Malaysia has abundant biomass waste from its oil palm, wood and agro-industries. Brammer and Bridgwater [10] stated that due to continuous running of an engine or turbine for example in bio-energy plants, the biomass may have to be dried. It has been widely used in palm oil mills, sawmills and wood processing factories to generate both electricity and steam and it can be transformed into both heat and electricity simultaneously through cogeneration. Among the utilization of renewable energy technologies (solar and biomass) which has been successfully applied in Malaysia are biomass boilers, palm oil industry boiler, co-generation plants, solar thermal technologies and photovoltaic technologies [6]. Among the biomass fuel materials that has been reported in biomass burner application are coconut shells [11], woodchips [12], [13], charcoal [14], paddy husk [15], fuel wood [16-18] and briquetted rice husk [19]. Hence, solar and biomass are the two main renewable energy sources of energy that extremely suitable for drying application.

1.2 Problem Statement

The drying process is essential to prevent microorganism from spoiling the product. Drying reduces water activity hence hinders quality decay. Solar energy exists in abundance renewable and is the most important source of heat for drying application.

The traditional method, open sun drying is extremely weather dependent and often results in contamination of the products by dusts, birds and insects and nutritional deterioration (caused by heterogeneous and insufficient drying). Mechanized dryers require fuel or electricity to operate and require expensive equipments, while the conventional solar dryer is used only when there is solar energy. As for any other solar system, there is a lack in availability of the solar irradiation for continuous operation especially during the cloudy days and at night.

Accordingly, there should be auxiliary source of energy to compensate for low or zero solar irradiation. In cases of low solar irradiation for example at night or during cloudy days, a backup heater is proposed. Biomass as fuel is investigated to power the backup heater. The biomass resource is considered as an organic matter in which the energy of sunlight is stored in chemical bonds. Biomass energy is generated when organic matter is converted to energy.

Since solar and biomass are two main sources of renewable energy, a proper usage of these sources produces food of better quality and provides reduction in drying time compared to open sun drying. Both sources will function together whereby solar irradiation is the main heat source integrated with biomass acting as a heating back up. It is important for the commercial producers to ensure the drying process is operated continuously so that they can increase their market production and avoid inferior products. Through solar-biomass mode of operation, drying will proceed successfully even under unfavorable weather conditions.

The latest research works were mostly limited drying of only one type of product. For example, the dryer is used specifically for food drying. Agricultural biomass product such as palm shell and fiber, rice husk, coconut shell and wood chips are very useful in the utilization of domestic fuel, agriculture and industries application and also for power generation [20]. These biomass wastes needs to be dried before proceeding into further processes and at this time, the application of solar dryer is practical to be applied since it provide higher rate of drying and hence increase the production. Hybrid dryer for multiple products is favorable for a farmer who produces more than one type of products (food and waste).

Nevertheless, there has been no report on a dryer capable of combining the drying techniques, the direct solar, the indirect solar, the clean warm air and the hot flue gases in a single drying unit. The present project will be investigated such hybrid dryer that can be used for multiple products.

1.3 Research Objectives

In view of problem statement, the most critical and interesting problem has been the interruption drying process of solar dryer for drying multiple products. Therefore, the objectives of this study are:

- To investigate the enhancement of solar drying by a thermal backup.
- To design and implement experimental model of hybrid dryer backed up by biomass heat source.
- To evaluate the performance of the dryer unit and the biomass backup unit by detailed experimental measurements at different operational condition.
- To evaluate the hybrid dryer unit by drying chillies, as food sample, and EFB, as waste sample.

1.4 Scope of Work

The analytical and numerical method would be based on the findings of the researches and formulae that being presented in books with alterations according to real conditions. The hybrid dryer model would be simulated and analyzed using CFD techniques. The study is carried out by four analytical techniques which are executed in the sequences below, where each step was based on results and findings from the previous step. The scope of study involved:

1.4.1 Analytical modeling and analysis

Within the analytical modeling, the design calculation of the dryer and the backup unit has been involved. The governing mathematical relation was identified, arranged

in process sequence converted to a computer program. The model would be a tool for the conceptual design. Also, analysis results could be obtained for comparison and extension of the application for prototyping purposes.

1.4.2 Experimental modeling with measurement

The experimental work composed of drying multiple types of product which are food and biomass waste. Experiments have been planned to consist of detection of the temperature distribution inside the dryer, the working fluid parameters, the evaporation rate and the heat supplied from the biomass burner. The experimental technique would be a verification tool for the computational and analytical models.

1.4.3 Computational simulation and analysis

The CFD simulation is carried out by using the available software in the department which is ANSYS[®] - FLUENT[®] and GAMBIT[®]. This technique would be used to simulate the model to analyze the performance of the solar dryer at various operational conditions. The visualization by CFD simulation would allow improvement of the dryer design by analyzing the flow and temperature in the dryer.

1.4.4 Comparison of the results

As justification of the numerical and analytical procedures, the results would be compared with the experimental results for three main cases of tests, which are:

- No-load case
- Chillies drying as food sample
- EFB drying as biomass waste sample

1.5 Organization of the Thesis

This dissertation is subdivided into six separate chapters. The introduction chapter describes the research background related to the evolution of solar drying systems, their main application and the feasible usage of biomass fuel as the alternative source

of heat. The limitations of solar drying were described in the problem statement. Furthermore, the objectives of the work, the scope of the study and the main features of the methodology have also been provided in the introductory chapter.

Chapter two contains of an extensive review on the drying mechanism and classification. It also describes a literature review of previous researchers and published work on solar dryer, biomass burner and hybrid solar dryer. The performance models adopted by previous researchers have been presented. Comments and some conclusion were provided at the end of the second chapter.

Chapter three presents the general methodology and mathematical formulation which were involved in the design approach of mixed mode solar dryer and biomass burner. The conceptual design, detailed design and materials selection were demonstrated. This chapter also underlines the solution procedures followed to solve and code the mathematical model using MATLAB[®].

Chapter four presents the experimental setup of biomass burner and solar dryer experiment and the obtained results. The burner was tested with three types of fuel and the best fuel was selected. The temperature distribution inside the solar dryer and collector performance was tested without loading materials. Two types of product had been dried which were chillies as food category and EFB as oil palm waste. The results were analyzed in details.

Chapter five presents the method of simulation and the results obtained at different operational conditions. The steps were shown in details including the modeling and meshing criteria, boundary conditions and the properties of parameters inserted into the CFD simulation. A concise idea was turned from the results analysis and discussion, and this facilitated evaluation of the developed model performance.

The last chapter provides conclusions gained from the preceding chapters. The major outcomes, which was the best drying technique from the conducted work was summarized in more details. The recommendations were pointed out in this chapter in purpose to improve the presented work.

CHAPTER 2

LITERATURE REVIEW

2.1 Chapter Overview

This chapter describes the drying principle, mechanism and classification of dryers. A review from traditional to modern drying method is reviewed in order to understand the evolution of solar drying application. In addition, detailed studies on the design characteristic of solar dryer and biomass burner by previous researches are presented. The development, performance and limitation of solar dryers conducted in the past had been investigated, and consequently the appropriate drying method was selected.

2.2 Drying Process

Drying is the process of reducing water or moisture content of products to a specific range in order to prevent microbial decay of the product. The application of solar energy which exists in an abundance total and renewable type of energy has been utilized since the immemorial of time. Among the dehydrated products are herbs, meats, fruits and vegetables. The reasons drying of these products are to improve the shelf life of product, to control textures properties such as crispness (biscuit), to standardize composition, to reduce weight for transport and the most importantly is to control the water activity [21].

2.3 Factors Influencing the Drying Rate

Drying is a combination of heat and mass transfer operation. The main aim of drying is to remove moisture as fast as possible at a temperature that does not seriously affect the flavor, texture and color of the food. Among the factors that influence the rate of drying are the nature of moisture, the nature of solids and the temperature [22].

2.3.1 Moisture Content of Solids

Moisture content can be expressed as the weight of water as a proportion of total weight either of the wet material (wb) or dry matter (db). The drying process takes place until there is no net transfer between the food and air. In this situation, it is called as equilibrium moisture content. It is varying depending on the types of material or product. According to Mujumdar and Menon [22], the moisture within the product is divided into three types which are bound, unbound and free moisture as explained below:

- Bound moisture is the moisture present as a liquid solution, trapped in the microstructure of the solid and exerts a vapor pressure less than pure liquid.
- Moisture in excess of bound moisture is called unbound moisture and it is needed to be removed by drying process.
- Free moisture can be bound or unbound and it can be removed at prevailing temperature. The portion of moisture not being held by chemical reaction within the substance.

There are two methods of removing unbound moisture which are evaporation and vaporization [22]. Evaporation occurs when the vapor pressure of the moisture on the solid surface is equal to the atmospheric pressure where it can be done by raising the temperature of the moisture to the boiling point. In vaporization, drying is carried by convection that is by passing warm air over the product. The moisture from product is transferred to the air and in this case, the saturation vapor pressure of the moisture over the solid is less than atmospheric pressure.

2.3.1.1 Sorption Isotherms

The relationships between the equilibrium relative humidity of the air (ERH) and the equilibrium moisture content within solids (M_e) is important in order to determine the end point of drying and for product stability evaluation during drying. This relationship at various temperatures is called moisture sorption isotherms as shown in Figure 2.1.

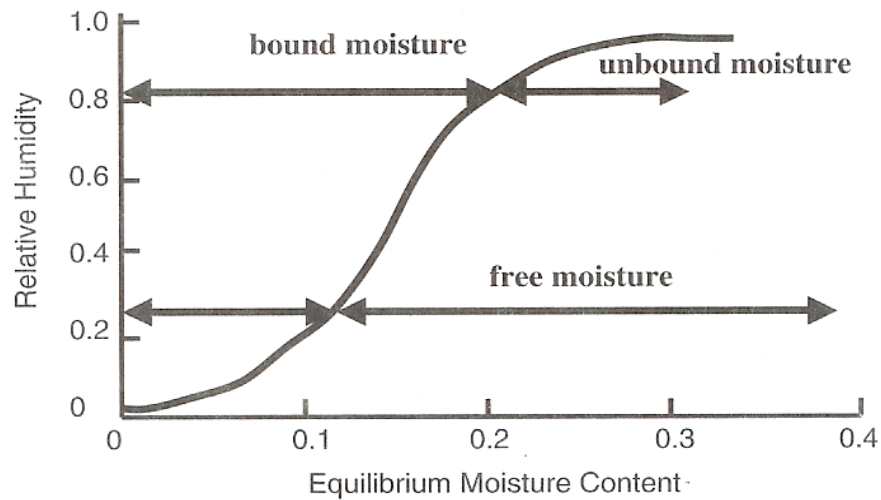


Figure 2.1: Moisture sorption isotherm [23]

Moisture sorption isotherms can be evaluated using two methods which are static and dynamic method [23].

- Under static method, the sample of known initial weight is placed in an environment of constant air humidity. The final moisture content is determined after equilibrium which can take several days.
- Dynamic method takes shorter period than static method. It can be done either by measuring the resulting air humidity at equilibrium from a sample of known moisture content enclosed in small headspace or using a continuous flow method. In this method, the equilibrium moisture content is measured after equilibration within enclosed sample where it circulated with temperature and humidity-controlled air.

2.3.2 Types of Materials

Van Brackel [24] classified solids subjected to drying into three types which are non-hygroscopic, hygroscopic and colloidal material as shown below:

- In non-hygroscopic material, the partial pressure of water in the material is equal to the vapor pressure of water. All the moisture content of a non-hygroscopic material is unbound moisture.

- A hygroscopic material includes almost all of dried materials such as food. The partial pressure of water becomes lower than the vapor pressure of water at a critical level of moisture content.
- In colloidal material, the liquid is physically bound and it does not have pore space. The evaporation occurs only at the surface. The examples of this type of material are soap, glue and many others.

2.3.3 Drying Temperature

Drying under controlled conditions of temperature and humidity helps the crop to dry reasonably rapidly to a safe moisture content level and to ensure a superior quality of the product [25]. If the temperature is too low in the beginning, microorganisms may grow before the food is adequately dried. If the temperature is too high and the humidity is too low, the food may harden on the surface. In addition, the rate at which drying air is moved through the chamber should ensure that a sufficient volume of fresh air is maintained to prevent saturation process [26]. For effective drying, air should be *hot and dry moving air*. According to Murthy [27], an optimum air flow rate is desired where slower flow rate may increase air drying temperature and a higher flow rate may decrease the moisture removed.

2.4 Drying Mechanism

Products that contain water behave differently on drying according to their moisture content and their composition structure. Mujumdar and Menon [22] came out with a typical rate of drying curve of a hygroscopic product. The drying curve is divided into three stages as shown in Figure 2.2.

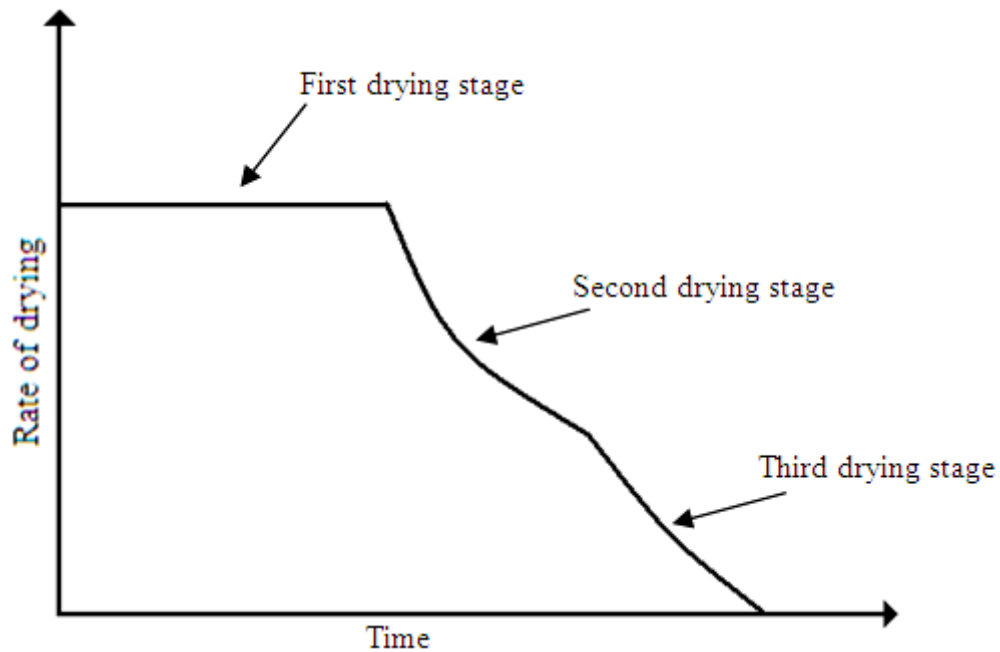


Figure 2.2: Typical rate-of-drying curve, constant drying conditions [22]

The drying rate is constant during the first stage. Vaporization occurs as the surface contains free moisture and led to some shrinkage where the moisture surface is drawn back toward the solid surface. At the end of the constant rate period, the moisture has to be transported from inside to the surface of solid. In the second stage, when average moisture content reached critical moisture content, dry spot is likely to occur. The moisture keeps decreasing until the liquid entirely evaporated. Further drying stage shows that the rate of drying falls more rapidly than before. In this stage, the heat transmission consists of heat transfer to the surface and heat conduction in the product. As the moisture concentration is lowered by the drying, the rate of internal movement of moisture decreases. The rate of drying continues until the moisture content falls down to the equilibrium value for the prevailing air humidity and then drying stops.

2.5 Drying of Food Products

The aim of most rural farmers is to dry food or vegetable in a short period of time in order to obtain high product and profit. Different types of product to be dried may require different range of drying temperature due to differences in initial and final

moisture content. Generally, the water content of well dried food is diverse from 5 to 25 percent.

The El Paso Solar Energy Association [28] provides basic guidelines to dry food where the temperature ranges between 37°C to 71°C will effectively kill bacteria and inactivate enzyme even though temperatures around 43°C are recommended for solar dryers and aims to remove 80 to 90% of moisture from the food. The allowable temperature of heat under solar or biomass burner supplied for most of the tropical fruits, vegetables and also fish drying into the drying chamber is about 60 to 70°C [11]. For safe storage, crops usually dried to a final moisture content of < 14% with equilibrium moisture content $\leq 14\%$ and RH of 80-90% is preferred [29]. The drying air temperature inside the drying chamber is depending on the type and moisture content of the product [30] as shown in Appendix A.

2.6 Drying of Biomass Product

Power plant boiler requires a nonstop operation. Due to high cost of diesel fuel, there are increasing demands in commercial scale on the biomass fuels since it is cheaper and available in abundance quantity. Biomass sources include food crops, grassy and woody plants, residues from agriculture or forestry, organic components of municipal and industrial wastes and animal waste. Among the biomass materials that has been widely applied as fuel are woodchip, sawdust, empty fruit bunch (EFB) and rice husk. The biomass materials may have to be dried first in order to support a continuous running of an engine and turbine [10].

According to Hasibuan and Daud [8], a hot flue gas in a diesel-fired rotary drum dryer has been applied in drying of EFB. However, the drying caused in low quality where the EFB product suffers from over-drying, browning and dust explosions. It can be concluded that the heat from direct fuel is applicable to be used as the source of heat for drying biomass product. The heat from direct fuel is expected to be higher than indirect fuel. By controlling the fuel, the direct heat temperature is assumed to be not too high and able to be applied for drying of biomass product. The range of supplied temperature should be observed first to prevent the over-drying. The effect

of dust explosion can be avoided by using a filter which places in between the burner and solar dryer.

2.6.1 Empty Fruit Bunch (EFB)

Palm oil industry uses its own solid waste, shell and EFB fiber as boiler fuel. The EFB is also burnt inside the incinerator to produce potash ash which is applied in the plantation as fertilizer. A stable and strong characteristic of EFB fibers lead it into the application of mattress and cushion manufacture, soil stabilization/compaction for erosion control, landscaping and horticulture, ceramic and brick manufacture and flat fiber board manufacture [8]. However, the EFB needs to be dried before further processing and here, the application of solar dryer with biomass burner is practical since it provides high drying rate which consequently increase the production. High initial moisture content in EFB may cause degradation, contamination and consequently damage the product quality. According to Rahim and Suffian [31], the initial moisture content of EFB is 80% and the optimum moisture content is less than 13%.

2.7 Drying Principle and Quality Changes

A good understanding on drying principle is important in order to ensure that the drying product is in good quality and can be stored for a longer period. Drying is a dual process of heat transfer to product from heating source and mass transfer of moisture from interior of product to its surface and consecutively to the surrounding air [32]. The process is complicated since it does not only involve the water evaporation on the solid surface but also the water movement from inside to its surface. The physical, chemical and biological reactions happened simultaneously during the drying process as discussed below.

- **Physical reaction**

It is the process of removing water inside the substance. Rockland [33] divided the water binding inside the food and crops into three types.

- (i) Unbound free water found in interstitial pores in which capillary forces and soluble constituents cause lowering of vapor pressure.
- (ii) Water molecules that are bound to ionic groups such as carboxyl and amino groups.
- (iii) Water molecules that are hydrogen bonded to hydroxyl and amide groups.

- Chemical reaction

The reaction occurs during the changes of raw materials into quality product.

- Biological reaction

It involves the microorganism activities which takes place during the drying process.

These reactions will affect the final and the acceptability of dried products. The quality changes in foods during drying are shown in Table 2.1. Most of food drying are associated with shrinkage in the final product and limited to texture and rehydration capacity. A “case hardening” phenomenon occurs when the drying is performed too rapidly [23]. Subsequent removal of water from the product will not be performed since the surface is covered with a thick crust. A chemical reaction result in significant quality losses which lead to discoloration and off-flavor generation. Loss of nutritional quality is mainly due to the effect of temperature and dehydration on vitamins and proteins. It is important to ensure that raw materials are free from pathogenic microorganisms at the beginning of drying since it is surrounded with saturated water environment.

Table 2.1: Quality changes in foods during drying [34]

Type	Factor	Quality Effect
Physical and structural	Shrinkage Cell structure damage Volatile retention	Volume, texture, rehydration ability Texture, rehydration ability, solute loss Aroma loss
Chemical and organoleptic	Browning reactions Lipid oxidation Pigment degradation Enzyme inactivation	Darkening, off-flavor development Rancidity, off-flavor development Color loss Flavor and pungency loss
Nutritional	Microbial death Protein denaturation Vitamin degradation	Microbial survival Loss of biological value Loss of nutritive value

2.8 Traditional Drying Method (Direct Open Sun Drying)

The most adapted drying application that been applied since ancient times is open sun drying. In the traditional method of drying, which is by an open sun, all the products are spread on a proper surface and it is directly dried under the sun as shown in Figure 2.3. Even though it is the cheapest and most applied method but this type of drying requires enormous manual labor and often results in food contamination by windblown dust and dirt, damage birds or rodent, nutritional degradation and irregular quality. Direct sunlight destroys some of the more fragile vitamins, enzymes and causes the food to lose color.



Figure 2.3: Direct open sun drying of fish in Peninsular Malaysia [35]

Amer et al. [36] dried 30 kg of ripe banana slices under open sun drying and solar drying for 8 hours on a sunny day. The moisture content reduced from an initial of 82% to 62% (wb) under open sun and 18% (wb) under solar drying. A low drying rate under open sun drying resulted in low quality dried product in terms of color, aroma and texture. Studies made by Mulozoki and Svanberg [37] revealed that the amount of provitamin A-carotenes in traditionally treated green leafy vegetables were highly reduced by open sun-drying. He found that due to direct exposure to sunlight, the open sun-dried vegetables had lower all-trans- α - and β -carotene and 9-cis-carotene contents compared with blanched and solar-dried vegetables.

Prasad and Vijay [38] have conducted experimental studies on *Zingiber officinale*, *Curcuma longa* l. and *Tinospora cordifolia* under open sun drying. The drying time of 18kg of all fresh products took 192-288 hour and the color was dark. They concluded that the quality under open sun drying was very low. Based on Ayensu [29] findings, it took nearly two times longer to dehydrate crops by open sun drying compared to the solar dryer. Prasad et al. [16] experimentally dried a batch of 500g rhizomes under open sun. The physical appearance in relation to surface color and color of breaking were observed visually. The open sun dried rhizomes were dark and most of them were affected by white fungus. The final product has been contaminated and resulted in a deteriorated quality.

Mastekbayeva et al. [19] described their findings on drying of chillies and mushroom under open sun drying. They stated that the low quality of dried product under this condition is due to the interrupted drying process. The tendency of mould to grow during the overnight storage is caused by moisture re-absorption. Besides, a crack tends to develop within certain product due to thermal stresses resulting from alternate heating and cooling of the product during day and night.

It can be concluded that *open sun drying is not the appropriate way for drying* application. Ramaswamy and Marcotte [23] had listed the primary disadvantages of sun drying which includes the difficulty on controlling drying conditions, the dependency on the other elements for instance solar availability, dry weather and wind speeds, requiring adequate exposure to the sun and also from the rain, insects and animals protection. Summary of previous works on open sun drying method is given in Table 2.2.

Table 2.2: Summary of experiment conducted by previous researchers on open sun drying method

Researchers	Type of product dried	Findings
Amer et al. [36]	Banana slices	Low quality in terms of color, aroma and texture
Mulozoki and Svanberg [37]	Green leafy vegetables	Reduced in Provitamin A-carotenes Lower trans- α - and β -carotene and 9-cis-carotene contents
Prasad and Vijay [38]	Zingiber officinale, Curcuma longa l. and Tinospora cordifolia (Herbs)	Dark color with low quality
Ayensu [29]	Food crops	Drying time is 2 times longer than solar dryer
Prasad et al. [16]	Turmeric Rhizomes (Herbs)	Dark surface color Affected by white fungus
Mastekbayeva et al.[19]	Chillies and mushroom	Growing of mould Cracks on surface

2.9 Solar Drying

Solar drying is an appropriate alternative of drying technology. It has been revealed to be an efficient alternative to traditional drying systems, especially in areas of good sunshine like Malaysia. Solar refers to the methods of using the sun's energy for drying in an enclosed zone which required low to moderate temperature below 80°C [39]. The application of solar dryer is able to reduce atmospheric pollution cause by conventional fossil fuels. Hence, the usage of solar thermal systems for drying has shown to be practical, economical and environmental friendly especially in isolated area where solar energy is the only heat source.

The drying process is basically involving 3 modes of heating which occurred simultaneously inside the solar dryer. The heat is transferred into the solar dryer through convection, conduction and irradiation. In convection, the heat transfer is due the genuine movement of the warmed matter. The evaporated moisture is removed from the solid surface by the hot air or gas. The energy that is transfer from particle to particle is called conduction. The source of heat is supplied from the heated surface and carried away the evaporated moisture. This process occurred in indirect type of

dryer and has higher thermal efficiency [22]. The energy is transported through space from the electromagnetic waves in irradiation. It consists of the various sources of electromagnetic irradiation with wavelengths ranging from the solar spectrum to microwave (0.2m to 0.2 μ m) [22]. The material absorbs merely a part of the solar irradiation depending on its wavelength.

The fundamental principle of solar drying is to supply product with more heat than the available ambient conditions, as well as increasing the vapor pressure of the moisture held within the crop and decreasing the relative humidity of the drying air [3]. These processes will subsequently increase product moisture carrying capacity and ensure low equilibrium moisture content inside the drying chamber.

2.9.1 Solar Dryer Classification

a. Based on the scale of productivity, David and Whitfield [40] have classified the solar dryer into three types and reviewed each of them in their paper presented in the International Conference on Solar Cooking, as shown below.

- Individual family units.

The usage is to dehydrate small quantities of fruits, vegetables and herbs for the purpose of extending the availability of these products at family level. It has the advantage of being portable.

- Medium scale commercial applications.

Suitable for individuals, groups, cooperatives and associations to supply a larger quantity of product in order to reach market demand. This dryer is able to increase the commercial yield of crops and exportation.

- Large scale commercial applications.

It is able to occupy a very large quantity of product with good temperature control and hygienic conditions but it requires a greater capitalization. This dryer has the ability to control climate and hygiene of the product which lead to immediate profit.

b. Based on the heat transfer mechanism, the classifications of solar-energy drying systems are based on their modes of heating and the technique of solar heat applied.

The available solar dryers systems are categorized into two major groups which are passive and active solar dryer [3]. The flow in passive or natural solar dryers are caused by the fact that warm air inside the dryer is lighter than the cooler air outside and moves up under buoyant force. Active or force convection solar dryers uses an external devices like fan or blower to create the airflow. It is also known as a hybrid solar dryer and performs very well in drying as compared to passive solar dryers.

c. Based on the mode of solar heating, Ekechukwu [3] separated the active or passive solar drying systems into three distinct sub-classes based on the design arrangement of systems components as well as the mode of heat utilization.

- Direct solar dryers.

The materials are placed in a transparent enclosure of glass or plastic. The sun heats directly to the material and enclosure and causes a heat buildup due to the “greenhouse effect”.

- Indirect solar dryers.

Sun does not act directly on material to be dried but the products are dried by hot air heated by the sun. It provides higher operating temperatures than direct dryers and can produce higher quality products [41].

- Mixed-mode solar dryers.

This type of dryer obtained a combination heat from direct solar irradiation and the heated air from solar collector for drying operation. The rate of drying is higher than indirect type solar dryers since it received heat from more than one source. Comparative studies have shown that it is the most efficient dryer between the natural convection solar dryers [42-44].

2.10 Solar Drying Overview

Obviously, a design is the main factor that will reflect the dryer effectiveness. Besides, the types of material used, inlet and outlet air location and the area exposed to solar highly determine the quantity of thermal heat supplied. An overview on the limitations, similarities and differences of solar drying had been done based on the works and investigation of previous researchers. The design construction,

characteristics and performance of the dryer had been looking deeply in order to come with better prototype design.

2.10.1 Direct Solar Dryer

A typical direct solar dryer usually consists of transparent cover, commonly glass or Perspex as shown in Figure 2.4. The function of transparent cover is to reduce the direct convective losses to the surroundings, to protect the products from exposure to the environment and to increase the temperature inside the dryer when heated with direct solar irradiation. Many types of direct dryer had been designed and experimentally studied by other researchers.

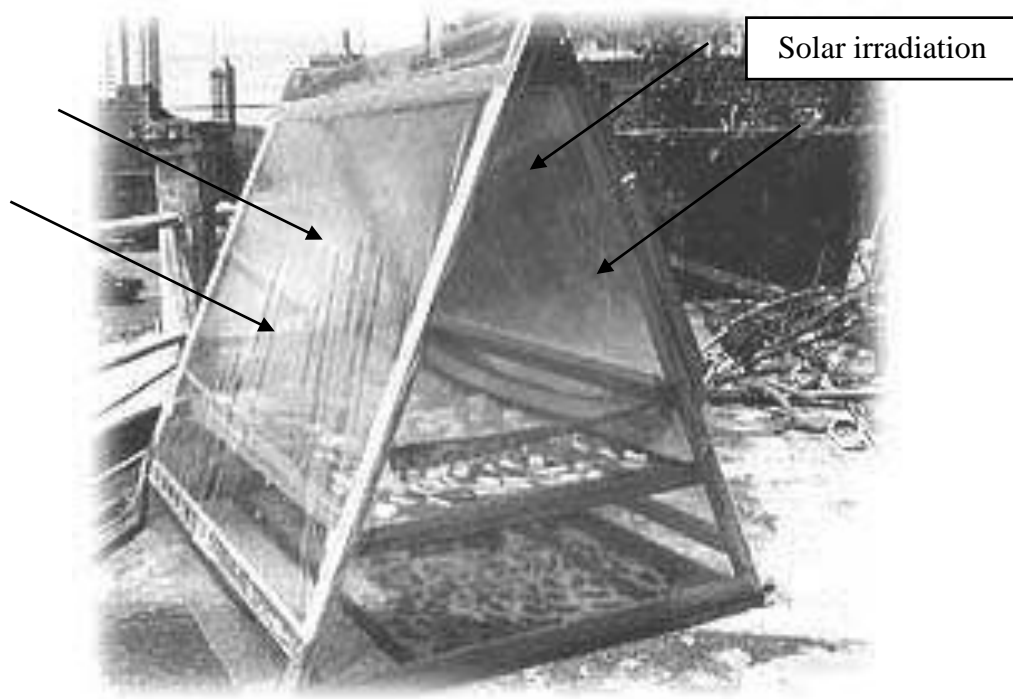


Figure 2.4: Direct solar dryer [40]

Sharma et al. [45] designed and tested a direct solar cabinet dryer that had same compartment as small box and made of wood. The drying chamber had been painted black to maximize solar absorption. The temperature recorded was relatively high, around 80°C [46]. The temperature rise was 25-30°C over the ambient [47] and dryer took 3-4 days when drying 10 kg of grapes.

Gbaha et al. [48] had applied a black painted sheet steel matt in his direct solar dryer designed. Treated wood had been used in the construction of the dryer to prevent any poor meteorological conditions and termites. The result indicates that the maximum temperature recorded in drying chamber was 59°C and the value changed according to solar irradiation. The dryer took 19 and 22 hours to dry cassava and sweet banana respectively.

Ezekoye and Enebe [49] designed and fabricated a domestic solar dryer for agricultural applications using plywood, Perspex glass, angle iron and wire mesh. The optimum temperature recorded inside the dryer was 67°C. It took five and eight days, respectively, to dry pepper and groundnuts at average dryer relative humidity of 43% and average temperature of 63°C.

A stair case solar dryer capable of containing large agricultural product quantity had been designed by Hallak et al. [50]. Double walled galvanized metal sheets had been used as its based and side covers. The upper surface was covered with transparent polycarbon sheet since it is non –breakable to allow solar irradiation. The highest temperature recorded on upper, middle and lower compartment were 78°C, 67 °C and 51°C respectively. The dryer is able to occupy 20kg of fruits and vegetables. The dryer took only 3 days to complete the drying process.

A glass roof solar dryer had two black painted inner side of drying platforms and a slanted long glass roof with cap. The air circulates from the bottom part and leave through the cap. It is identical with solar green house. A foldable solar dryer that operates on the same principles of glass roof solar dryer had been design by Nair and Bongirwar [51]. The outside and inside wall respectively had been covered with black painted aluminum sheet and polythene sheet. The dryer was able to dry 100kg of product at a time.

Even though the system provides a favorable thermal in drying application, it still suffers significant disadvantages due to unstable solar insulation. The fluctuating drying temperature may result in a longer drying time and allow growth of spoilage microorganism due to improper drying process which consequently produces a low quality product.

Besides that, the product to be dried is exposed to solar irradiation and thus resulting in discoloration and vitamin loss in a certain product [52]. Summary of previous works on the dryer design shape and material is given in Table 2.3.

Table 2.3: Summary of dryer design shape and material used by previous researchers in direct dryer fabrication

Researchers	Dryer design	Dryer material	Max dryer temperature recorded
Sharma et al. [45]	Solar cabinet dryer	Wood	80°C
Gbaha et al. [48]	Portable box type	Wood and blade of glass	59°C
Ezekoye and Enebe [49]	Domestic solar dryer	Plywood and Perspex glass	67°C
Hallak et al. [50]	Stair case solar dryer	Galvanized metal sheets and polycarbon sheet	Upper : 78°C Middle : 67 °C Lower : 51°C
Nair and Bongirwar, [51]	Glass roof solar dryer	Glass body, black painted aluminum and polythene sheet	-

2.10.2 Indirect Solar Dryer

Indirect solar dryer produced a high product quality by maintaining a low temperature. It is suitable to be applied in the preparation of crops such as sweet potatoes and grapes [53] whose vitamin content can be easily destroyed by sunlight or under hot air heated by the sun. The system consists of separate solar collector and drying chamber. The product does not expose directly to the solar irradiation but received the hot air from solar collector. The movement of the heated air into the drying chamber is either cause by natural draft or by means of a fan as shown in Figure 2.5.



Figure 2.5: Indirect solar dryer [54]

Azad E. [55] designed and tested an indirect solar for agricultural product consisting of a black painted solar collector which made from wooden frame insulated by polystyrene foam. The fiberglass sheet covered on top to reduce the heat lost and black painted rocks as a thermal storage, placed on the insulator. Wind-operated ventilator at the top of the dryer chamber had been used to increase air circulation rates. He had tested the dryer with 3 modes operation which were open sun, direct with indirect and only indirect mode by drying grapes. Under direct with indirect experiment, the maximum collector outlet temperature recorded was 62°C and the maximum dryer temperatures from Tray 1 (bottom) to Tray 5(top) were 55, 52, 47, 43.5, 39°C respectively. He indicates that by utilizing the thermal storage, the drying process keeps continuing even under shaded midday period and sundown. The grape took 3 to 4 days to dry under solar drying and 6 days for sun-dried. Indirect mode took a longer drying time but resulting in better quality. Direct with indirect mode offers the advantages in faster drying rate much and almost uniform moisture content reduction among the trays yet poor quality. He found that direct irradiation resulting

in red and 'black' of the grape surfaces which means that the quality had been deteriorated while in indirect mode the grape maintained in green color.

An indirect solar dryer with natural ventilation for drying grapes had been studied by Eissen et al. [56]. The solar collector was made of a transparent foil cover and a black absorber sheet. The solar collector collects the solar irradiation and heats up the entering air from the inlet. The maximum temperature recorded in the drying chamber was 50°C when the ambient temperature was 30°C. The drying time required was 7–8 days with loading capacity of 100kg/m² drying chamber.

Dissa et al. [57] had done an experimental of indirect solar dryer for drying mango slices. The absorber was a mixed type of a corrugated iron absorber and a porous absorber which made of an aluminum mesh. The bottom side of dryer had been insulated with glass wool and shaving in order to increase the drying temperature. The drying unit made of wood with maximal capacity of 2 kg per tray. The recorded dryer temperature of Tray 1(bottom) until Tray 3 (top) reached 46, 50 and 64°C at 12pm.

Another indirect type natural convection solar dryer for fruits and vegetables had been developed by El-Sebaai et al. [58]. The solar air heater was made of painted matte black copper sheet covered with glass and sand as storage material. The chamber and black painted chimney made from wood and galvanized iron respectively. The experiment was conducted without storage (RUN1), with storage (RUN2) and chemically treatment material with storage (RUN3) for drying seedless grapes, apples and figs and green peas. They had found that the dryer is suitable for drying agricultural product since the average inlet drying chamber temperature was between 45.5°C and 55.5°C and the thermal storage caused further moisture loss at night.

Khalil et al. [59] designed and constructed a solar dryer for drying of fruits and vegetables. The system consists of three separated parts which were solar collector, drying cabinet and air blower which had been connected by a plastic pipes. Black painted galvanized steel containing (5%) black chromium powder had been used in collector to increase the absorbing capability. They had used V-corrugated collector

which tilted at 60 degree to increase the heat transfer area [60] and absorptivity to solar irradiation [61]. The air blower supplied 370 W powers to the system. The dryer had been tested to dry grape, apricots and beans at three different flow rates. The temperature recorded from grapes and apricots were 65°C and 60°C respectively. They had found that the most effective factor on the drying rate is the temperature of the air inside the cabinet and the effect variation of speed of air inside the drying cabinet can be neglected if it is small.

Based on the findings of the previous researches, it can be concluded that this type of dryer is suitable only for product that easily gets affected or deteriorated by drying temperature. However, indirect solar drying has several limitations. This dryer consumed a long period to complete the drying process in order to acquire a good quality product. Furthermore, a low drying process may result in low production. Summary of previous works on the indirect dryer design is given in Table 2.4.

Table 2.4: Summary of indirect dryer design conducted by previous researchers

Researchers	Thermal heating medium	Max dryer temperature recorded
Azad E. [55]	Black painted collector made from wooden insulated by polystern foam Black painted rocks	Tray 1(bottom): 55 °C Tray 2: 52 °C Tray 3(middle): 47 °C Tray 4: 43.5 °C Tray 5(top): 39 °C
Eissen et al. [56]	Transparent foil cover and a black absorber sheet	50°C
Dissa et al. [57]	Corrugated with porous iron absorber which made of an aluminum mesh	Tray 1(bottom): 46 °C Tray 2: 50 °C Tray 3(top): 64 °C
El-Sebaili et al. [58]	Black painted copper sheet solar air heater Sand as storage material	Average inlet drying chamber temperature: 45.5 °C – 55.5 °C
Khalil et al. [59]	Black painted galvanized steel containing (5%) black chromium powder	Grapes : 65°C Apricots : 60 °C

2.10.3 Mixed Mode Solar Dryer

A mixed mode solar dryer obtained the heat for drying from the combination of direct and indirect solar irradiation as shown in Figure 2.6. The dryer consist of transparent

wall cover to allow direct solar irradiation and solar collector to enhance air heating for faster drying process. Among the different types of natural convection solar dryers, the mixed-mode type has been demonstrated to be superior in the speed of drying [42-44].



Figure 2.6: Mixed mode solar dryer [62]

Simate [63] carried out optimization of mixed mode and indirect mode natural convection solar dryer and compared the performance. He found that under the same drying capacity of 90kg of maize, mixed mode dryer require a shorter collector length than indirect mode dryer which consequently save the cost of fabrication. Besides, the product in this dryer has more the more uniform moisture content distribution due to additional drying from direct irradiation.

Forson et al. [64] had developed a mixed mode natural convection solar dryer to dry cassava chips. The experiment was compared with the laboratory model to generate the required experimental data under controlled laboratory conditions. The result indicates that the rate of drying inside dryer is higher than room-air drying since it received direct and indirect heat. Furthermore, they had discovered that the drying process in this dryer took place even during the night.

Other studies on mixed mode solar dryer for preserving salt greengages had been conducted by Li et al. [65]. It consist three collectors with a total area of 6m², three fans powered by silica photovoltaic. The experiment had shortened the drying period of 60 kg greengages from 48 days under open sun to 15 days. The average temperature rise in chamber was 18 °C to 19°C. However, in order to obtain uniform drying, the samples were needed to exchange trays.

Bolaji and Olakusi [66] presented performance evaluation of mixed mode solar dryer. The dryer was design and constructed using locally sourced material to dry food. The no-loadexperiment result indicates that the highest temperature recorded in the dryer is in the mid-day. The maximum temperature recorded at solar collector and drying cabinet were 63°C and 65°C respectively. The no-loadexperiment result indicates that the hourly variation of the temperatures inside the cabinet and collector were higher than the ambient temperature during the most hours of the day-light. The dryer removed 85.4% moisture content of 6.2 kg yam chips in one day of 10 hours drying time. The dryer able to dry food items rapidly to a safe moisture level which ensures a superior quality of the dried product.

Singh et al. [52] had developed a low cost and multi-shelf portable solar dryer. The dryer was an integral, natural circulation and direct/indirect type. Multi-shelf design utilized the heated air across the trays and provides uniform drying in all trays due to the intermediate heating of air in between trays. The performance of dryer was tested by drying of fenugreek leaves. The maximum stagnation temperature was 75°C. They had identified that the thermal efficiency keeps reducing after several days of drying because it requires more energy to remove same quantity of product moisture. However, to overcome this problem, they had introduced a semi-continuous mode of drying for better drying efficiency on all drying days.

Based on the literature, it can be concluded that the mixed mode solar dryer provides more advantages compared to the other natural convection solar dryer. The drying time reduced since it received heat from two heat sources and consequently increases the production. Nevertheless, the drying process is totally depending on the presence of solar irradiation. The process will be interrupted especially during the cloudy and rainy day. Hence, the study on a biomass back up heater is necessary to

provide a continuous drying and shortens the drying time. Summary of previous works on the mixed mode is given in Table 2.5.

Table 2.5: Summary of mixed mode solar drying studies done by previous researchers

Researchers	Findings
Simate [63]	More uniform moisture content distribution
Forson et al. [64]	High rate of drying Drying process occurred even during the night
Li et al. [65]	Solar dryer functioned effectively by preventing regaining moisture
Bolaji and Olakusi [66]	Temperatures inside the cabinet and collector were higher than the ambient temperature on most hours of the day-light
Singh et al. [52]	Uniform drying in all trays Thermal efficiency keeps reducing after several days to dry same quantity of product moisture

2.11 Overview on the Supporting Elements of Solar Dryer

It is essential to consider the previous investigation and the findings pertaining the supporting elements to the solar dryer, which are the solar collector for indirect solar drying, the backup heater for the mixed mode solar drying.

2.11.1 Solar Collectors in the Solar Dryers

Solar collectors are normally designed together inside the dryer to increase the drying temperature inside solar dryer. The functions of solar collector are the same as heat exchangers where it transforms solar irradiation energy to internal energy of the transport medium [67]. The collectors absorb and supply heat to the product being dried through the flowing fluid such as air. The materials that are commonly used for solar collector plates are copper, aluminum, and stainless steel. The larger the area of solar collector thus the larger the heat being absorbs and transmitted. A corrugated metal sheet has a larger area than flat plat collector, hence it gives high performance. Among the factors that affecting amount of solar-energy absorbed by a solar-energy air heater are discussed below.

- The level of insulation.

High level of insulation produces a greater energy in solar collector. Different places may have different level of insulation and it also varies according to the time of the year. Hence, a proper size of solar collector in corresponding to the typical solar insulation is needed.

- The solar collector orientation.

The orientation of solar collector at site is ideally facing either North or South with the right slope. The inclination angle δ , the angle between the sun's direction and the equatorial plane is given by Equation 2.1 [68-70]

$$\delta = 23.45 \sin(360(284 + n) / 365) \quad (2.1)$$

where (n) is the day in the year which varies from n = 1 to n = 365.

The slope, β at solar noon of a particular day at site, can be calculated using Equation 2.2.

$$\beta = \delta + \phi \quad (2.2)$$

where (δ) is the angle of declination and (ϕ) is the latitude of the location.

Many researchers had defined varieties of collector orientation. According to Ghaba et al. [48], the solar energy received by a collector is at maximum if the inclination angle (i) of the solar collector with horizontal is such as: $(\phi - 10^\circ) \leq i \leq (\phi + 10^\circ)$. Duffie and Beckman [68] and Brewer et al. [71] stated that the collector tilt for maximum collection of incident solar irradiation for all year-round operation can be taken as the latitude of the site where it is located in practice. In addition, Kalogirau [72] had mentioned that the optimum tilt angle of the collector is equal to the latitude of the location with angle variations of 10-15 more or less depending on the application of the flat plate collector. Saleh and Badran [73] stated that perpendicular collector may gain a maximum energy of solar at all time along the day. However this technique requires an expensive tracking system. Based on Kalogirau [67], the flat plate collector slope angle can be calculated using Equation 2.3. In this

project, the design tilt angle (β_{opt}) to allow maximum collection of incident solar irradiation all year-round was taken as 10° .

$$\text{Collector slope angle} = \text{Latitude} + 5 \text{ to } 10^\circ \quad (2.3)$$

- The absorptance of the absorber surface.

The nature and colour of the coating on the incident angle determines the amount of solar energy absorbed by solar collector [67]. A low emissivity, good thermal conductivity and thermally stable during operation and stagnation are among the factors that influence the absorptance of irradiation. The transmittance of the cover material

A high transmittance cover material is the best material since it able to effectively trap the re-radiated heat from the absorber plate. Other factors that also influencing on the cover qualities are low heat absorptivity, stability at the operating and stagnation temperatures, resistance to breakage, durability under adverse weather conditions and low cost [74]. In drying industry, plastics are widely used as the cover material compared to glass mainly because the glass has high weight, low shatter resistance and require high cost. The properties of some cover materials are given in Appendix B.

2.11.2 Thermal Backup for Hybrid Drying

The purpose of burner as shown in Figure 2.7 is to compensate the solar energy during cloudy and rainy days and also to provide enough energy for full-scale drying operation at night as well for faster drying process. Biomass backup heater can be used as a supplement heat for faster drying [17]. The source of supplied heat from the burner is highly dependent on the types of material being dried such as food or biomass types. For biomass waste drying, direct heating is applied since the temperature is higher than indirect heating. For a good EFB quality, the supplied heat flue gas temperature range temperature should be known first to prevent over-drying.

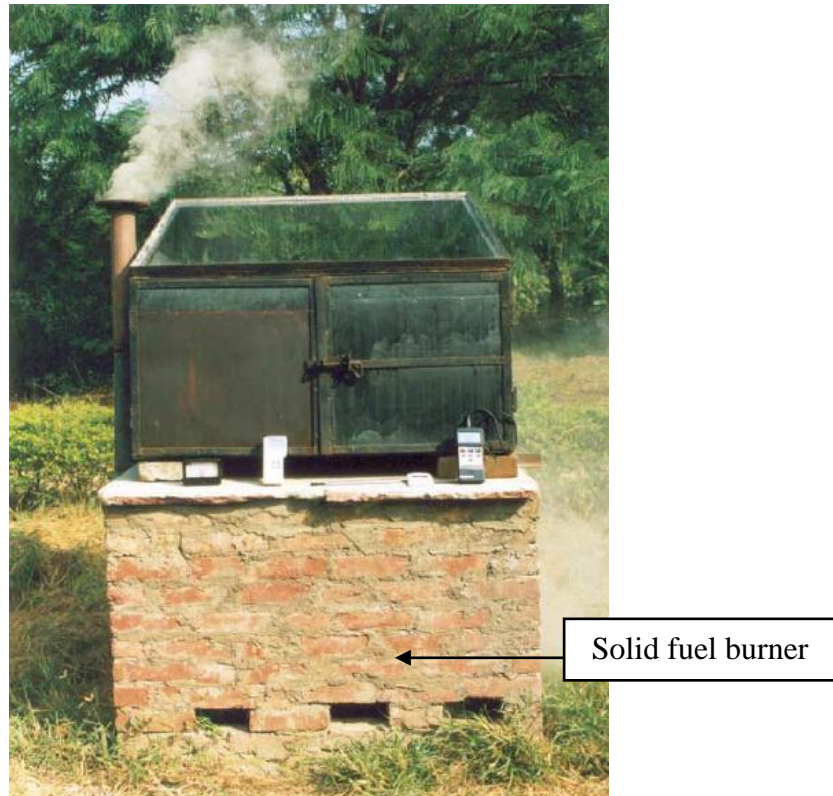


Figure 2.7: Hybrid dryer (a combination of thermal and solar drying method) [38]

The combustion product from complete combustion of biomass generally contains nitrogen, water vapor, carbon dioxide and surplus of oxygen. If there is a surplus of solid fuel due to incomplete combustion, the products of combustion are combustible gases like Carbon monoxide, CO, Hydrogen, H₂ and traces of Methane and non-useful products like tar and dust [75]. These combustible gases are not suitable for drying food application. The composition of the flue gases is reviewed in Table 2.6.

Table 2.6: Distribution of pyrolysis products for dry wood under combustion conditions [76]

<i>Product</i>	<i>Mass fraction</i>
H ₂ O	0.25
CO	0.183
CO ₂	0.115
H ₂	0.005
Light hydrocarbons	0.047
Tar	0.20
Char	0.20

Madhlopa and Ngwalo [12] designed a biomass backup heater (Refer Appendix C) which composed of drum, rectangular duct and flue gas chimney. The biomass burner which made from brick consists of rock pebbles as a thermal storage. The burner had been attached with 2.1m long gas chimney to increase the gas velocity and to prevent flue gas from entering drying chamber. It is able to operate 10 hours and 6 hours with door closed and open respectively and requires 8 kg of wood shaving per night. The rate of combustion had been controlled by opening or closing the door of biomass burner. The temperature inside the dryer had maintained at 41-56 °C.

Thanaraj et al. [15] designed and tested a furnace connected with a rotary solar hybrid dryer using paddy husk fuel at different feeding rate. The furnace consisted of a cylindrical shape heat exchanger using a 20 gauge metal sheet and a baffle to maximize the heat transfer. The wall was made from normal bricks, clay and cement. The steps were constructed from cast iron fire bars with 3.5cm gap at an angle of 45° to the horizontal. The temperature was controlled by adjusting the feeding rate of fuel to the furnace. They observed that the best feeding rate is 10 kg/hr with drying chamber temperature of 60°C.

A biomass stove which consists of a perforated tray grate and three metal baffle plates (Refer Appendix D) had been developed by Prasad and Vijay [38]. The brick chamber was surrounded by 13 rectangular holes for air inlet. Indirect heating was applied to protect the product from contamination by smoke, soot and ash of flue gases. The biomass stove had been located at the bottom of drying chamber with a rock slab in between to avoid the excessive temperature and also functioned as a thermal storage. The temperature had been controlled by modulating the air inlet and combustion rate of the biomass burner. They used 6 kg of charcoal and observed that the rock slab resulted in uniform drying inside the drying chamber. The temperature recorded at the bottom tray was 59.5°C.

The same drying system arrangement also had been reported by Tarigan and Tekasakul [18]. The biomass burner (Refer Appendix E) had been constructed from concrete wall and surrounded with a thermal storage which made from brick. The air inlet located at the bottom edge of burner to support the fuel combustion. The bricks separated the clean warm air from the fuel gas and maximized the heat stored from

burning fuel. The chimney was attached at the upper edge to gain heat from exhaust gas and smoke where it will heat up the internal wall and consequently heat the trays. They had utilized 50 kg wood per night and temperature recorded in drying chamber was 65°C. However, high temperature was recorded near the heat storage, around 93°C since it was in contact with top surface bricks. Large piece of fuel wood enabled the fire to burn more slowly and can last longer time.

Bena and Fuller [17] developed a biomass back-up heater (Refer Appendix F). The baffle was located inside the burner to give time for complete combustion and to lengthen the heat path. The burner was added with adjustable air inlet valve to control combustion. A thermal storage made from a layer of concrete located in between the dryer and burner. Approximately 9 kg of fuel wood per night had been burnt and the resulted temperature inside the dryer maintained below 65°C. This temperature is the maximum drying temperature for most fruits. They had tested and found that the combustion of large fuel pieces last longer than small pieces fuel. The combustion able to sustain up to 5 hours and dryer temperature maintained ~10°C above the ambient air and consequently prevented the re-absorption of moisture.

A biomass stove-heat exchanger insulated with castable refractory mortar (Refer Appendix G) had been designed by Mastekbayeva et al. [19]. The biomass burner consisted of a cross-flow shell and tube heat exchanger. The heat exchanger was insulated with rock wool and clad with aluminum sheet to reduce thermal losses. DC fans were located near the heat exchanger to facilitate the air. They used 6 kg of rice husk briquettes and found that the heat last for 2 hours. The maximum recorded temperature was 50.9°C and it quite uniform until the end of combustion.

Serafica and del Mundo [11] designed a biomass gasifier stove connected with of hybrid solar dryer for fish drying (Refer Appendix H). It had been constructed from galvanized iron sheet and composed of fuel hopper, reactor, primary air inlet, combustion chamber and hood connector. The biomass gasifier consists of shell and fin heat exchanger configuration. Coconut shells had been used as a fuel .The heat delivery and combustion rate were controlled by using a butterfly valve at the primary air inlet. The hot air temperature was about 60 to 70°C.

Bhattacharya et al. [13] had also designed a gasifier stove for fruits and vegetables drying (Refer Appendix I). The gasifier stove consisted of fuel storage hopper, reaction chamber, primary air inlet and combustion chamber. Wood chips were used as fuel of the gasifier-stove. They had installed a thermostat and set the permissible temperature of fruits and vegetable drying at 70°C inside the drying chamber to control the closing and opening of a butterfly valve at the inlet of the gasifier stove.

Fuller et al. [77] had designed a low cost wood burner which made from steel drum (Refer Appendix J). The burner was enclosed with brick chamber and consists of grate to support the solid fuel, a metal baffle to lengthen the exhaust gas flow, concrete top to prevent excessive swings and valve to control the air supply. The experiment was conducted with five kilogram of fuel wood and kindling had been used to initialize combustion. They had identified almost third of the energy available in the wood was lost in the flue gases. A lightweight insulated structure is expected to reduce the heat losses. Summary of previous works on the biomass burner as a backup heater of solar dryer is given in Table 2.7.

Table 2.7: Summary on the usage of biomass burner as a backup heater of solar dryer by previous researchers

Researchers	Biomass Burner Design	Type of fuel	Max dryer temperature recorded
Madhlopa and Ngwalo [12]	Drum, rectangular duct and flue gas chimney	Wood shaving	41-56 °C
Thanaraj et al. [15]	Furnace consist of cylindrical shape heat exchanger made from metal sheet and a baffle	Paddy husk	60°C
Prasad and Vijay [38]	Stove with perforated tray grate and three metal baffle plates	Charcoal	59.5°C
Tarigan and Tekasakul [18]	Concrete burner with brick thermal storage	Wood	65°C
Bena and Fuller [17]	Burner consists of baffle and concrete layer thermal storage	Wood	Maintained below 65°C
Mastekbayeva et al. [19]	Burner consists of a cross-flow shell and tube heat exchanger	Rice husk briquettes	50.9°C
Serafica and del Mundo [11]	Gasifier stove consists of shell and fin heat exchanger	Coconut shells	60 to 70°C
Bhattacharya et al. [13]	Gasifier stove which installed with thermostat	Wood chips	Permissible temperature 70°C
Fuller et al. [77]	Wood burner made from steel drum	Wood	-

2.12 Overview of Gas to Gas Heat Exchanger Design

The larger the area of both fluid sides, the greater the performance of heat exchanger and it can be done by adding the secondary surfaces which is fins. Wang et al. [78] experimentally studied the strip fin heat exchanger with 3 different densities. They had found that the pressure gradient and heat transfer coefficient increases with fin density. Besides, the pressure gradient increases faster than heat transfer coefficient as velocity increase. He had also listed other factors that influence performance of heat exchanger are geometrical dimension, components characteristics under cycling temperatures and pressures, the surfaces coating layer and thermal conductivity of material used.

The physical process of a clamshell heat exchanger commonly used in residential gas fired furnace had been studied by Lei Fang [79]. The clamshell was created by joining two steel panels containing half channel. The furnace heat exchanger which made from aluminized steel separates the high temperature flue gas stream from the low temperature circulating air stream while at the same time transferring thermal energy from the former to the latter. He had found that the density increases and volumetric flow rate decreases as the flue gas is cooled while travel downstream. Besides, the dimples in heat exchanger caused large pressure drop without enhancing heat transfer. After removing the dimples, the result indicates better performance on both pressure drop and heat transfer.

Tomimura et al. [80] worked out experimentally on a multi layered type of gas to gas heat exchanger using porous media. According to them, multi layered type of heat exchanger had higher overall heat transfer coefficients than conventional heat exchanger and also exhibit excellent reaction characteristics as a steam reformer. A large temperature drop and large amount of converted radiant energy can be created by using porous metal plate with high porosity material [81]. Based on their results, the enthalpy of the high temperature gas was effectively transferred to the porous metal plate through extremely high heat transfer coefficient between the flowing gas and the porous plate. The designed model had low pressure loss in piping and simpler for layer extension structure.

Al-Omari [82] tested and studied the combustion and heat transfer characteristics in a biomass furnace. Date stones and palm trees stalks had been used as the fuel. The experimental work was done with different fuel feed conditions and combustion flow rates. He had used a digital weighing scale to monitor and record the fuel mass in the bed during the combustion process. LPG combustion was found to be more convenient and effective to initiate the combustion around the 2 to 3 minutes which is stabilized and guided by means of conical bluff body. He concluded that the heat transfer is depending on the feeding rate. High flow rates will enhance the rate occurred in bed and the furnace.

Table 2.8: Summary of the studies on gas-to-gas heat exchanger by previous researchers

Researchers	Heat Exchanger Design	Findings
Wang et al. [78]	Strip fin heat exchanger	Pressure gradient and heat transfer coefficient increases with fin density. Geometrical dimension, components characteristics under cycling temperatures and pressures, the surfaces coating layer and thermal conductivity of material used
Lei Fang [79]	Clamshell heat exchanger	Density increases and volumetric flow rate decreases as the flue gas is cooled
Tomimura et al. [80]	Multi layered gas to gas heat exchanger using porous media	Temperatures inside the cabinet and collector were higher than the ambient temperature on most hours of the day-light
Al-Omari [82]	Conical bluff body	Heat transfer is depending on the feeding rate
Kevin [83]	Shell-and-tube exchanger	Excess pressure drop capacity, the re-evaluation of fouling factors, the use of augmented surfaces and enhanced heat transfer

Kevin [83] had conducted studies on shell-and-tube exchanger. He stated that heat exchanger enhancement can be divided into both passive and active methods. Passive methods include extended surfaces, inserts, coiled or twisted tubes, surface treatments, and additives. Active techniques include surface vibration, electrostatic fields, injection, and suction. He had concluded that to increase heat exchanger performances, first to ensure it is performing correctly in the beginning, excess pressure drop capacity, the re-evaluation of fouling factors and their effect on

exchanger calculations, and the use of augmented surfaces and enhanced heat transfer. Table 2.8 summarizes the findings of previous researches on the G-to-G HEXs.

2.13 Chapter Summary

Based on the studies of the previous works on the drying techniques, it could be concluded that many types of solar dryer had been developed and evolved from traditional drying method. The dryer performance is different according to design criteria and drying method. The appropriate drying temperature of most tropical food products is 40°-70°C. Direct exposure open sun causes lower all-trans- α - and β -carotene and 9-cis-carotene contents of vegetables. Hence, direct sun is not recommended for food drying. A mixed mode type of solar dryer had shown to be superior in the speed of drying compared to other different types of natural convection solar dryers.

The limitation of each type of solar dryer had been identified. The combination of solar dryer with a thermal backup heater had shown to provide heat continuously for drying application without interruption. The usage of the gas to gas heat exchanger (G-to-G HEX) is crucial to make sure that the gas that will be used for food drying application is clean, free from smoke, soot and ash in order to protect the food from being contaminated. It is important to maintain the quality of dried products in terms of cleanliness, color and taste. In addition, the usage of the flue gases from diesel fired drum dryer causing over drying and produced low quality EFB as fuel. The final moisture content of dried EFB is less than 13%.

As a conclusion from the literature, it was found that there was no technology combining the direct solar, the indirect solar, the clean warm air and the hot flue gases in single drying unit. The present project will be aim to investigate such hybrid dryer for different types of materials.

CHAPTER 3 METHODOLOGY AND DESIGN APPROACH

3.1 Chapter Overview

This chapter presents methodology of this study, and it can be considered as introductory chapter for model development. The conceptual design and mathematical formulation which are involved throughout the designing process of the system are clarified. The drying system consists of two units which are solar dryer unit and thermal backup. Detailed design procedures and material selection for the model construction unit are discussed. The solution procedures had been solved using mathematical model formulation MATLAB[®] and Excel.

3.2 Operational Principles of the Mixed Mode and Hybrid Solar Dryer

A mixed mode solar dryer configuration was proposed and investigated by previous researchers. According to Simate [63], this dryer performs greater drying rate since it received heat from both direct and indirect solar irradiation and suitable to be applied in tropical humid areas where climatic conditions favor sun drying of agricultural products [84]. Generally, hybrid solar dryer operates with solar irradiation as the main source of energy and a backup heater as auxiliary source when there is inadequate irradiation especially during the cloudy days or at night. In such case, continuous drying is possible. It also can be applied to extend the period of drying beyond sunshine hours.

In the present developed system, when the dryer is operated under solar, some of the heat from direct solar irradiation enters through the transparent cover and being absorbed by crops and the corrugated black painted Aluminum solar collector. The heated surfaces warm the surrounding air, which rises by natural convection, passing

through the drying trays and picking up the moisture. The moisture finally exits the dryer through the chimney on the upper side. These processes reduce the pressure inside the solar dryer and consequently draw the ambient air through the inlet holes at the side of solar dryer. A continuous flow of air inside the solar dryer is thus established. The developed system is designed with options to dry food or solid waste. The flow of drying process of hybrid drying is shown in Figure 3.1.

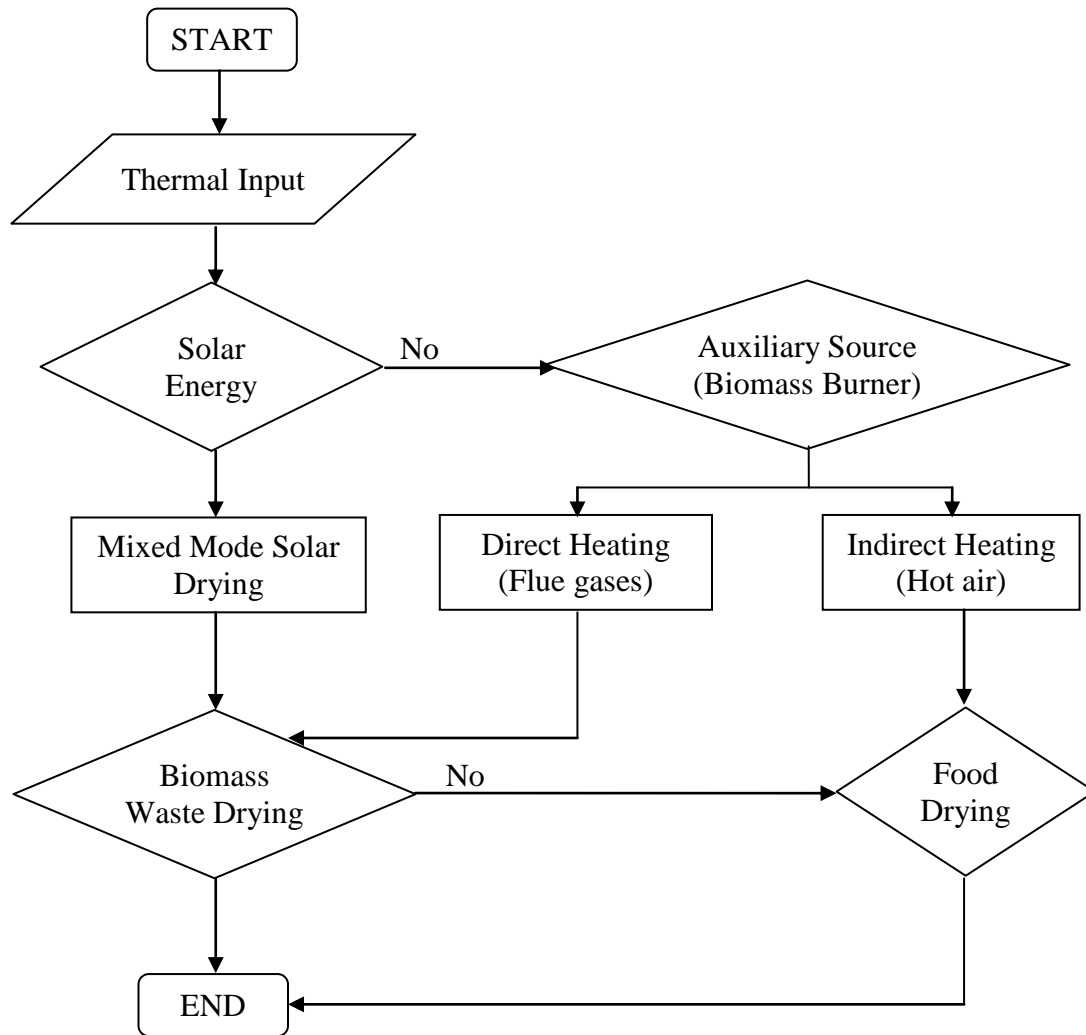


Figure 3.1: The drying flow of hybrid solar dryer with biomass backup.

During periods of low or zero solar irradiation, the backup heater is applied. The heat supplied from backup unit is highly depending on the type of product to be dried. In order to dry food, a heat exchanger has been used to separate the flue gas from the clean warm air therefore the food is protected from contamination by the smoke, soot and ash. Waste drying product does not require any specific temperature limit and

quality control, thus the heat from direct fuel can be used as the source of heat. The warm air rises up into the drying chamber, evaporating and picking up crop moisture as it passes through the trays, and then escapes through the top vents as before. The maximum allowable temperature in the drying chamber either under solar or backup heat is between 50 to 65°C.

3.3 Geometrical Design Procedure of the Dryer

The conceptual design, material selection and design calculation of solar dryer is described in detail. The aims of dryer construction are on the uses of simple materials, tools and skills.

3.3.1 Conceptual Design

Design process is important in order to enable the specified properties of the product to be obtained. Several methods and designs of solar dryer reported previously were taken into consideration glass roof solar dryer [51] , solar dryer with natural ventilation [56] and solar cabinet dryer [45]. The design of the dryer was separated into several features.

3.3.1.1 Solar Collector

The function of solar collector is to absorb the heat from the incoming solar irradiation. The total of heat absorb is depending on the material thermal conductivity and the surface area. The top surfaces of the collector were concentric and inclined at an angle of 10° and painted black to maximize the capture of solar irradiation. Besides, it had a corrugated surface which provides large area which consequently increased the total of heat absorbed.

3.3.1.2 Body

The roof was designed with a slope to ensure that the evaporated water can easily flow contact with the roof surface toward the chimney. Both sides of the roof were

elongate to prevent rain or outside water drop from entering the airflow holes as shown in Figure 3.2. Small holes were made at the bottom side wall of the dryer for air inlet. A door was located at the front side of the dryer to ease the process of positioning the product.

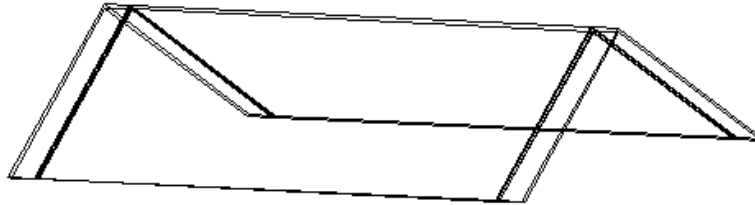


Figure 3.2: Sketching of the roof

3.3.1.3 Floor

The floor was attached together with the solar collector. It was designed with a certain slope to prevent water accumulation. Four holes, two in each side were made at the floor side walls for biomass burner connection. The holes were design at the bottom of the collector to guarantee distribution of the heat inside the dryer. The heat flow is the same as when using solar even thought biomass source being used. A thin Aluminum plate supporter was screwed around the border of solar dryer to increase the stability of the model. The sketch of the floor is shown in Figure 3.3.

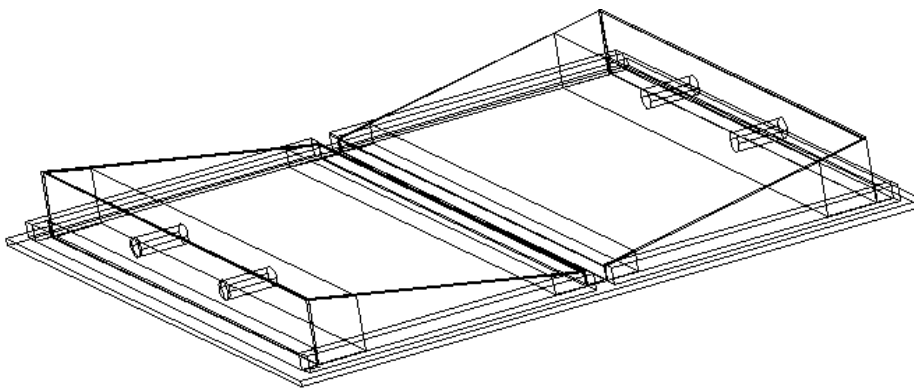


Figure 3.3: Sketching of the floor

3.3.1.4 Racks

The solar dryer consists of five racks which are located inside the drying chamber. The racks have an alternate rectangular hole in the middle to allow the warm air circulation as shown in Figure 3.4. The rectangular holes were covered with wire mesh to prevent the crops from dropping throughout the rectangular hole. The usage of wire mesh was to allow the heated air to flow from the bottom through the top part of the solar dryer.

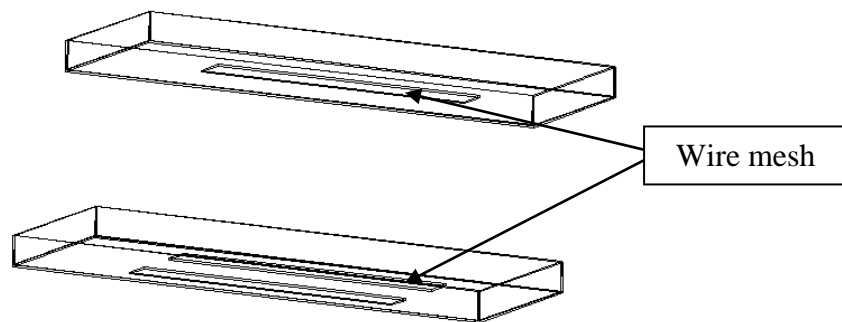


Figure 3.4: Sketching of the racks

3.3.2 Dryer Material Selection

In the material selection, basic requirement such as functional requirements, process ability requirements, cost, reliability and resistance to service conditions must be met.

3.3.2.1 Solar Collector

Solar collector plate is the main contribution to the heat transfer process. The material should have high thermal conductivity, adequate strength and good corrosion resistance. According to Table 3.1, copper is generally preferred because of its high thermal conductivity and resistance to corrosion. However, due to market availability and economic concern, aluminum is chosen for this project. A corrugated Aluminum surface had been used instead of flat surface since it provides larger area.

Table 3.1: Thermo-physical properties of candidate metals used for collector plate.

Reproduced from [85]

Material	Density (kg/m ³)	Specific heat (J/kg·K)	Thermal Conductivity (W/m·K)
Aluminum	2719	871	202.4
Copper	8954	383	386
Zinc (pure)	7144	384	112
Brass (70/30)	8522	385	111
Steel	7833	465	54

3.3.2.2 Selective Coatings

The nature and color of the coating on the incident angle determines the amount of solar energy absorbed by solar collector [67]. A low emissivity, good thermal conductivity and thermally stability during operation and stagnation are among the factors that influence the absorptance of irradiation. The properties of common absorber materials are shown in Table 3.2. The black matte paint was selected for the coating of the absorber faces, since it is locally available and cheap compared to black Nickel or black Chrome plating.

Table 3.2: Properties of absorber materials. Reproduced from [86]

Coating	Substrate	Absorptivity, α	Emissivity, ε	Maximum temp.	Durabil ity
Black nickel	Iron, copper, zinc/aluminium	0.85±0.96	0.05±0.15	288°C	Medium
Black chrome	Nickel/aluminium copper, iron	0.82±0.96	0.04±0.15	427°C	Very good
Black copper	Copper	0.85±0.95	0.10±0.15	316°C	-
Copper oxide	Copper, iron, aluminium	0.87±0.90	0.08±0.16	-	-
Anodic aluminium	Aluminium	0.90±0.96	0.10±0.23	-	-
Metal carbide	Copper, glass	0.82±0.93	0.02±0.05	-	-
PbS paint	Any	0.90	0.30	-	-
Selective paint (coralur)	Most	0.93	0.30	-	-
Black paint	Any	0.95±0.97	0.95±0.97	-	-

3.3.2.3 Cover Materials

The characteristic of the cover plate has to be able to transmit maximum solar energy to the absorbing plate, minimize heat loss from the absorbing plate to environment and to shield the absorber plate. Thermal and optical properties of some of the cover plate materials are listed in Table 3.3. The transmittance of glass depends on its iron content, which means lower the iron content has higher transmittance for solar irradiation. Tempered glass is the most common cover material for solar collectors due to high durability and stability when exposed to UV irradiation and also has higher reduction on irradiation.

Transparent plastic material such as acrylic polycarbonate plastic, plastic films of Tedlar and Mylar and commercial plastic such as Perspex and Lexan may also used for cover plate. In terms of performance, it is less effective in reducing radiated heat losses from the absorbing plate and cannot withstand the stagnant temperatures encountered in hot environment. However, the main advantages of plastic materials are the cost, light weight and resistance to breakage. Perspex had been selected as the wall of the designed model since it is easier to find and fabricate.

Table 3.3: Thermal and optical properties of cover plate materials.

Reproduced from [85]

Material	Index of refraction	Density (kg/m ³)	Specific heat (J/kg·K)	Thermal capacity (W·hr/m ² ·K)
Glass	1.518	2489	754	1.659
Fiberglass reinforced polyester	1.540	1399	1465	3.61
Acrylic (Plexiglass)	1.490	1189	1465	1.534
Polyester (Mylar)	1.640	1394	1046	0.051
Polytetrafluoroethylene (Teflon)	1.343	2148	1172	0.036
Polyvinyl Fluoride (Tedlar)	1.460	1379	1256	0.049
Polycarbonate (Lexan)	1.586	1199	1193	1.260

3.3.3 Design Calculation

The design of solar dryer was focusing on the estimation of solar collector area. The steps began with the setting on parameter assumption of boundary condition and a

mathematical calculation. The presented design calculation was based on drying of 2.5 kg palm fiber (EFB) basis.

3.3.3.1 Design Parameters

The selection of the design parameters was based on the studies of solar drying and biomass backup heater design journal. The dryer was assumed to have near collector air temperature, T_1 around 55°C at surrounding temperature, T_{amb} of 30°C. The drying chamber temperature, T_{cham} is around 50 to 65°C. The selected temperature is suitable for drying all types of product and able to inactivate the growth of microorganism. The assumed outlet dryer temperature, T_{od} is 35°C, it is slightly low since it contains the picked up moisture content. The parameter assumption of solar dryer is shown in Figure 3.5 and Table 3.4.

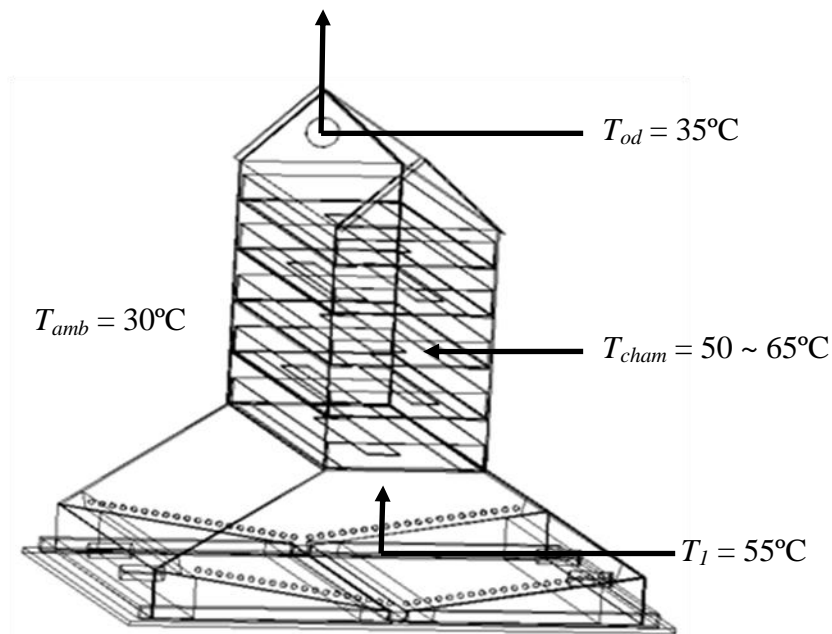


Figure 3.5: The parameter assumption of solar dryer

Table 3.4: Boundary conditions as used in the design

No.	Items	Value
1	Mass of product, m_p	2.5 kg
2	Initial moisture content, M_i	75% w.b [31]
3	Final moisture content, M_f	6% w.b [31]
4	Near collector air temperature, T_1	55°C
5	Relative humidity of air near collector, RH_1	25%
6	Maximum allowable temperature, T_{cham}	65°C
7	Relative humidity inside chamber, RH_2	45%
8	Temperature difference, $\Delta T_d = T_{cham} - T_1$	10°C
9	Total solar irradiation, ΣI	17-21 MJ/m ² daily
10	Collector efficiency, η_c	30% [87]

3.3.3.2 Mathematical Modeling

The estimation of the collector area was based on the procedures described by Ampratwum [87] for drying dates (a cabinet type), Basunia and Abe [88] for drying rough rice, and Ayensu [29] for drying of crops (convective solar dryer). More recently El-Amin Omda *et al.* [89] had applied all those mathematical models that are generally used by previous researchers in designing the solar dryer for drying mango slices (a box type).

The mass of water evaporated, m_w in kg is calculated from Equation 3.1

$$m_w = m_{pi}(M_i - M_f)/(100 - M_f) \quad (3.1)$$

The average drying rate, m_{dr} in kg H₂O/hr is determined from the mass of moisture to be removed and drying time, t_d in Equation 3.2.

$$m_{dr} = m_w / t_d \quad (3.2)$$

The mass flow rate of air needed for drying, \dot{m}_{ad} is calculated by using Equation 3.3 given by Sodha *et al.* (1987) [90].

$$\dot{m}_{ad} = m_{dr} / (w_f - w_i) \quad (3.3)$$

The total useful energy, E received by the drying air in kJ is given by Equation 3.4.

$$E = \dot{m}_{ad}(h_f - h_i)t_d \quad (3.4)$$

Considering a safety factor of 1.4, the area of the solar collector, A_c , in m² is calculated using Equation 3.5.

$$A_c = 1.4(E/\Sigma I\eta_c) \quad (3.5)$$

where:

ΣI = the total global irradiation on the horizontal surface in kJ/m^2

η_c = the collector efficiency, 30% [87]

The air pressure difference, ΔP in Pa across the drying bed is taken by the density difference between the air near collector, T_1 and the ambient air, T_{amb} in $^\circ\text{C}$ as determined by Equation 3.6. The pressure head, H (height of the hot air column from the base of the dryer to the point of air discharge from the dryer) is in m and the acceleration due gravity, g value is 9.81 m/s^2 .

$$\Delta P = 0.00308g(T_1 - T_{amb})H \quad (3.6)$$

The quantity of heat required for drying, Q_d in Watt to evaporate the H_2O is calculated from mass of water evaporated and the latent heat of evaporation, as shown in Equation 3.7.

$$Q_d = (m_w \times h_{fg})/t_d \quad (3.7)$$

The volumetric flow rate, \dot{V}_a is calculated based on the heat required, Q_d by using Equation 3.8.

$$\dot{V}_a = \frac{Q_d}{\rho_{air} \times c_p \times \Delta T_d \times t_d} \quad (3.8)$$

3.3.3.3 Values of design parameters

The optimum tilt angle of the collector could be taken as the sum of the latitude of the location with angle variations of $10\text{-}15^\circ$ more depending on the application [67]. In this design, (β_{opt}) to allow maximum collection of incident solar irradiation all year-round was taken as 10° . The area of the solar collector is highly dependent on the weight and the initial and final moisture content of the product to be dried. The estimated value of the collector area was 1.17m^2 . The results of design calculations and the schematic picture of solar dryer with full dimension are shown in Table 3.5 and Figure 3.6 respectively. The fabricated solar collector was 1.23m^2 which agreed to the design calculation since it was within the range of estimated design.

Table 3.5: Design calculation results

Eq.	Items	Value
3.1	Mass of water evaporated, m_w	1.88 kg
3.2	Average drying rate, m_{dr}	0.23 kg·H ₂ O/hr
3.3	Mass flow rate of air for drying, \dot{m}_{ad}	3.66 kg dry air/hr
3.4	Total useful energy, E	5.39 MJ
3.5	Solar collector area with S.F of 1.4, A_c	1.17 ~ 1.23 m ²
3.6	Air pressure difference, ΔP	0.26 Pa
3.7	Quantity of heat required for drying, Q_d	154 Watt
3.8	Volumetric flow rate of air, \dot{V}_a	23.01 m ³ /hr

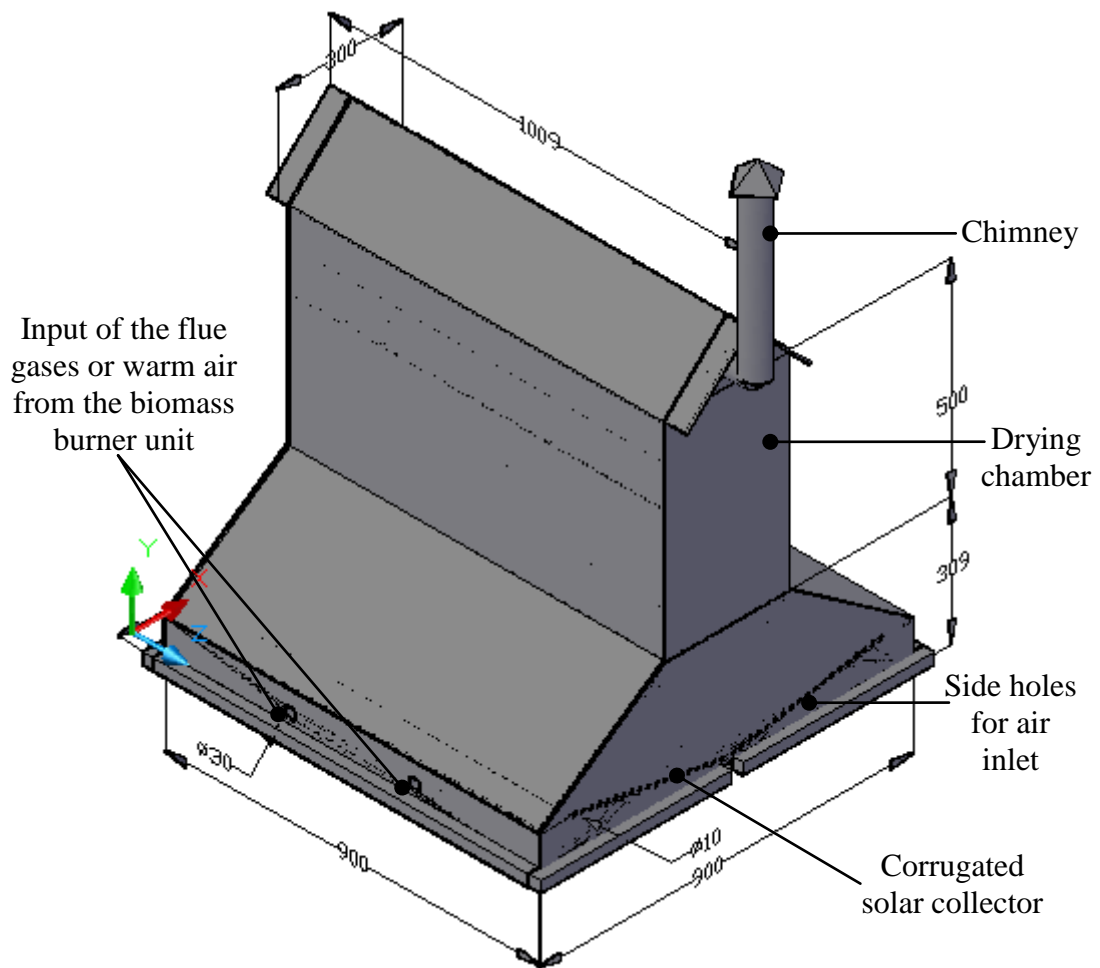


Figure 3.6: Schematic of solar dryer with full dimensions (in mm)

3.4 Design of the Thermal Backup Unit (TBU)

As for any other solar system, there is a lack in availability of the solar irradiation for continuous operation. The application of the mixed mode solar dryer is limited only on

a sunny day. To overcome this problem, a thermal backup is applied especially during inadequate irradiation and at night therefore a continuous drying is possible. Besides, it can be applied to extend the period of drying beyond sunshine hours. A biomass burner was proposed to supply heat for solid waste (biomass) and food drying application. Therefore the TBU was designed to supply two types of thermal medium which are hot clean air (indirect heating) and flue gases (direct heating).

The main purposes of using G-to-G HEX is to separate the clean warm air from the flue gas. In burner, the biomass fuel combustion heated the wall of the G-to-G HEX and allowed the transmission of the heat to the ambient air, resulting in temperature raise. The process produces a heated clean air for food drying application. The G-to-G HEX would be uniquely used in the present project as supporting element for multi-function solar dryer.

The mode of heat supply from the TBU to the dryer is dependent on the type of product to be dried. The combustion of biomass fuels is almost the same as any other hydrocarbon combustion which will create poisonous gases that is harmful to human and surely not suitable for drying food application. So the usage of the G-to-G HEX is crucial to ensure that the gas that will be used for food drying application is not poisonous and clean. The G-to-G HEX was designed as part of the TBU. It was representing parallel flow heat exchanger with extended surfaces (fins) to enhance the process of heat transfer. The process of heat supply from TBU to the dryer is shown in Figure 3.7.

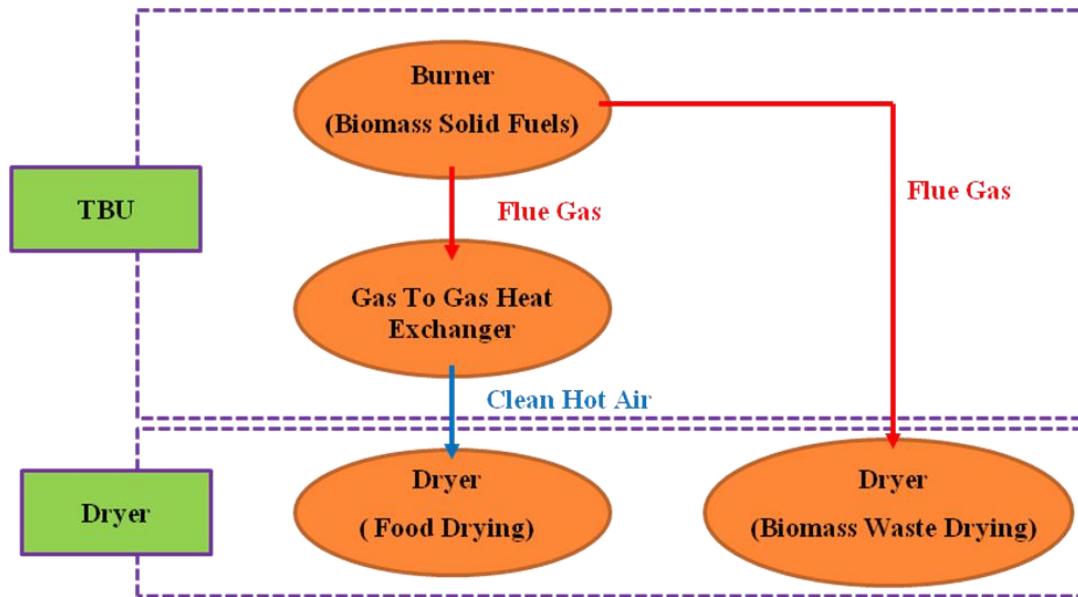


Figure 3.7: The process of heat supply flow diagram

3.4.1 Conceptual Design of the TBU

The unit consists of two main zones. The lower zone is for the solid biomass combustion. The upper part is the G-to-G HEX. The upper part has a cylindrical shape comprises two zones; inner cylindrical hot zone and outer annulus cold zone. The features are described in more details as below.

3.4.1.1 Gas-to-gas heat exchanger (G-to-G HEX)

The heat exchanger should have a high heat transfer coefficient. Larger area of heat exchanger may produce more heat. Hence eight rectangular plate fins was built together surround the heat exchanger to increase the surface area and to enhance the heat transfer. The thickness of the fins is neglected since it is considered as a thin plate. The proposed design configuration of the heat exchanger is shown in Figure 3.8.

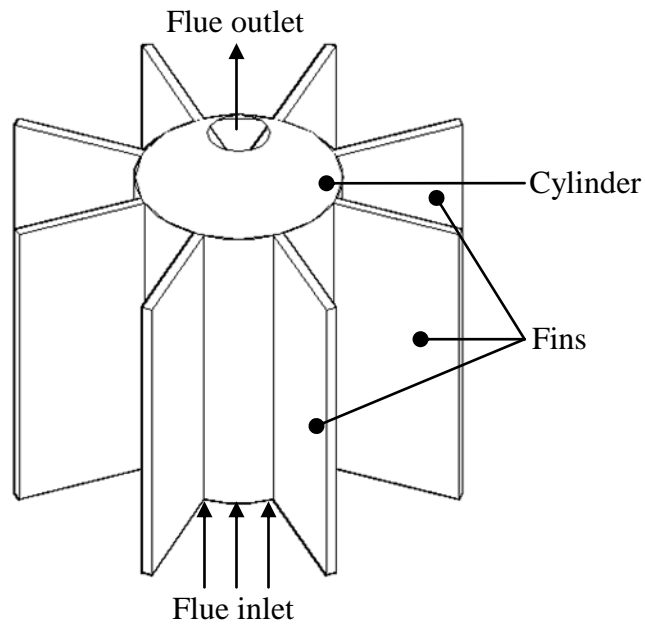


Figure 3.8: The gas-to-gas heat exchanger design and its component

The G-to-G HEX wall will be heated by hot flue of fuel combustion and the transfer of the heat to the ambient air will increase its temperature and consequently produce a heated clean air which is also known as indirect heat for food drying application. No specific clarity for drying of waste product, therefore the direct heat from flue gas is to be applied as the source of heat. The flow path of the heat is shown in Figure 3.9.

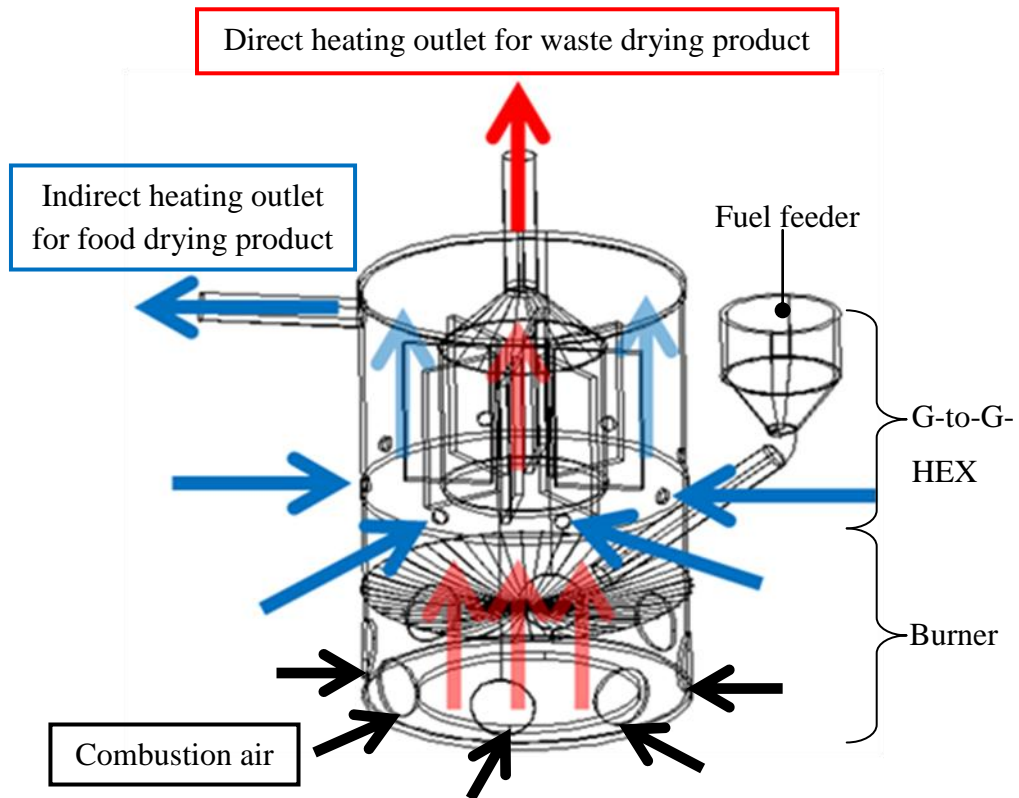


Figure 3.9: The flow path of the heat inside the biomass burner

3.4.1.2 Body of Burner

Heat loss may affect the efficiency of the TBU. In order to prevent the heat loss from the burner to the environment and to maximize the heat supply to the dryer, the body of the biomass burner was insulated with double layers of insulator. Wool and aluminum sheet were covered surround the outer body of the burner.

3.4.1.3 Chimney

Since shorter chimney affects the air flow rate and drying rate of material, the chimney was installed with height of 1.5 m and diameter of 63.5 mm. High chimney may enhance a buoyancy force and able to increase the velocity of the air inside the burner in addition to provide proper channel for the outlet gases. The ‘chimney effect’ creates proper ventilation without using a ventilator.

3.4.2 Material Selection

Heat exchanger has a function as a major of heat transfer surface, and also as a barrier to prevent flue gas to mix with the clean ambient air. Since the burner will experience a high combustion temperature, the selected material must have a good characteristic in the required criteria, which are melting point, corrosive, assembly easiness, thermal conductivity, and price.

3.4.2.1 Gas-to-gas heat exchanger

Five types of material are considered reliable for the process. Table 3.6 signifies the decision matrix leading to the final choice. All the materials are rating between 0 and 5 to each cell of the table, bound to the influence of the corresponding. Based on the material selection, stainless alloy with thermal conductivity, k of 14.9 W/m was chosen since it scored evaluation. Even though the thermal conductivity is low, this material able to sustain high combustion temperature, easy to fabricate and excellent for joining (welding).

Table 3.6: Decision Matrix Table of Gas-to-gas Heat Exchanger

	A	B	C	D	E	Total
Pure Copper	5	3	2	5	3	18
Low carbon steel (AISI 1010)	4	3	5	2	4	18
Aluminum	4	4	3	3	2	17
Stainless alloy (AISI 304)	4	5	5	2	4	20
Titanium	5	5	3	2	1	16

Criteria : **A**: Melting point; **B**:Corrosive; **C**:Assembly easiness;

D:Thermal conductivity; **E**:Price

Choice : **1**:very bad; **2**:medium; **3**:good; **4**:very good; **5**:perfect

3.4.2.2 Burner body

The biomass burner body was made from galvanized iron. Galvanized iron has a good fire resistance characteristic which can sustain up to 1500° C. Galvanized iron also having fair corrosion resistance and it is very excellent for shape forming especially welding.

3.4.3 Design Calculation

The TBU design was emphasized on the G-to-G HEX. The design of heat exchanger was based on the studies of convection-conduction heat transfer. The scope was related to the design criteria, material and the effectiveness of the biomass burner with gas-to-gas heat exchanger.

3.4.3.1 Boundary Conditions

During the combustion, the flue gas flowed up through the inner passage, and the ambient air flowed up the outer zone. The thermal process was similar with the process undergone in parallel double pipe heat exchanger. Previous measurements have shown that the inlet flue temperature, T_{fi} is around 320°C with velocity of flue, V_f of 0.5m/s. The flue moved up within the inner cylindrical passage by natural draft assisted by a chimney. During its up flow, the hot flue exchanges heat with air via the wall of the inner pipe and the extended surfaces. Eight holes with 25.4 mm drilled on the outer surface to permit ambient air to flow to the outer zone of the G-to-G HEX. The air enters to the annulus outer zone of the heat exchanger at ambient temperature, $T_{amb} \sim 30^\circ\text{C}$ and moves up due to buoyancy effect assisted by a chimney. The estimated temperature of hot air outlet from the G-to-G HEX, T_{ao} is around 80°C. This temperature had been selected after considering the heat losses through the tube connection between burner and dryer. In fact, the required temperature in the dryer is around 50-65°C. The overall cross sectional unit design and boundary conditions is shown in Figure 3.10.

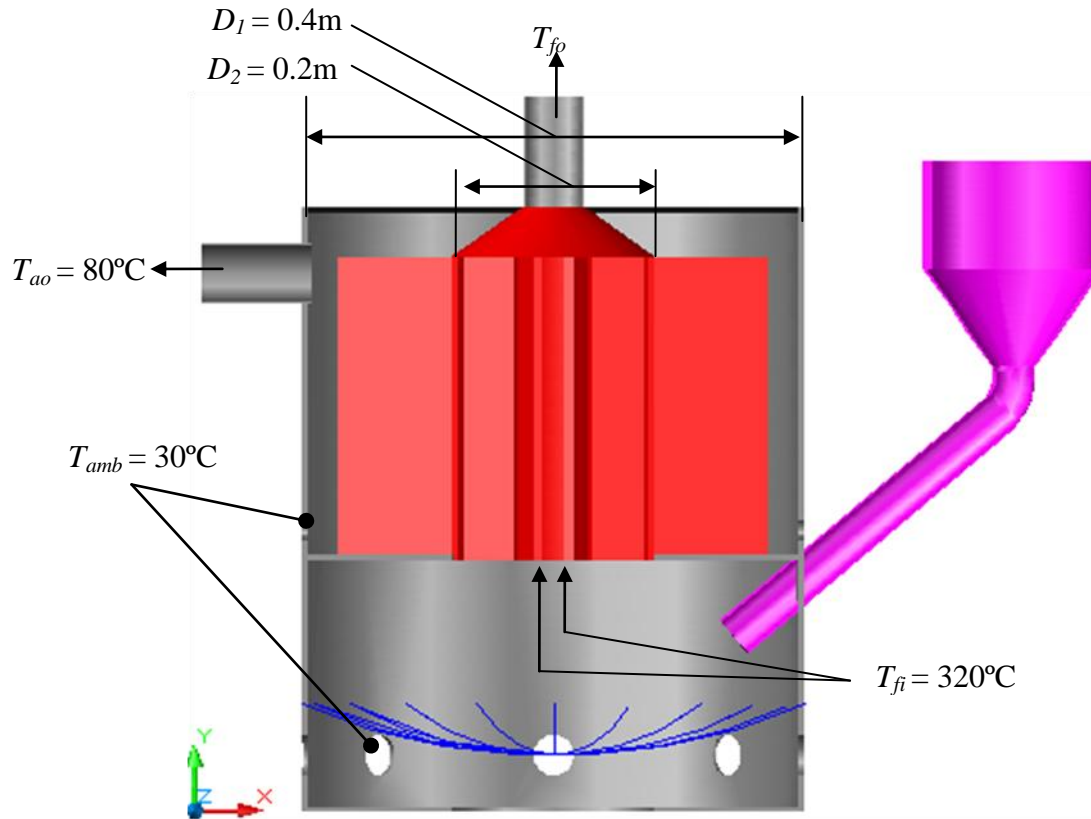


Figure 3.10: The overall cross sectional unit design and boundary conditions (unit shown are not in scale)

3.4.3.2 Mathematical Modeling

The TBU was designed based on the calculated heat needed for the drying process. Only internal flow was considered and fins thickness could be neglected. The heat required for drying, Q_d is obtained from the dryer design. It is the same as the calculated heat supplied from the G-to-G HEX of thermal backup unit, Q_{TBU} . The value was used in order to design the heat exchanger inside the burner. To calculate Q_{burner} and the outlet temperature of flue, T_{fo} , the following equation was used.

$$Q_{TBU} = \dot{m}_{ad} c_p (T_{ao} - T_{amb}) = Q_d \quad (3.9)$$

The illustration of flue heat flow inside the heat exchanger is shown in Figure 3.11.

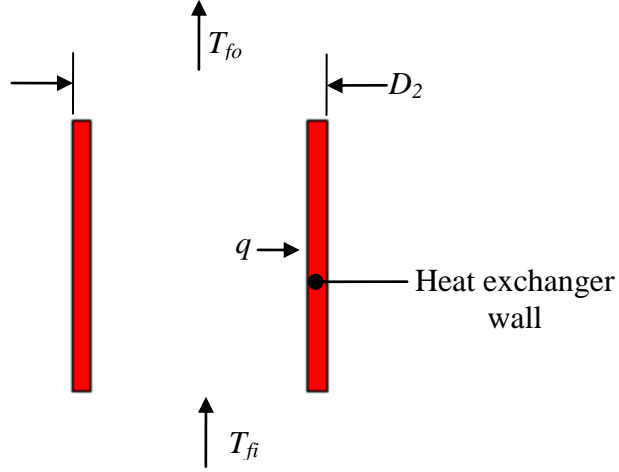


Figure 3.11: Flue heat flow through the heat exchanger

In the flue flow side,

$$Q_{TBU} = \dot{m}_f c_{pf} \Delta T_f = \rho_f A V_f c_{pf} (T_{fi} - T_{fo})$$

Hence,

$$T_{fo} = T_{fi} - \frac{Q_{TBU}}{\rho_f A V_f c_{pf}} \quad (3.10)$$

The type of flow for flue was determined by calculating Re numbers as shown in Equation 3.11.

$$Re = \frac{\rho_f V_f D_2}{\mu_f} \quad (3.11)$$

where if:

Re < 2300: Laminar flow

Re > 2300: Turbulent flow

Grashof number, Gr was calculated from the difference of mean flue temperature, \bar{T}_{flue} and inside wall temperature T_{wi} of heat exchanger. \bar{T}_{flue} was obtained by determining the average between the previous measurement of inlet flue temperature, T_{fi} and the calculated flue outlet temperature, T_{fo} .

$$Gr = \frac{g\beta(\bar{T}_{flue} - T_{wi})D_2^3}{\nu^2} \quad (3.12)$$

Ratio of Gr/Re^2 determines the mode of convective heat transfer [85]:

- $0.1 < Gr/Re^2 < 10$; Natural convection + Forced convection, i.e. combined
- $Gr/Re^2 < 0.1$; Forced convection
- $Gr/Re^2 > 10$; Natural convection

The Nusselt number, Nu was determined based on the type of the flow from Re , and also the mode of heat transfer based on Gr/Re^2 ratio. Noted that the Re number determines the type of flow whether laminar or turbulent. Then based on Gr/Re^2 ratio, the mode of convective heat transfer which is forced, free of combined could be determined.

i. If Re is laminar flow condition

a. For free convection,

$$Nu = CRa^n \quad (3.13)$$

where:

- for laminar, $C=0.59$ and $n=1/4$
- for turbulent, $C=0.1$ and $n=1/3$

and Rayleigh number, Ra was calculated by:

$$Ra = GrPr \quad (3.14)$$

where:

Pr = Prandtl number

Accurate correlation was suggested by Churchill and Chu [91] for $Ra \leq 10^9$.

$$Nu = 0.68 + \frac{0.67Ra^{1/4}}{[1 + (\frac{0.492}{Pr})^{9/16}]^{4/9}} \quad (3.15)$$

b. There are two different empirical relations suggested in the literature to evaluate Nusselt number for forced convection, where:

- By assuming fully developed flow of the flue, the Nu is shown to be [92]

$$Nu = 3.66 \quad (3.16)$$

where surface temperature, T_s is constant (if Nu is less than 3.66, consider Nu is 3.66)

- For the case of considering the flow at entrance conditions, the suitable correlation for Nu number of combined entry length, the Sieder and Tate [93] correlation is more suitable as shown in Equation 3.17.

$$\overline{Nu} = 1.86 \left(\frac{Re Pr}{L_t / D} \right)^{1/3} \left(\frac{\mu}{\mu_s} \right)^{0.14} \quad (3.17)$$

where:

$$L_t = 4.4 D Re^{1/6}$$

- c. For combined convection,

$$Nu_{combine} = (Nu_{force}^3 + Nu_{natural}^3)^{1/3} \quad (3.18)$$

- ii. If turbulent flow condition

- For free convection [94],

$$Nu = \left[\frac{576}{\left(Ra \frac{S}{L} \right)^2} + \frac{2.87}{\left(Ra \frac{S}{L} \right)^{0.5}} \right]^{-1/2} \quad (3.19)$$

- For forced convection, the well-known Dittus-Boelter [95] equation was applied.

$$Nu = 0.023 Re^{0.8} Pr^n \quad (3.20)$$

where:

$n = 0.3$ for cooling, and $n = 0.4$ for heating.

Finally the convection heat transfer coefficient of flue, h_{flue} is calculated after the Nu number was obtained.

$$h_{flue} = \frac{Nu.k_f}{D_2} \quad (3.21)$$

The illustration of heat transfer across the wall of heat exchanger is shown in Figure 3.12.

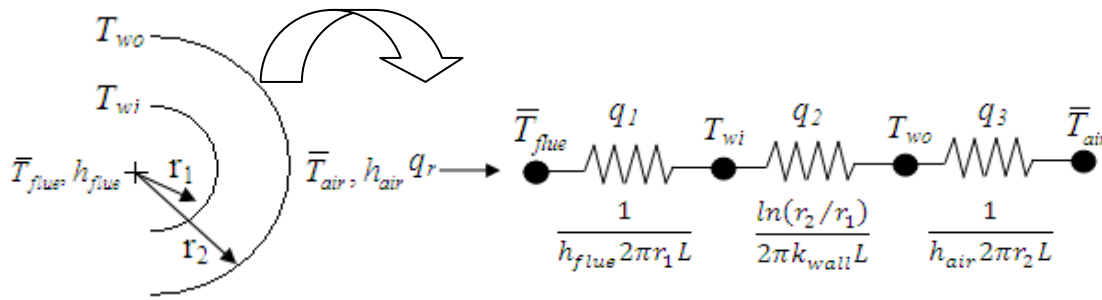


Figure 3.12: Heat transfer network from flue to air side

The characteristic length, L_c or height of the heat exchanger was obtained by maintaining the same amount of the calculated heat required for drying.

$$Q_d = Q_{TBU} = q_1 = q_2 = q_3 \quad (3.22)$$

The heat transfer from the flue to the inside wall:

$$q_1 = h_{flue} A_f (\bar{T}_{flue} - T_{wi}) \quad (3.23)$$

Across the wall of heat exchanger:

$$q_2 = \frac{2\pi L k_{wall} (T_{wi} - T_{wo})}{\ln \frac{r_1}{r_2}} \quad (3.24)$$

And from the outside wall of the cylinder to the air flow zone:

$$q_3 = h_{air} A (T_{wo} - \bar{T}_{air}) \quad (3.25)$$

where:

$$A_f = A_{win} + A_{fin sin}$$

$$A = A_{wo} + A_{fin so}$$

The design procedure aimed to estimate the geometries of the G-to-G HEX. The outer and inner diameters were presented as 0.4 m and 0.2 m respectively. The width of the extended eight fins was selected as 0.01 m. The height of G-to-G HEX, L_c was the target to be determined by the mathematical procedure identified above.

The steps of procedure were repeated again using the previous calculations across the wall of heat exchanger of hot air side. The type of flow for air is determined by calculating Re number as shown in Equation 3.26 using properties at air temperature.

$$\text{Re} = \frac{\rho V_d D_h}{\mu} \quad (3.26)$$

where:

$$V_d = \dot{V} / A$$

$$A = \pi r_2^2 - \pi r_1^2$$

$$D_h = 4A/P$$

$$P = \pi D_1 + \pi D_2$$

Gr_L number for air was calculated by finding the difference across T_{wo} and \bar{T}_{air} using Equation 3.27. The calculation was followed after finding of the nature of convection heat transfer based on Gr/Re^2 .

$$\text{Gr}_L = \frac{g\beta(T_{wo} - \bar{T}_{air})L_c^3}{\nu^2} \quad (3.27)$$

The Rayleigh number, Ra_L was obtained from Equation 3.14 which involves the previous Gr and Pr of air.

By adapting the same criteria of $0.1 < Gr/Re^2 < 10$, the convection heat transfer in the airflow zone was checked and the relevant Nu equation is used to calculate h_{air} . For the case of natural convection, the relation in Equation 3.13 was applied. For forced convection heat transfer, Dittus-Boelter relation was used as shown in Eq. 3.20. If the case was combined, thus the Nu was evaluated as in Equation 3.18.

The convection heat transfer coefficient of air, h_{air} was obtained by substituting the values of Nu which depended on the type of flow into Equation 3.21 by using properties of air annulus hydraulic diameter.

The total area, A of heat transfer to the air flow zone was comprised of the outer wall of the inner cylinder and the total surface area of the eight extended fins as in Equation 3.28.

$$A = A_{cylinder} + A_{fins} \quad (3.28)$$

where:

$$A_{cylinder} = L_c \pi D_2$$

$$A_{fins} = 2nL_c(L_{fo}/2)$$

Finally, the new characteristic length, L'_c was calculated by using the same Q calculated from dryer shown in Eq. 3.29 followed by iteration until it reached a setting error, L_c measured – L_c old equal to 0.001. The purpose of iteration is to estimate the accurate value based on the initial assumption. The newly calculated characteristic length, L'_c of the G-to-G HEX was:

$$L'_c = \frac{Q_{TBU}}{h_{air} \times A \times (T_{wo} - \bar{T}_{air})} \quad (3.29)$$

3.4.3.3 Design Algorithms

The mathematical modeling of the G-to-G HEX unit has been converted to a computer program in MATLAB[®] environment. The boundary conditions of the TBU are shown in Table 3.7. The calculated heat required for drying, Q was 154 Watt and this value was used by deliberating with the TBU calculation.

Table 3.7: Boundary condition of the TBU unit

No.	Items	Value
1	Mean Air Temperature, \bar{T}_{air}	55°C
2	Heat required for drying, Q_d (obtained from dryer)	154 Watt
3	Volumetric flow rate (from dryer) with SF 1.2, \dot{V}_a	30 m ³ /hr
4	Velocity of flue inside the inner cylinder, V_f	0.5 m/s
5	Cylinder diameter, D_1	0.4m
6	G-to-G HEX diameter, D_2	0.2m
7	Number of fins, n	8
8	Length of outer fins, L_{fo}	0.08m
9	AISI 304 thermal conductivity, k	14.9 W/m·K
10	Initial assumption of characteristic length, L_c	0.4 m

The programming was divided into two parts. The first part was concerned with the flue side to calculate h_{flue} and the second part was concerned with the air side across the heat exchanger, to calculate the correct height, L'_c . The algorithms of the flue and air side analysis are shown in Figure 3.13 and Figure 3.14. The execution of the program involved many iteration processes.

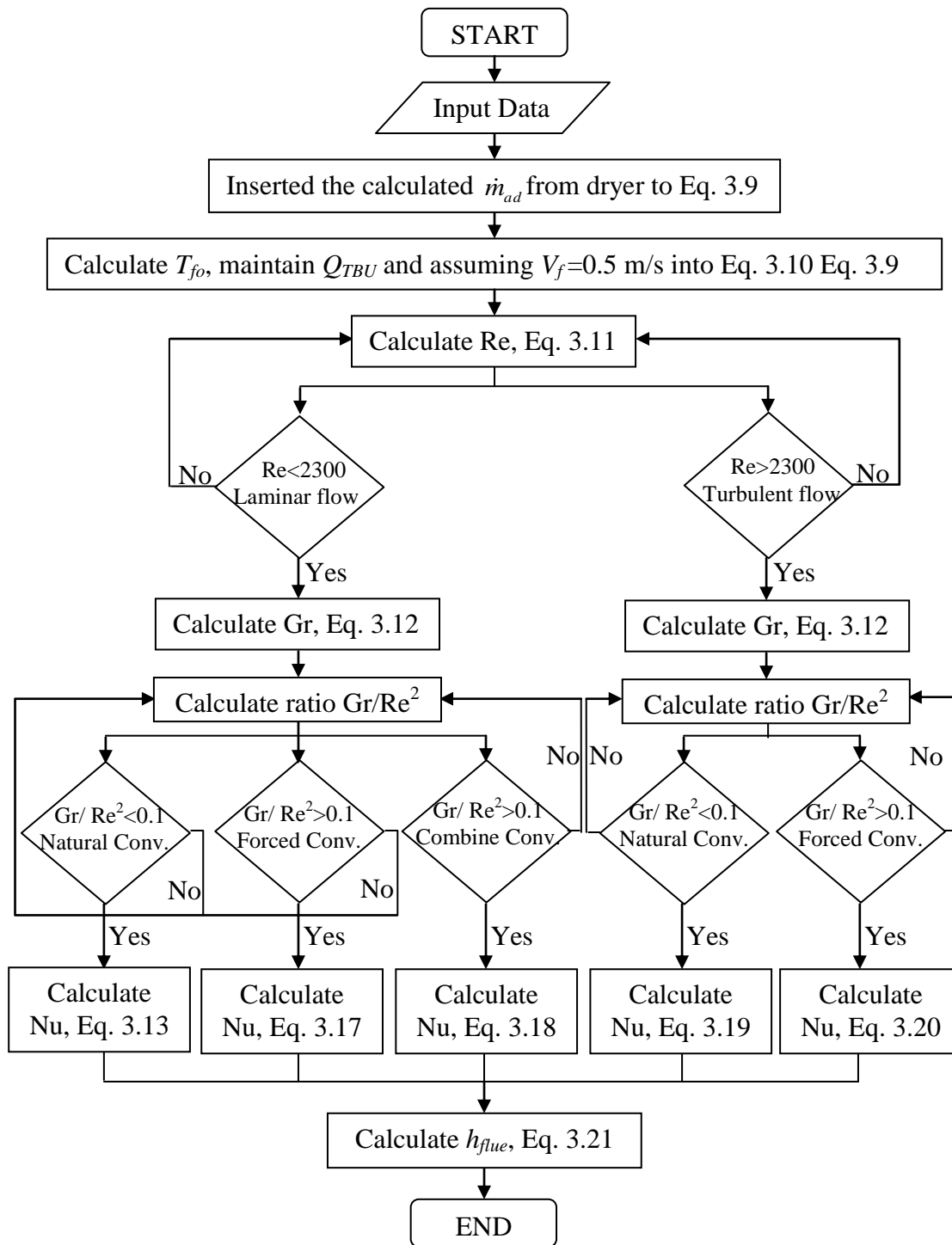


Figure 3.13: Algorithm of the flue side analysis

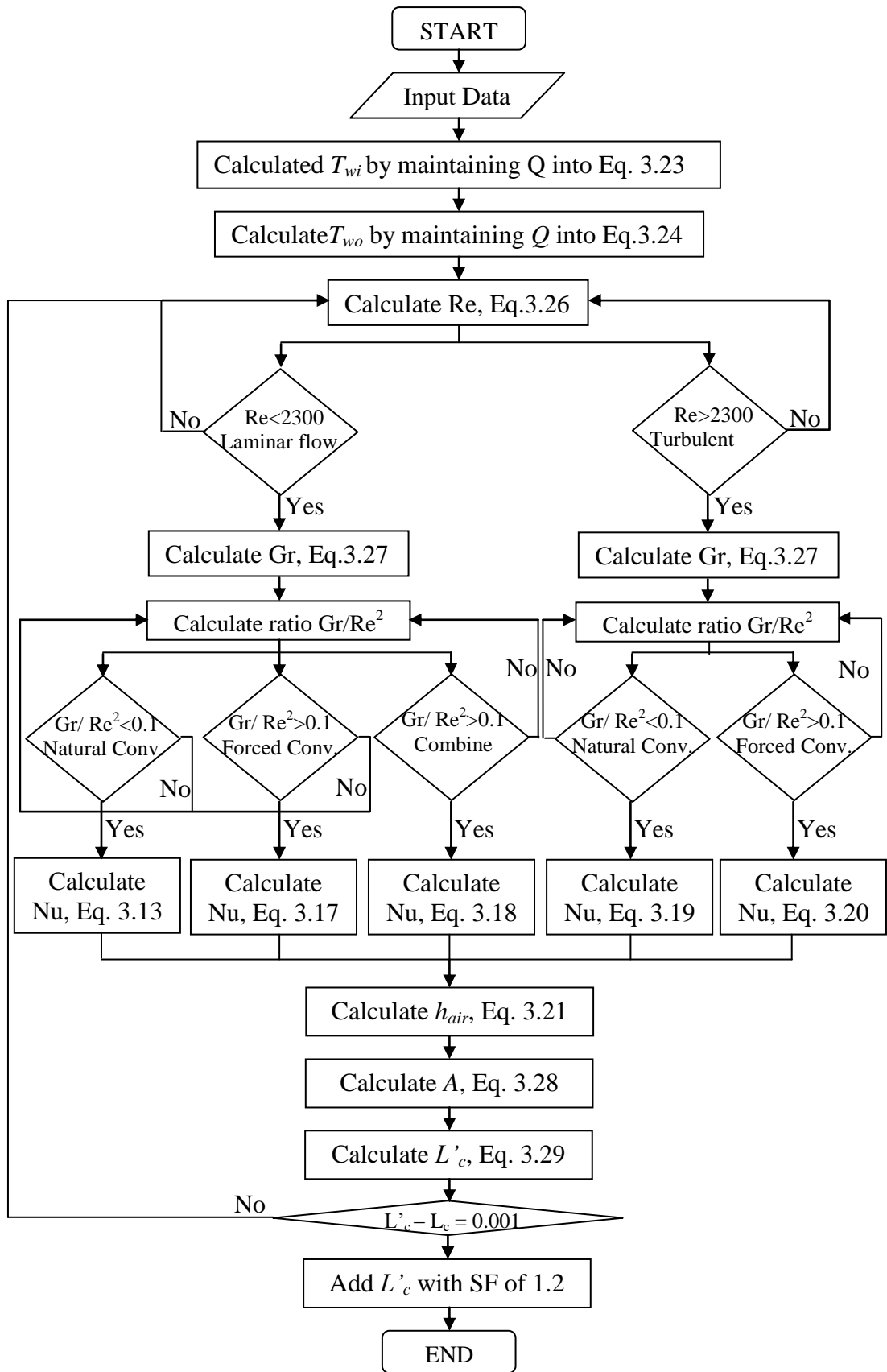


Figure 3.14: Algorithm of the air side analysis

The initial characteristic length, L_c is assumed to be 0.4m and the final length is obtained from the iteration until the difference of error between the new and old length reaching approximately to 0.001. The results of iteration are shown in Figure 3.15. The calculated L_c that obtained at final iteration was 0.33 m.

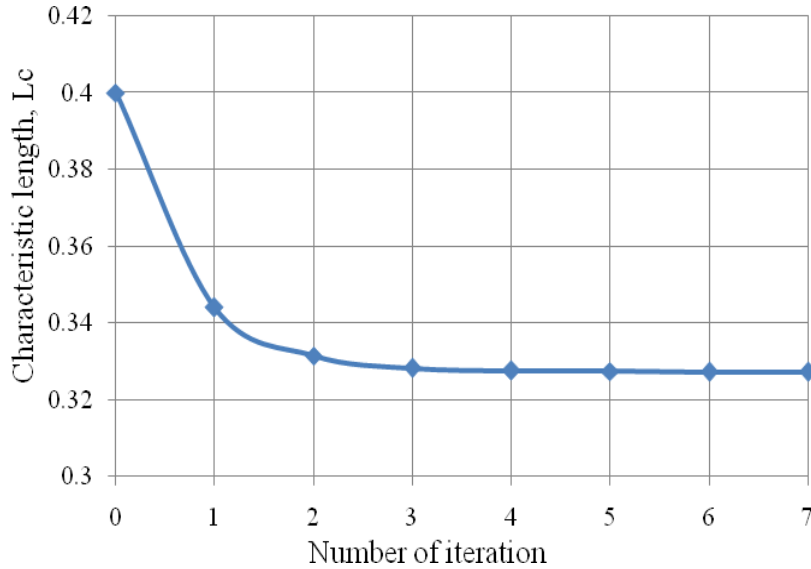


Figure 3.15: Characteristic length, L_c versus number of iteration

3.4.3.4 Values of Design Parameters

The flue convective heat transfer coefficient, h_{flue} calculated from the flue side was $3.41 \text{ W/m}^2\cdot\text{K}$. In the air side analysis, the calculated Re was 319.17 which indicates that the flow was laminar with air convective heat transfer coefficient, h_{air} of $4.78 \text{ W/m}^2\cdot\text{K}$. The results of design calculation of the burner at final iteration are shown in Table 3.8.

The value of h_{flue} obtained from calculation was compared with the typical values of the convection heat transfer coefficient for gases in Incropera et al. [85]. For free convection of gases, the range is from 2 to $25 \text{ W/m}^2\cdot\text{K}$ which means that the calculated value of h_{flue} , $3.41 \text{ W/m}^2\cdot\text{K}$ is valid. The final L_c is to be multiplied by safety factor of 1.2 to compensate for the losses to the exchanger surroundings. Thus, the final L_c calculated for the design of burner is 0.4m. The results of the calculated final length and the component of TBU are shown in Figure 3.16 and Figure 3.17.

Table 3.8: Result of the TBU design calculation

No.	Item	Value	Remarks
1	Inner wall temperature, T_{wi}	132.5°C	
2	Outer wall temperature, T_{wo}	132.46°C	
3	Convective heat transfer coefficient, h_{flue}	3.41 W/m ² ·K	
4	Heat from TBU, $Q_d = Q_{TBU}$	154 Watt	
5	Hydraulic diameter for airflow zone, D_h	0.19m	
6	Reynolds number in the air flow zone, Re	319.17	Laminar
7	Grashof number in the air flow zone, Gr	1.295x 10 ⁸	
8	Ratio Gr/Re ²	1272	Natural convection
9	Nusselt number in the air flow zone, Nu	57.98	
10	Rayleigh number in the air flow zone, Ra	9.327 x 10 ⁷	
11	Convective heat transfer coefficient, h_{air}	4.78W/m ² ·K	Within the typical values in literature
12	New characteristic length with SF 1.2, L'_c	0.4m	

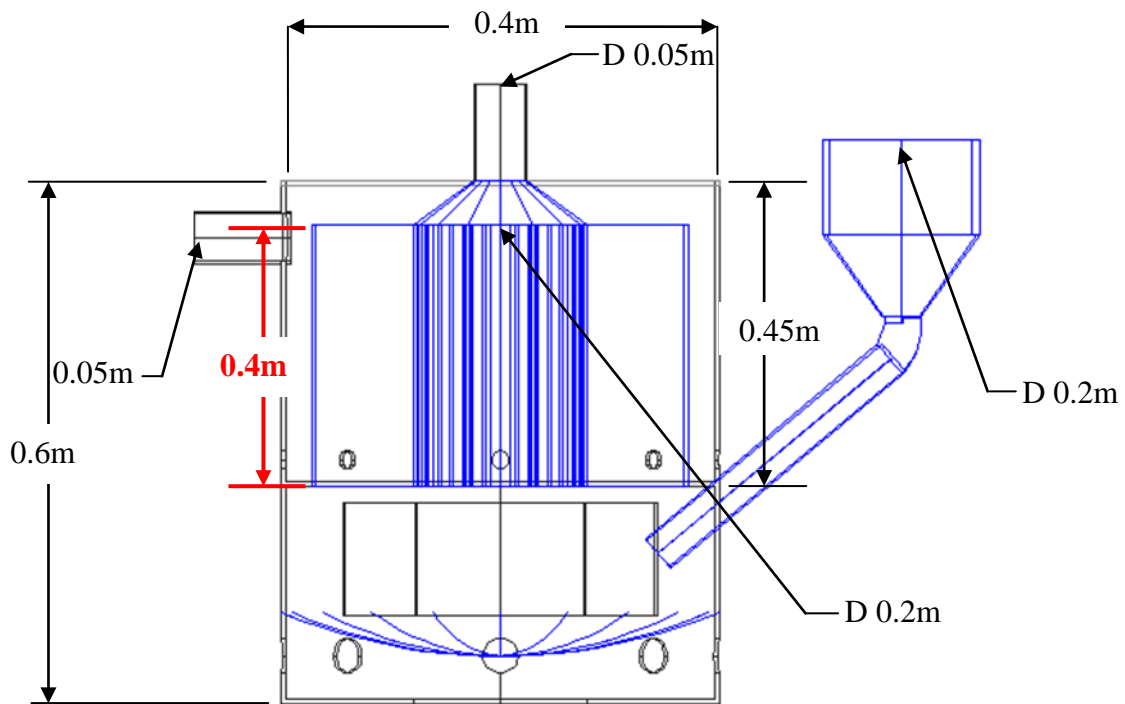


Figure 3.16: The sketch length of the heat exchanger inside the TBU (unit shown are not in scale)

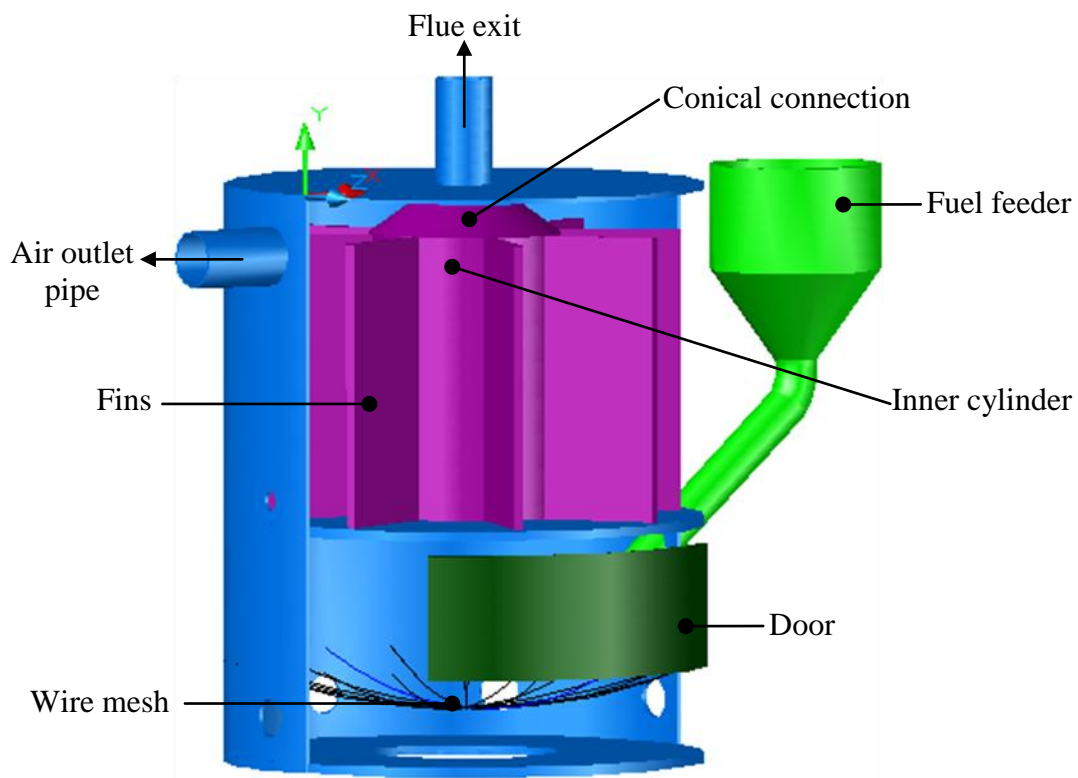


Figure 3.17: Sketch of the components of the TBU

3.5 Chapter Summary

This chapter described mainly on the procedure involved in model development. The operational principles of both solar dryer and biomass burner were presented. The designs of both models were divided into several parts starting from conceptual design, material selection and design calculation. The dryer and burner designs were based on the studies of related journals and books. Design calculation is the most crucial part since it affected on the process of units fabrication. The results of calculation for each unit were shown and AutoCAD design software had been used to present the detailed schematic solar dryer and biomass burner.

CHAPTER 4

EXPERIMENTAL VERIFICATION

4.1 Chapter Overview

This chapter presents the experimental results that have been conducted throughout the project. The experiments were divided into two parts, which were the TBU and the dryer unit. Three different types of solid biomass wastes, which were rice husk, EFB and wood chips, have been tested in the experimentation on the TBU. The solar dryer experiments were divided into two, no-load and loading experiment. The no-load experiments focused on the thermal performance of the dryer under different operational modes. Chillies and EFB from food and waste product category respectively have been dried under loading experiments. The efficiencies of the solar collector and the drying efficiencies were presented at the end of this chapter.

4.2 Experimental Procedure and Measuring Instrumentation

The first stage of experiment had been conducted on the TBU. The performance of TBU was evaluated by using different types of biomass fuel at different feeding rate for four hours to obtain the required temperature and velocity which were suitable for drying application. Only the hot air temperature (indirect heating) was evaluated since the quality of food product is highly dependent on it. The required hot air outlet temperature from the TBU should be within 80 to 100°C after considering the heat loss along the tube hose which connect the TBU and the dryer. The experiment programs are shown in Figure 4.1.

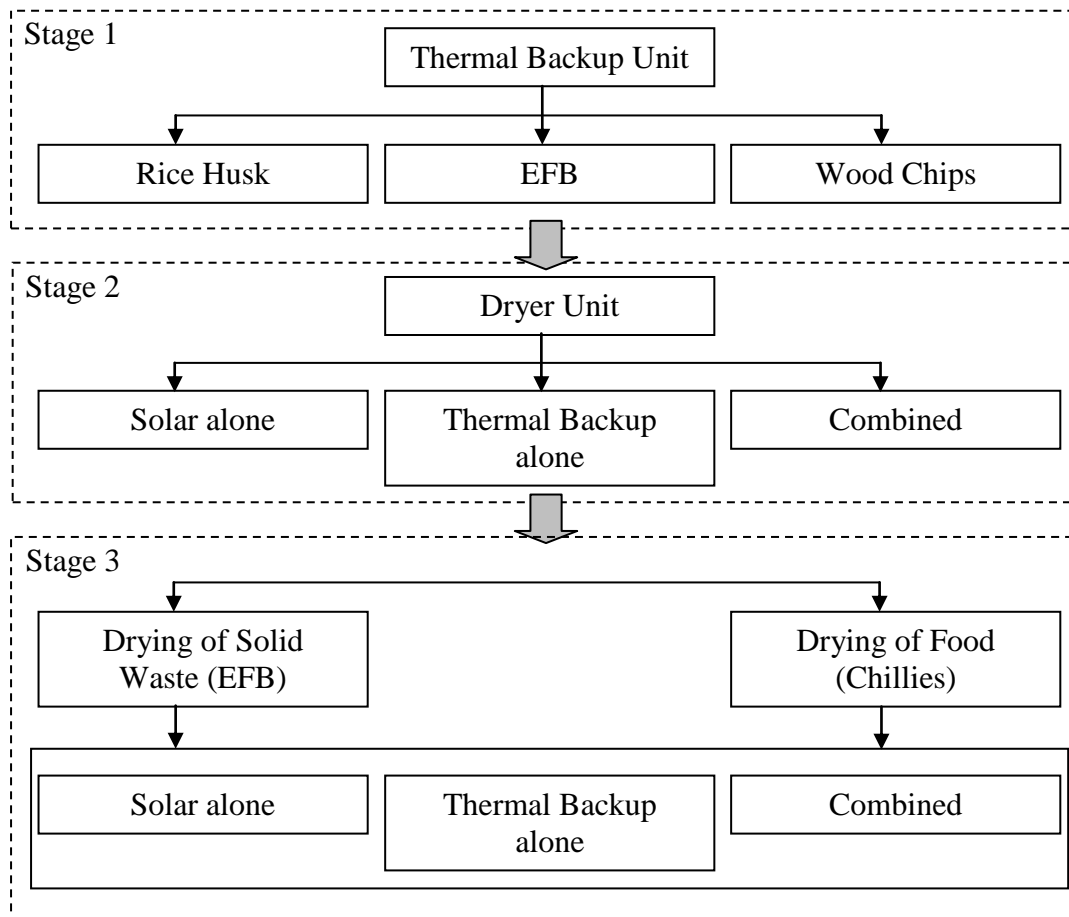


Figure 4.1: Experimental program

Next, the second and third stage experiments were carried out on the dryer unit. The experiments were separated into no-load and loading experiments respectively. The best type of fuel selected from the biomass burner experiment had been used throughout these experiments. In no-load experiments, the temperature distribution inside the dryer was plotted to ensure that the temperatures were within the required range before continuing with drying products. Both stages of experiments were divided into several modes which includes the application of thermal backup. The trays were numbered from the bottom to the top of drying chamber. The location of the trays according to the numbering and the dryer experimental setup are shown in Figure 4.2.

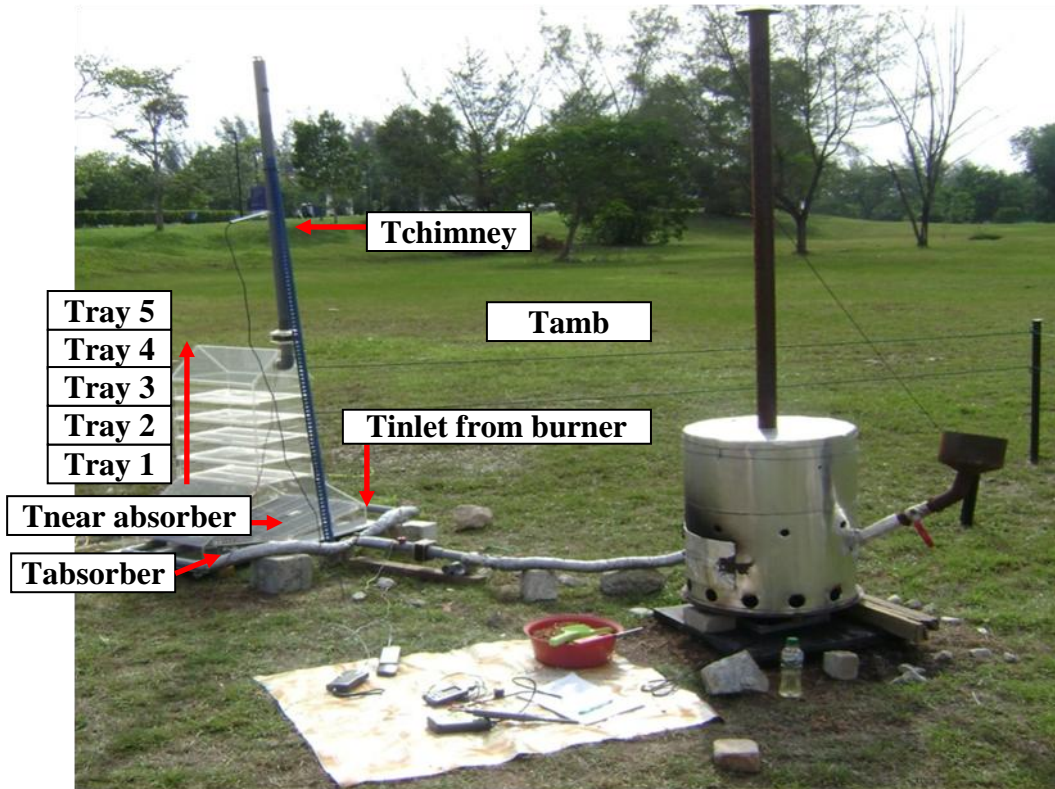


Figure 4.2: Experimental Set-up of Hybrid Mode Solar Dryer

The details of the parameters measured during the experiment were summarized as in Table 4.1.

Table 4.1: The details of parameter measured

Parameter	Locations
Temperature	<ul style="list-style-type: none"> • Ambient air • Absorber plate • Near absorber • Trays • Chimney flow • Inlet (Heat supplied form burner)
Relative Humidity	<ul style="list-style-type: none"> • Ambient air • Absorber plate • Near absorber • Trays
Weights	<ul style="list-style-type: none"> • Biomass fuels • Chillies • EFB
Speed of air flow	<ul style="list-style-type: none"> • Chimney flow
Solar Irradiation	<ul style="list-style-type: none"> • Outside dryer

The relative humidity and air temperature inside the chamber were measured using digital hygrometer/psychrometer (NPI 597), while the absorber temperature was recorded using data logger (FLUKE HYDRA). Solarimeter (KIMO instruments) was used to record the solar irradiation and anemometer (Testo 435) was used for the airflow velocities. The weight was measured using digital scale model FEJ-5000 (max 5kg). The outlet of TBU by hot air and flue temperature were recorded using portable hot wire probe (K-type thermocouple).

4.3 Thermal Backup Unit Experiments

This experiment was mainly focusing on the performance of TBU by using different types of biomass fuel and different feeding rates for 4 hours to obtain the required temperature and velocity that is suitable for the drying application. Only the hot air temperature is evaluated since the quality of food product is highly dependent on it. The biomass fuels that have been tested were rice husk, empty fruit bunch (EFB) and wood chips. The required hot air outlet temperature was within 80 to 100°C after considering the heat loss along the tube hose. The best type of fuel was selected based on thermal performance of the burner and would be applied as fuel for the further experiment. The experimental setup of the biomass burner experiment and the location of the hot air temperature recorded are shown in Figure 4.3.

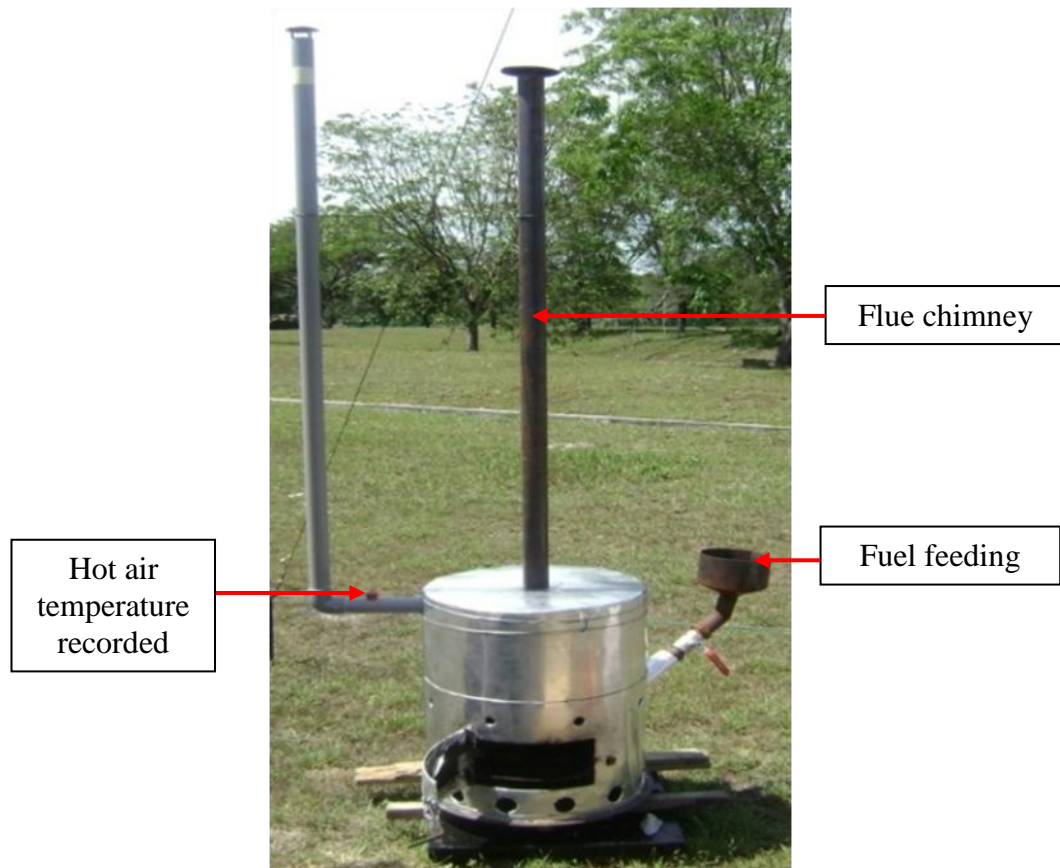


Figure 4.3: Experimental set-up of the TBU

4.3.1 Solid Biomass as Burning Fuel

Biomass fuels have many advantages to the environmental and economy since it is cheap, clean and a type of renewable source of energy. The usage of biomass fuel as the source of electricity has been widely applied nowadays especially among the factories. Felcra Nasaruddin which located near Universiti Teknologi PETRONAS, Perak produces its own electricity using their waste product which is EFB through cogeneration process to save their operating cost. Besides, Kapur et al. [96] have studied on the electricity generation from rice husk which applied in Indian rice mills. They have developed nomographs to estimate the required rice husk in parboiling, drying and milling operations. In this project, three types of biomass fuel which are rice husks, empty fruit bunch (EFB) and wood chips had been tested in the experiment. The calorific value of the fuel is shown in Table 4.2.

Table 4.2: Calorific value of the biomass fuel [97-99]

No.	Type of Biomass	Calorific Value (kJ/kg)
1	Rice Husk	12 557
2	Empty Fruit Bunches fibers (EFB)	19 068
3	Wood Chips	15 192

The calorific value of biomass is an indication of the energy chemically bound in it. Calorific value is the most important property to determine the energy value. During the combustion process it converts into heat energy. The design and control of the biomass combustor are depends strongly on the calorific value of the biomass fuel.

The outlet temperature of the rice husk, EFB and wood chips combustion was taken every one hour with different feeding rate and the results were compared with the required assumption value to investigate the performance of the unit. The potential of the fuel as a backup heater for solar dryer was discussed and the best biomass fuel would be selected.

4.3.2 Results of Rice Husk

The experiment was conducted in the afternoon where the initial ambient temperature was 38°C in average. The initial reading taken at the air outlet temperature of TBU was 40°C. This experiment was conducted with three different weights which were 0.5 kg, 1.0 kg and 1.5 kg for 4 hours of operation. These weights were chosen to ensure that the fuel supplied enough heat and sustain for the 4 hours of continuous operation. The results of rice husk fuels are shown in Figure 4.4.

It is observed that at feeding rate of 0.125 kg/h, the hot air of burner took about two hours to be heated up and reached the maximum air temperature of 76°C. The rice husk fuels at this time undergo nearly a complete combustion. The temperature slightly declined after adding the fuel since the combustion became lesser. At the final hour, the fuel was exhausted and the air temperature drops to 40°C. The feeding rate of 0.125 kg/h is insufficient to sustain the required air temperature.

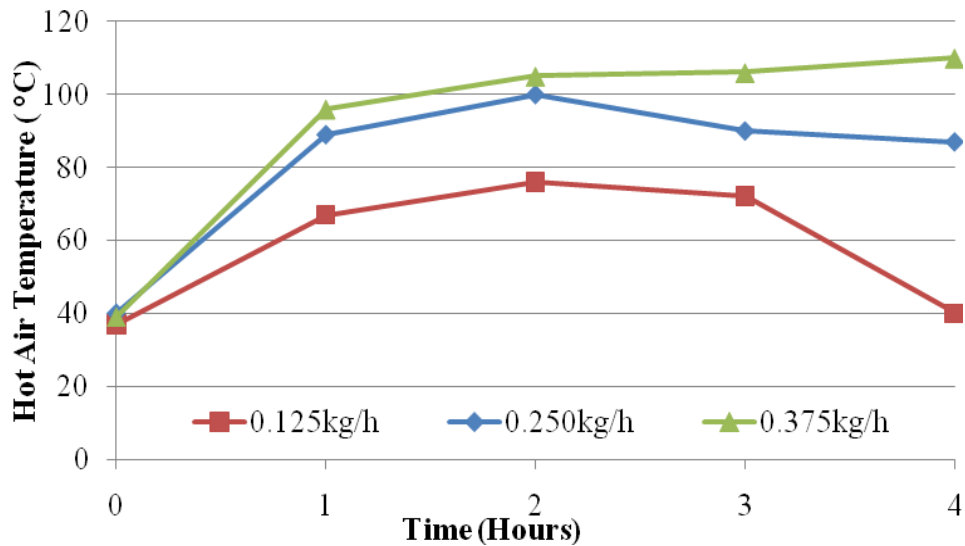


Figure 4.4: Hot air outlet temperature obtained from burning of rice husk

Next, the experiment was carried out with a feeding rate of 0.250 kg/h. The graph indicates that the hot air temperature of burner lay within the required temperature even at the first hour of combustion. The temperature kept increasing up to 90°C and then declines slightly due to termination of feeding. On the following hour, there were a temperature decline but it stayed within the required drying temperature until the end of experiment. The experiment was repeated with the final feeding rate of 0.375kg/h. It is observed that the temperature recorded for the first hours almost reaches 100°C and it was kept increasing until the end of the experiment. In this feeding rate, the maximum recorded air outlet temperature was 110°C, far beyond the required temperature which will affect the quality of drying product.

The best feeding rate of rice husk fuel observed from the tests was at 0.250kg/h since the recorded heat temperature fall within 80 to 100°C along the period of experiment. However, based on the analysis, it was found that rice husk fuel has several disadvantages. It was not easy to ignite and maintain the heat. Fire starter medium such as kerosene was used to instant the process in the early morning but there was a higher tendency for the fuel to re-flaming if the burner receives adequate air supply. Furthermore, rice husk was found to produce a lot of heavy smoke during the combustion.

4.3.3 Results of EFB

The EFB was obtained from the Nasarudin Palm Oil Factory (FELCRA) in Bota, Perak. It has been dried first under the open sun for several hours due to high initial moisture content. Three varying total weight of EFB which were 1.0 kg, 1.5 kg and 2.0 kg were burned for four hours. The results are shown in Figure 4.5.

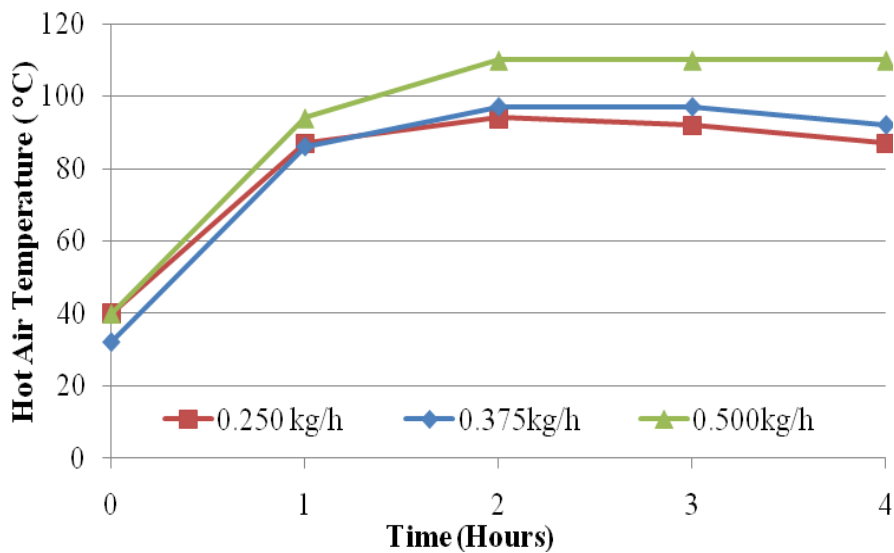


Figure 4.5: Hot air outlet temperature obtained from burning of EFB

As could be noticed, all the feeding rates were observed to produce higher and more stable heat than the rice husk. The combustion of EFB fuels were shown to occur continuously. The feeding rates of 0.250 kg/h and 0.375 kg/h produces heat within the required temperature throughout the experiment. A slight temperature decline at the ends showed that the burning process of EFB is quiet constant and not affected much. The temperature was maintained until the end of experiment for a feeding rate of 0.5 kg/h but it is too high to be applied in the present drying application. There were some difficulties in using EFB fuels. Same as rice husk, EFB was hard to ignite hence the uses of turpentine as igniter is needed. Besides, it needs to be stirred regularly in order to ensure that all the fuel is completely burned.

4.3.4 Results of Wood chips

Wood chips are the excess form of wood craft processes and come in very small. A varying total weight of 1.0 kg, 1.25 kg and 1.5 kg woodchips fuel were tested. The results are shown in Figure 4.6.

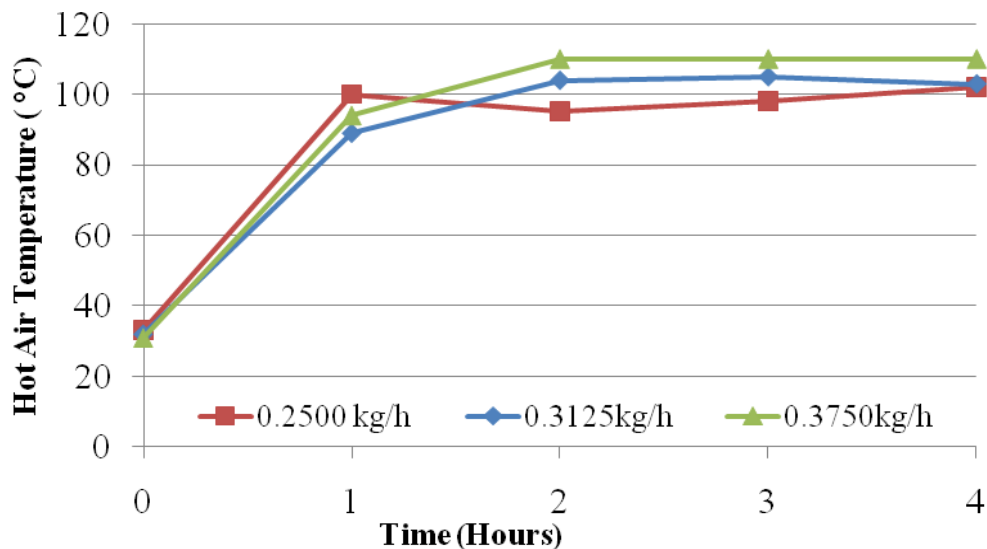


Figure 4.6: Hot air outlet temperature obtained from burning of wood chips

From the graph, it could be observed that wood chips combustion has produced a stable air temperature throughout the experiment. The highest air outlet temperature of 98°C was recorded at feeding rate of 0.2500 kg/hr during the first hour of combustion. It shows that the burner was heated up very fast at this feeding rate as compared with the feeding rate of 0.3125 kg/h and 0.375 kg/h. The temperature slightly declined after it reached complete combustion in the first hour and increased in the next hour until the end of experiment yet still maintained in the required temperature range. The feeding rate of 0.3125 kg/h and 0.375 kg/h shows that the temperature kept increasing and resulted in high air outlet temperature which exceeded the required drying temperature. That is not suitable for drying application. Hence, the first feeding rate is the best feeding rate since it maintained the air temperature below 100°C. As a general observation, wood chips fuels are easy to handle as compared with the rice husk and EFB. It is not difficult to ignite and able to sustain the heat. Besides, the combustion is even, produced light smoke and heated up the burner very fast.

4.3.5 Verification of TBU Design

The analyses of measurement results demonstrated that the designed and fabricated TBU was capable to produce the temperature and flow rate of the hot air required for the drying application. Wood chips with a feeding rate of 0.250kg/hr have been selected as the fuel of the burner. To justify the mathematical procedure which was adopted for the TBU design, a comparison has been carried out between the temperatures used in mathematical calculation and the measurement results. As shown in Table 4.3, the highest percentage of difference is 25% for the heat from burner and the others are below 5%. The low percentage difference indicates that it is in a good agreement and the procedure is verified.

Table 4.3: The percentage difference between mathematical calculation and experimental result

No	Items	Mathematical Calculation	Experimental Result	Percentage Difference (%)
1	Inner wall temperature, T_{wi}	132.5°C	140°C	5%
2	Outer wall temperature, T_{wo}	132.5°C	126°C	5%
3	Convective heat transfer coefficient, h_{flue}	3.41 W/m ² .K	3.27W/m ² .K	4%
4	Convective heat transfer coefficient, h_{air}	4.78W/m ² .K	4.85W/m ² .K	2%

4.4 No-load Dryer Experiment

The aim of the no-load experiment was to study the thermal characteristics of solar collector and the drying chamber under different modes. The temperature across the trays were recorded and compared. The results obtained would be compared with the simulation results, for validation of the numerical procedure. The mode of heating was divided into five as shown below.

- Solar
- TBU by hot air
- TBU by flue
- Solar + TBU by hot air
- Solar + TBU by flue

The no-load experiment was conducted without any drying materials. The performance of solar collector was examined under this experiment. The drying modes consisted of drying under solar, hot air and flu gas from the TBU and a combination of backup modes with solar. The temperatures were recorded from the alternate tray position as shown in Figure 4-2. The experiments were conducted from 9am to 5pm daily and separated for 4 days to reduce the uncertainty. Sawdust with a feeding rate of 0.250kg/hr had been selected as the fuel for the burner. The ignition of biomass fuel was started at 9.00am and feed at 2 hours interval until 5.00pm. The average values of the 4 days repeatability were plotted according to the mode of drying.

4.4.1 Experimental Analysis of Solar Collector Performance

The average transient temperatures of the absorber plate, outlet air (chimney), ambient and solar irradiation were measured and the results were plotted. The results are shown in Figure 4.7. This experiment was conducted with unloaded test to obtain the solar collector performance. The experiment was carried out from 4th to 7th April 2010. It was observed that the rise in temperature in the collector is sufficient for the purpose of most agricultural products drying even the average value of the solar irradiation was fluctuated. The ambient temperature was more or less uniform throughout the day which was around 28 to 33 °C. The maximum average air temperature at the collector was recorded as 70°C at the solar irradiance level of 650 W/m². As the irradiation increased, the collector temperature also increased therefore the collector temperature was highly depending on the solar irradiation. According to Pangavhane et al. [100], the wind conditions, ambient air temperature, incident solar irradiation and collector design highly influenced the mass flow rate of the drying air inside the dryer.

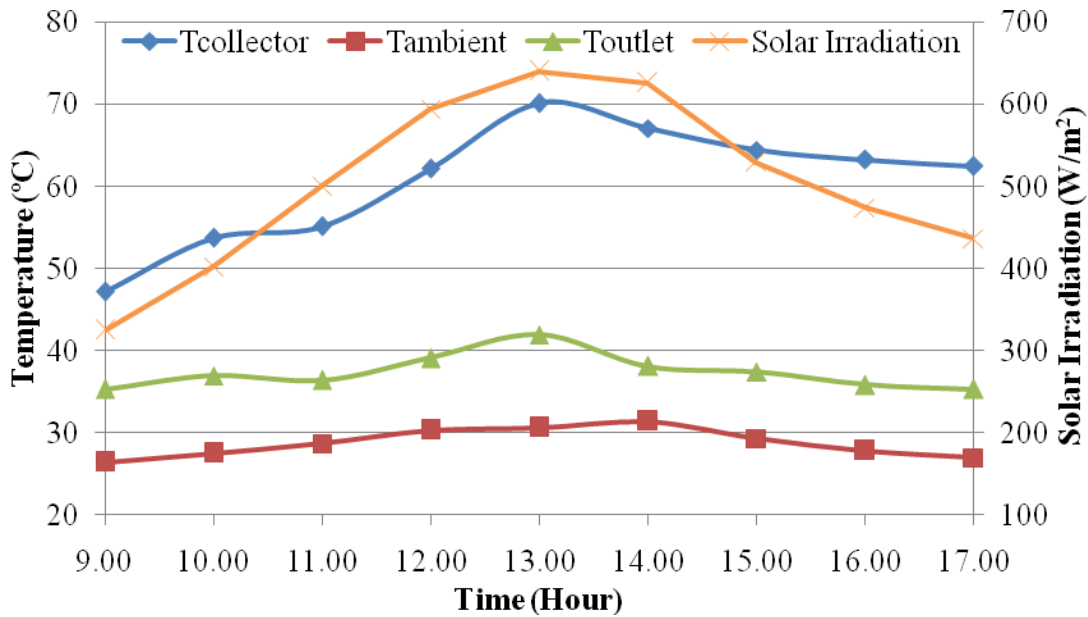


Figure 4.7: Transient measured values of temperature at collector, ambient, outlet air of dryer and solar irradiation

4.4.2 Experimental Analysis of Dryer under Solar Mode

The solar drying mode was operated only by using the heat source from solar irradiation. The solar dryer was left under the sun and the average temperature distribution inside the dryer had been recorded. The results are shown in Figure 4.8. Those results were used as a bench mark for evaluation of other drying modes.

The average temperature at Tnear collector was supposed to be the highest. However at 11.00 am to 2.00 pm, the measurements were affected by cloudy and rainy environment. Since Tray 3 is located in the middle of the trays, the received heat from natural convection is not high enough compared with the lower trays, in one hand. On the other hand, it absorbs solar irradiation lower than the upper two trays. Besides, the location was in the shaded area due to the shadow of the other trays and only small area able to expose to solar irradiation. The highest recorded temperature among the trays was in Tray 5 since it is located on the top tray and received direct solar irradiation. The temperature recorded at this tray was between the ranges of 48 to 65°C.

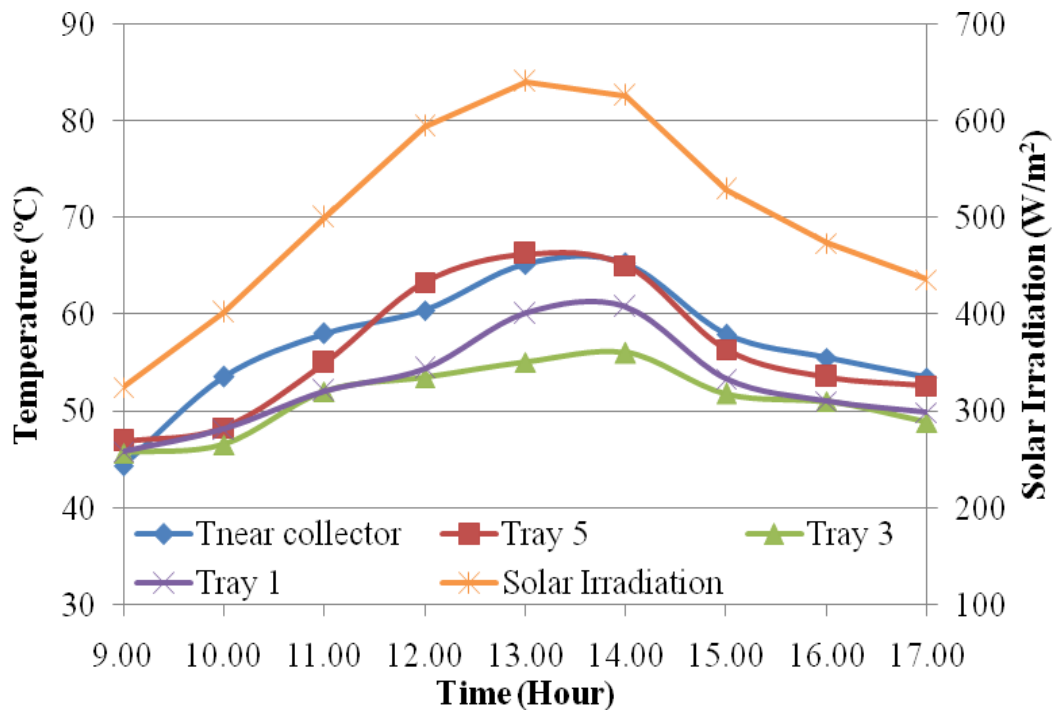


Figure 4.8: The average temperature of dryer under solar mode

The measured temperatures fluctuated along the day since they were totally depending on the solar irradiation. The highest temperature was recorded in Tray 5 (top), followed by Tray 1 (bottom) since it were located near to the heat source. The measured temperature of Tray 3 (middle) was the lowest. When solar irradiation was available, some was absorbed directly by the wall of dryer and the major was transmitted to inside of the dryer. Some of the transmitted was absorbed by the black painted absorber plate which was located at the bottom part of dryer. Consequently, heat would flow from bottom to the top part of dryer by natural convection. The process of irradiation entering and escaping the dryer is shown in Figure 4.9.

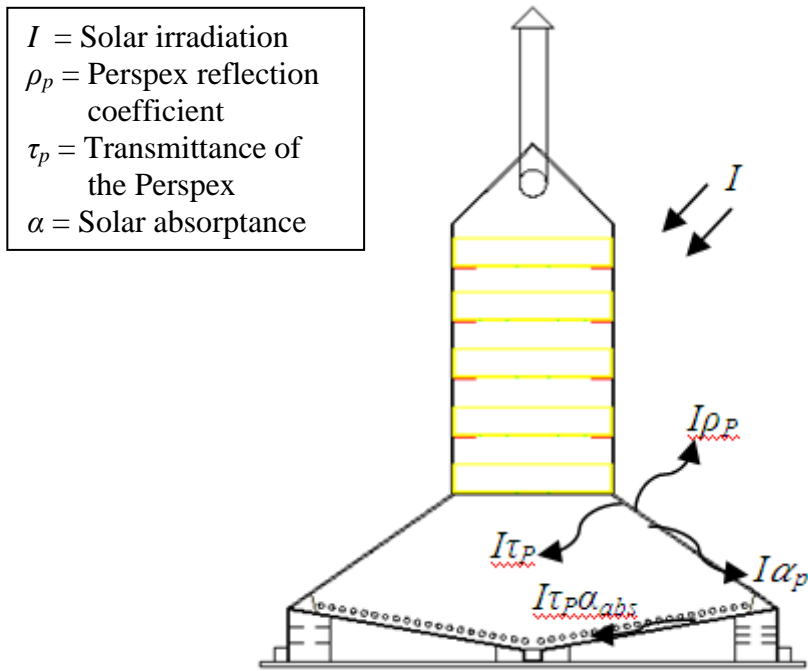


Figure 4.9: Irradiation entering and escaping surface

4.4.3 Experimental Analysis of Dryer under Thermal Backup Mode

This experiment was conducted in a shaded area where there was low or no direct solar irradiation. The shading was to simulate cloudy ambient and night. The backup modes were divided into two experiments. The first experiment had been conducted by connecting only the clean hot air from the TBU into the solar dryer. The flue gas and the clean hot air were separated by the heat exchanger which had been designed inside the burner and was named as clean hot air thermal backup mode. In the second experiment, flue gas was directly supplied into the solar dryer without the usage of heat exchanger. This mode was named as flue thermal backup mode and the results were compared with clean hot air mode. The average results of four days measurement of dryer temperature of clean hot air and flue mode of thermal back up were shown in Figure 4.10 and Figure 4.11 respectively.

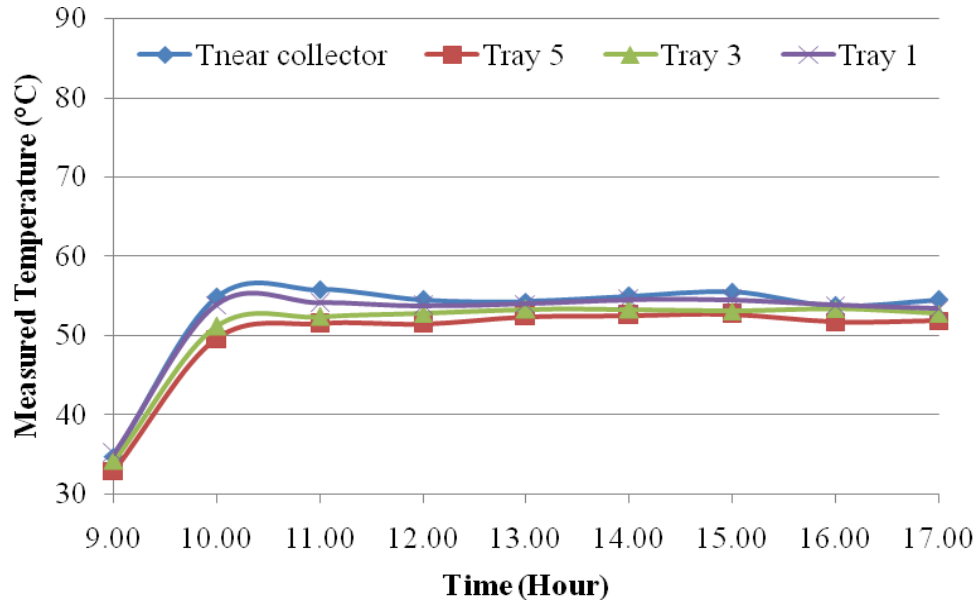


Figure 4.10: The average measured temperature of dryer under clean hot air thermal backup mode

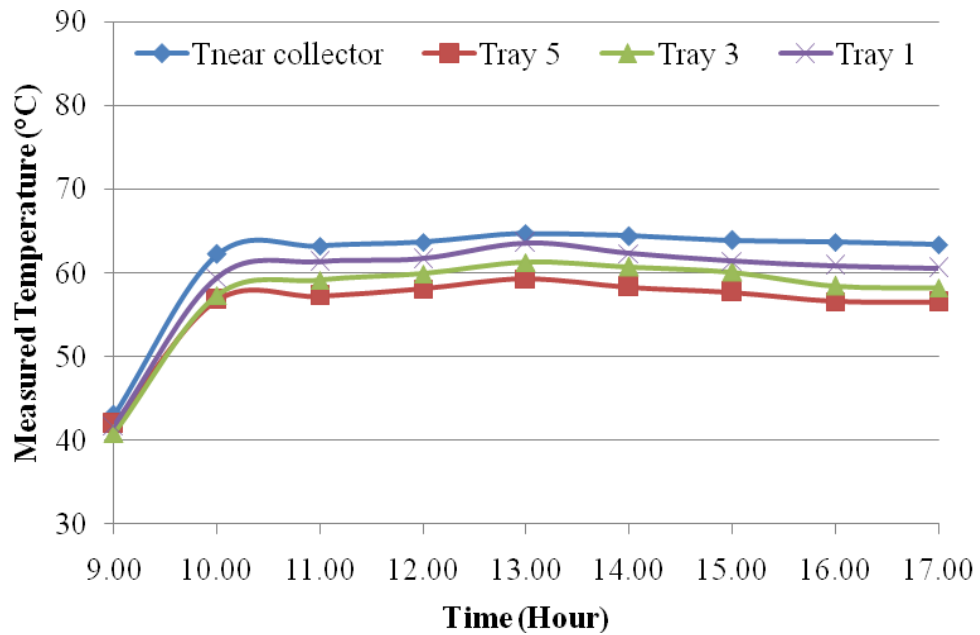


Figure 4.11: The average measured temperature of dryer under flue thermal backup mode

The graphs indicate that the average temperatures of separated clean hot air and flue thermal backup mode are quite constant throughout the day. The temperature differences between the trays are small. The highest temperature recorded was in Tray 1 since it is located near the source of heat, followed by Tray 3 (middle) and Tray 5

(top) for both modes. The temperature reduction was due to heat losses to the surrounding and some has been absorbed by the trays as the heat flows from bottom to the top. The flue thermal backup up heating temperature was slightly higher than clean hot air backup heating which was around 57 °C to 64°C. While, the temperature recorded in hot air backup heating was around 52 to 56°C. It can be concluded that the thermal back up caused a uniform distribution of temperature over the five trays. Besides, it also caused a stable temperature in the dryer over the drying period, in contrast to the solar mode which follows the solar irradiation.

4.4.4 Experimental Analysis of Dryer under Hybrid Mode

In hybrid drying mode, solar irradiation and thermal backup were used as the sources of heat. The results of the separated solar with clean hot air and solar with flue thermal backup modes are shown in Figure 4.12 and Figure 4.13, respectively.

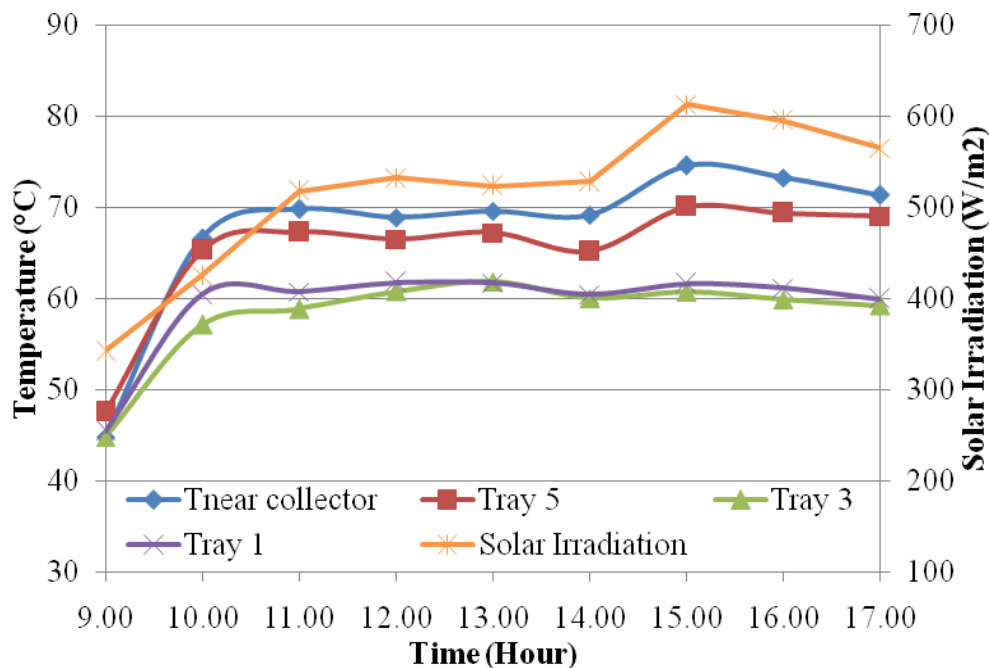


Figure 4.12: The average measured temperature of dryer under solar with clean hot air thermal backup mode

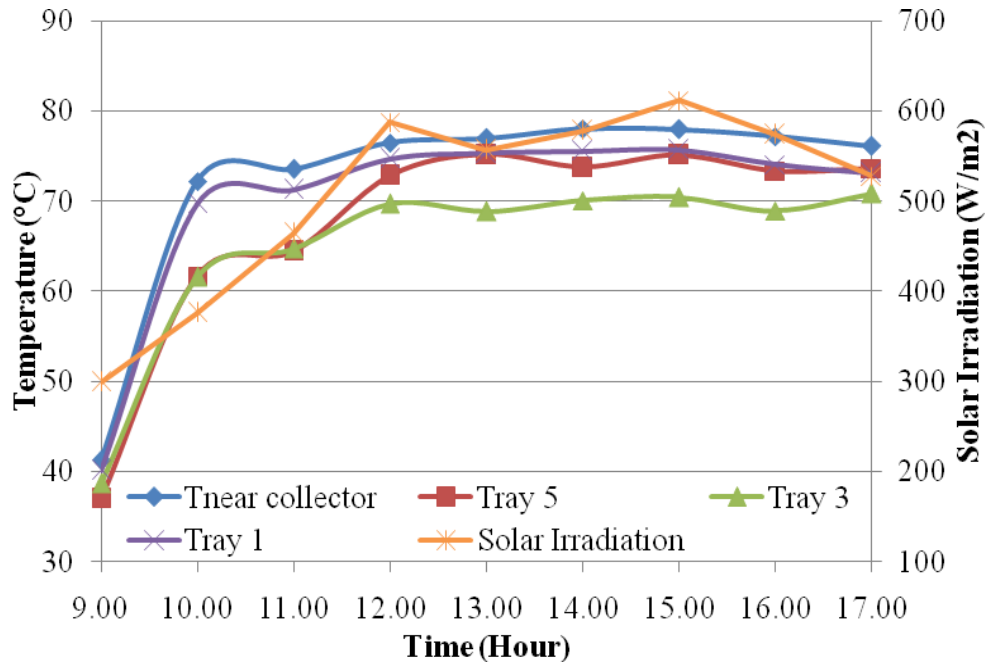


Figure 4.13: Variation of measured temperatures inside the dryer for solar with flue thermal backup mode

The hybrid mode result of solar with clean hot air thermal backup mode in Figure 4.12 indicates that the recorded average temperatures fluctuated throughout the day since they were highly dependent on the solar irradiation. The highest temperature was recorded in Tray 5 (top), since that in addition to the heat supplied from TBU, the temperature was enhanced from the absorbed direct solar irradiation. This followed by Tray 1 since it was exposed to the high temperature of the air flowing up. Tray 3 (middle) had the lowest temperature because it was affected by the shadow. The average temperature recorded in the drying chamber was within 56 to 73°C. The low averages of solar irradiation before 3pm were due to the cloudy and rainy day data.

Solar with flue thermal backup mode is shown in Figure 4.13. On a sunny day, the recorded solar irradiation was supposed to be in a bell shape. The graph indicates that the recorded temperature was quite stable even though the average solar irradiation was low in the afternoon. The pattern of temperature on each tray was same as in direct thermal backup mode but the temperature was slightly higher which was between 61 to 78°C. These temperatures could be reduced by decreasing the feeding rate of biomass fuel to the burner in order to meet the drying temperature requirement.

It could be concluded that with the same feeding rate of fuel, the heat supplied from flue-TBU mode was hotter than hot air-TBU mode.

4.5 Loading Experiment

The loading experiment had been conducted by drying of food and waste product which are chillies and EFB respectively. The aim of this experiment is to analyze the drying performance of the system by using various kind of product under different modes. The indirect heating from burner was applied for drying of food while direct heating for biomass product. The weight of product had been measured every hour until it reaches the required final moisture content. The modes of drying for both products are shown below.

a) Chillies

- Open sun drying
- Solar
- TBU by hot air
- Solar + TBU by clean hot air

b) EFB

- Open sun drying
- Solar
- TBU by flue
- Solar + TBU by flue

4.5.1 Experiments of Chillies Drying

The third stage of experimentation was continued with loading experiment. Chillies had been selected as food material to be dried. The drying chamber consists of 5 trays and the location of the trays is shown in Figure 4-2. For all modes of experiment, the initial mass of chillies to be dried on each tray was 500g. The mass reduction of

chillies was recorded every 2 hours from 9am until 5pm daily until the moisture content on each tray was reduces from 80% to 5% according to recommendation of Hollick (1999) [32]. The experiments were conducted under different modes of drying which were solar, clean hot air (indirect thermal backup) and solar-hot air. Control samples were dried simultaneously in open sun under the same weather conditions for comparison.

4.5.1.1 Solar Drying Mode of Chillies

The first chillies drying experiment was conducted with only the source of heat from solar. The drying process and measurement were done continuously until the drying product reach its final moisture content. The results of chillies drying under solar mode are shown in Figure 4.14.

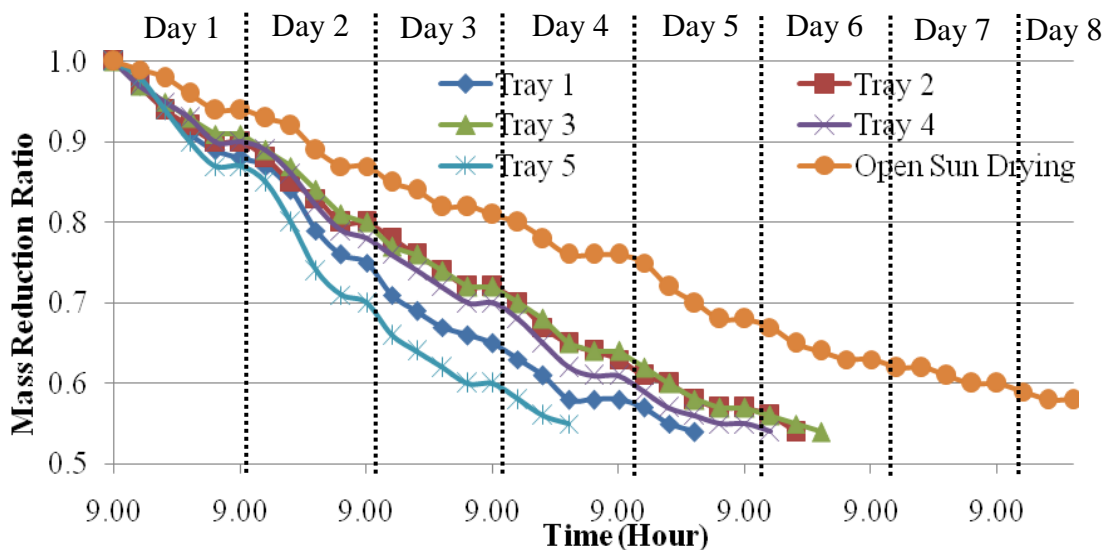


Figure 4.14: Drying of chillies under solar mode only

It was observed that the open sun drying required 174 hours to dry the chillies while each of the trays inside the dryer required different time, but all dried faster than the open sun drying. Tray 5 took only 78 hours since it was located at the top of drying chamber and the whole area was exposed to the solar irradiation. Next followed by Tray 1 since it is located near the solar collector, therefore the heat received from the hot air was higher. The other trays took around 122-126 hours to complete the drying process due to the shaded area. The mass reduction ratio

difference between the trays was slightly large. The summary of chillies drying periods under solar mode is shown in Table 4.4. It could be concluded that the location of the trays highly affected the drying performance.

Table 4.4: Summary of chillies drying periods under solar mode

Location	Total time (hours)
1. Open sun drying	174
2. Solar drying	
Tray 1	102
Tray 2	124
Tray 3	126
Tray 4	122
Tray 5	78

4.5.1.2 Thermal Backup Drying Mode of Chillies

Since chillies were under food category, it was dried using the clean hot air thermal backup mode. This mode transfers only the hot air into the solar dryer. The results are shown in Figure 4.15.

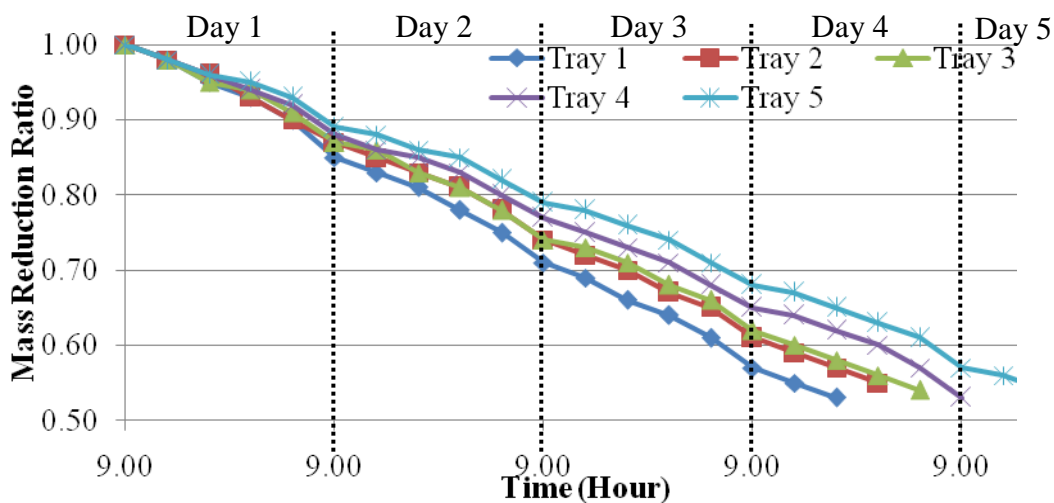


Figure 4.15: Drying of chillies under clean hot air thermal backup mode

The graph indicates that the chillies required around 76 to 100 hours to complete the drying process under hot air thermal backup mode. Sawdust has been used as the biomass fuel and the ignition started at 9am and the fuel feeding was continued at 2 hour interval until 11.00pm daily. The fuel feeding rate was constant at 0.5kg/hr throughout the drying process for all experiments. The lower the location of trays, the

faster the drying since it was located near the heat source. The difference between Tray 1 and Tray 5 was about 24 hours. Therefore the heat supplied from the TBU was quite constant to dry even at different tray location. Table 4.5 shows the summary of chillies drying periods under thermal backup mode.

Table 4.5: Summary of chillies drying periods under clean hot air thermal backup mode

Location	Total time (hours)
Tray 1	76
Tray 2	78
Tray 3	80
Tray 4	96
Tray 5	100

4.5.1.3 Hybrid Drying Mode of Chillies

The hybrid drying mode was conducted with heat source from solar and clean hot air thermal backup mode. During the night, the drying process worked continuously with the presence of heat source from clean hot air thermal backup. The results of drying chillies under hybrid mode are shown in Figure 4.16.

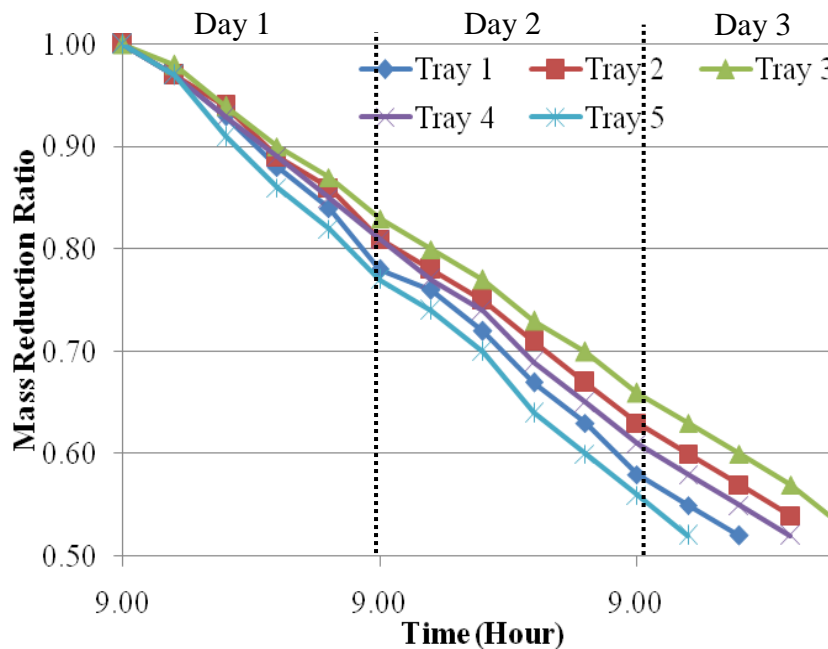


Figure 4.16: Drying of chillies under hybrid mode

The result indicated that the drying process took only 50 to 56 hours to dry the chillies. The trays drying pattern was same as in only solar mode with considerable time reductions. This mode performed two times faster than solar mode only. The differences of mass reduction ratio between the trays were very small which indicated that the heat supplied from the TBU enhanced the drying process even during the night time. The summary of chillies drying periods under hybrid mode is shown in Table 4.6.

Table 4.6: Summary of chillies drying periods under hybrid mode

Location	Total time (hours)
Tray 1	52
Tray 2	54
Tray 3	56
Tray 4	54
Tray 5	50

The overall comparisons of chillies drying modes under different modes are shown in Figure 4.17. It can be concluded that the hybrid mode is the best mode of drying since it took the shortest drying periods to reach the chillies final moisture content.

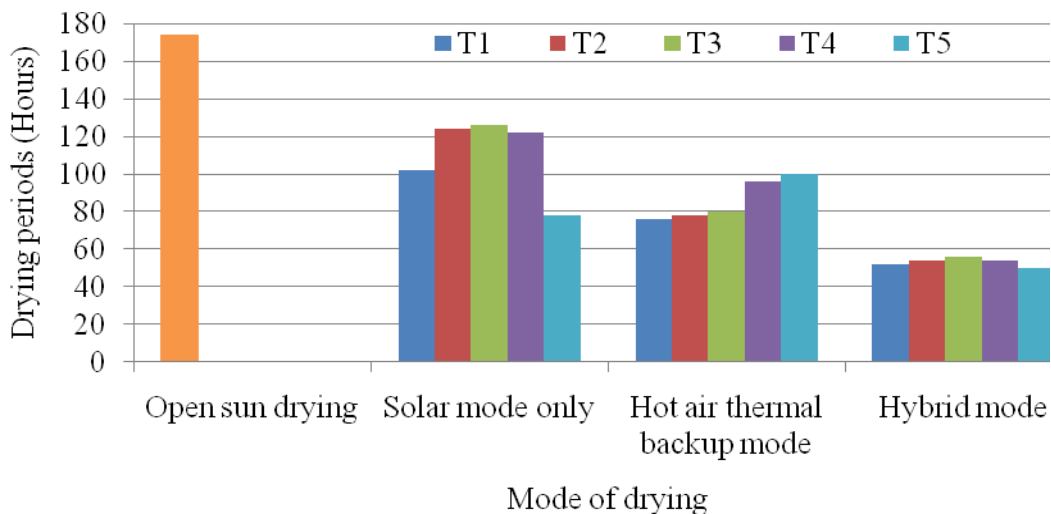


Figure 4.17: The overall comparison of chillies drying under different modes

4.5.2 Experiments of EFB

EFB has been selected as a sample of the biomass waste product to be dried. Same as previous loading experiment, each of the trays was loaded with 500g of EFB. The mass reduction of EFB was recorded every 2 hours from 9am until 5pm daily until the moisture content on each tray reduces from 75% to 6% as recommended by Rahim and Suffian (2006) [31]. The experiments were divided into three different modes of drying which are solar, flue thermal backup and solar-flue thermal backup. The open sun drying experiment was carried out under the same weather conditions of solar dryer and also performs as a reference sample for comparison.

4.5.2.1 Solar Drying Mode of EFB

Firstly, the EFB was dried by using the heat source from the solar irradiation. The weight reduction was measured continuously until it reached 5% final moisture content. The results are shown in Figure 4.18.

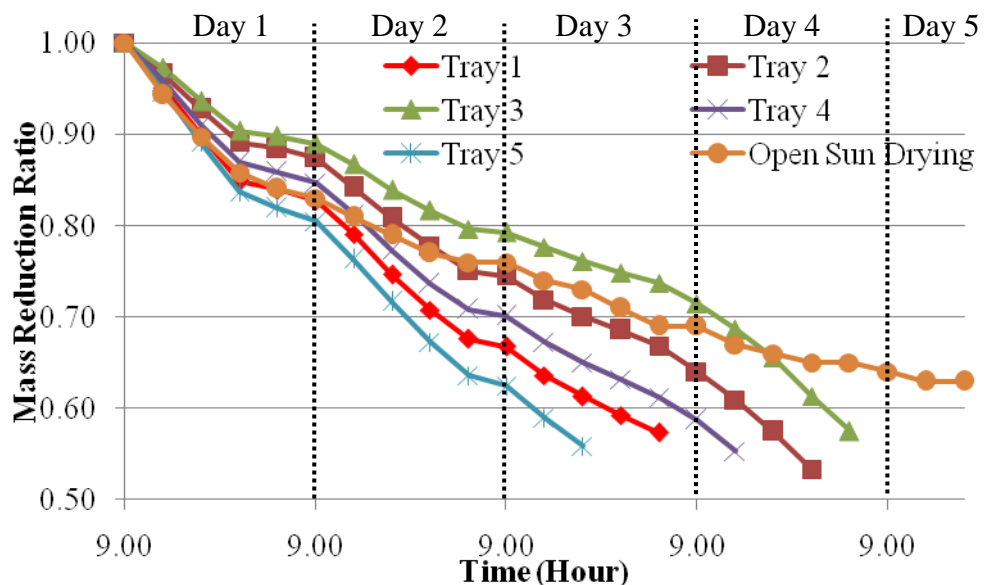


Figure 4.18: Drying of EFB under only solar mode only

The results indicated that the solar drying mode required around 52 to 80 hours to dry EFB, while it required 100 hours under open sun drying. The rate of open sun drying is slower than solar dryer as it could be observed from the slope of weight reduction measured results. The EFB was in shredded pieces therefore it took shorter

time than chillies to dry. Tray 5 took the shortest time to complete the drying since it located at the top and it exposed to solar irradiation, totally. This followed by Tray 1 since it was located near the solar collector and the heat flow through convection process was the highest. Tray 4 and Tray 2 stop nearly at the same drying time since it were located at the interval of the heat source. Tray 3 took the longest time to dry because it was located in the middle. It could be concluded that under this mode, the trays which located below Tray 5 having problem with the shadowed area. This causes a large difference of mass reduction ratio among the trays. The summary of EFB drying periods under solar mode is shown in Table 4.7.

Table 4.7: Summary of EFB drying periods under solar mode

Location	Total time (hours)
1. Open sun drying	100
2. Solar drying	
Tray 1	56
Tray 2	78
Tray 3	80
Tray 4	74
Tray 5	52

4.5.2.2 Thermal Backup Drying Mode of EFB

The EFB was dried using the flue thermal backup mode. The flue from the burner was directly connected to the solar dryer. The drying process was run continuously even at night since it was not affected by the presence of solar. The results are shown in Figure 4.19.

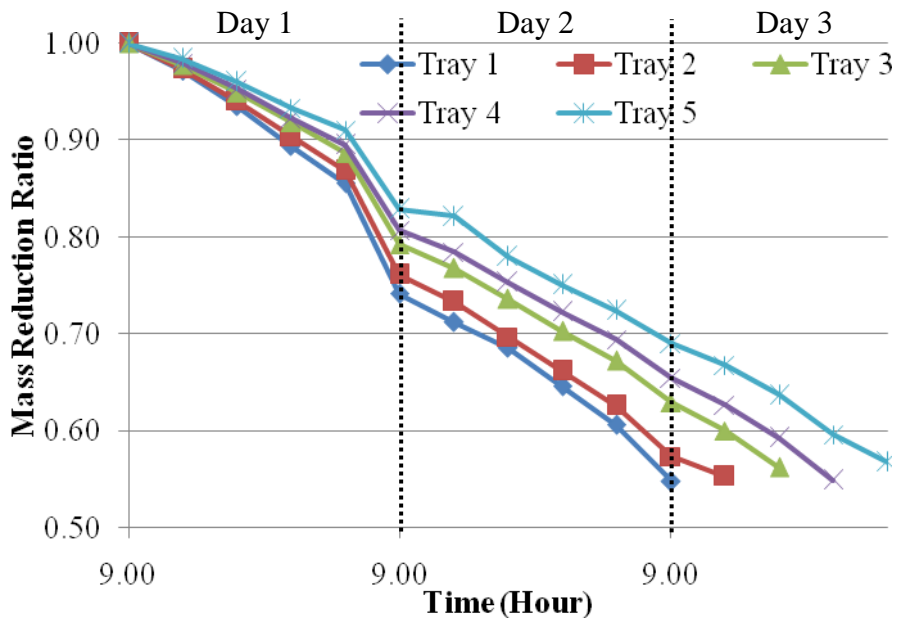


Figure 4.19: Drying of EFB under direct thermal backup mode

The results indicated that under flue thermal backup mode, the drying process took about 48 to 56 hours to dry the EFB. The ignition started at 9am and the fuel feeding was continued at 2 hour interval until 11pm daily. The summary of EFB drying periods under flue thermal backup mode is shown in Table 4.8. It was observed that the lower the trays, the faster the drying complete since it was exposed to the source of heat. The time difference between the trays to reach the final moisture content is constant at 2 hour interval.

Table 4.8: Summary of EFB drying periods under flue thermal backup mode

Location	Total time (hours)
Tray 1	48
Tray 2	50
Tray 3	52
Tray 4	54
Tray 5	56

4.5.2.3 Hybrid Drying Mode of EFB

The combined drying mode was conducted using the source of heat from solar and the flue from the TBU. At night, the drying process runs continuously with the presence of biomass mode. The results are shown in Figure 4.20.

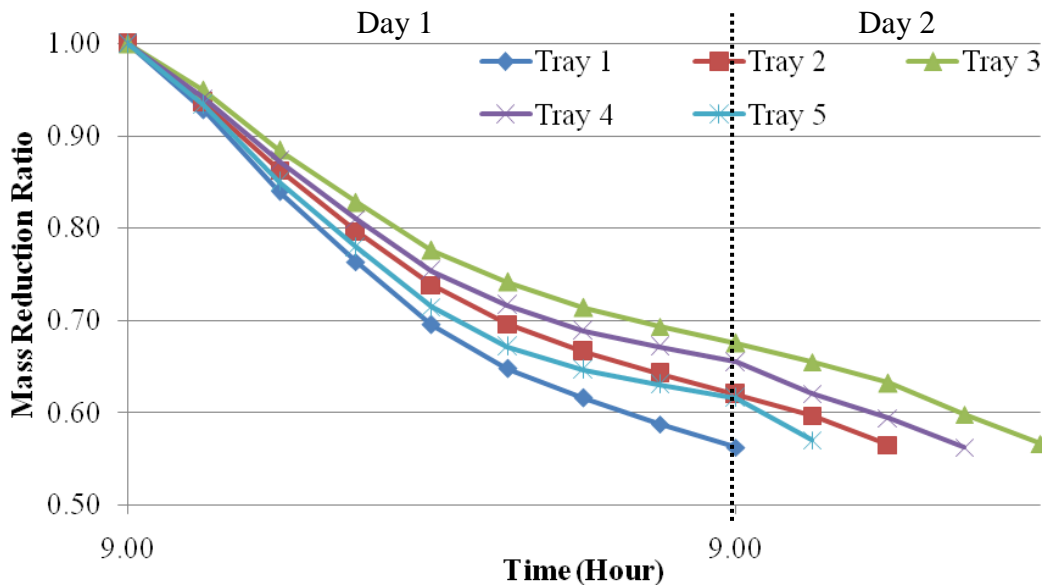


Figure 4.20: Drying of EFB under hybrid mode

Hybrid mode took about 24 to 32 hours to complete the drying process. Compared to the same mode of chillies drying, the drying rate of EFB was faster since the temperature of flue heat was higher than hot air heat. Based on the graph shown in Fig. 4-20, Tray 1 requires 24 hours to dry EFB since it received a continuous heat from the flue and it did not rely on the availability of solar irradiation. Tray 5 and

Tray 2 took 26 and 28 hours respectively to complete the drying process and followed by Tray 4 and Tray 3 at 30 and 32 hours. The location of the tray and also shadowed area causes the difference of drying rate at each tray. The summary of EFB drying periods under hybrid mode is shown in Table 4.9.

Table 4.9: Summary of EFB drying periods under hybrid mode

Location	Total time (hours)
Tray 1	24
Tray 2	28
Tray 3	32
Tray 4	30
Tray 5	26

The overall comparisons of EFB drying modes under different modes are shown in Figure 4.21. It can be concluded that the hybrid mode is the best mode of drying since it took the shortest drying periods to reach the EFB final moisture content.

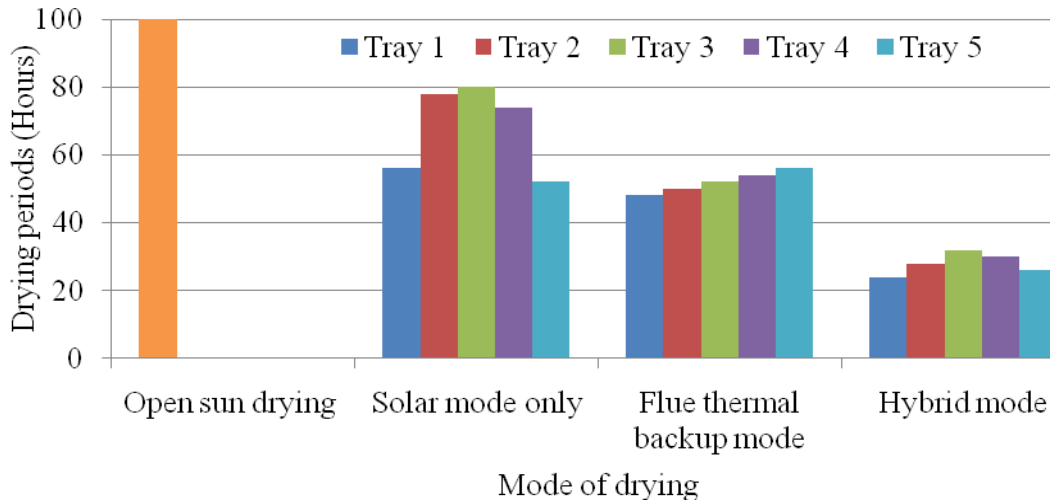


Figure 4.21: The overall comparison of EFB drying under different modes

4.6 Thermal Analysis of the Solar Collector

The thermal analysis of the solar collector was calculated based on the experimental measurements. It depends on collector performance to convert the solar irradiation to thermal energy and thermal losses to the surroundings. The convection occurred mostly at the top and bottom of the absorber. The absorber plate was assumed to be in horizontal since most of the heat transfer occurred on the upper and bottom side and not through the both sides as inclined plate. The buoyancy force is exclusively normal to the surface [85]. Inside the dryer, a cold collector surface is facing downward and a hot collector surface is facing upward. The flow is driven by descending and ascending parcels of fluid [85]. The solar thermal efficiency depends essentially on thermal losses from outer surfaces of solar collector [59]. The governing equations are based on Incropera et al. [85].

The type of flow in the free convection is determined by calculating the Rayleigh number, Ra . It is based on the characteristic length, L_c of the geometry.

$$Ra = GrPr \quad (4.1)$$

where if:

- $Ra < 1000000000$: Laminar flow
- $Ra > 1000000000$: Turbulent flow

$$Gr = \frac{g\beta(T_{ab} - T_1)L_c^3}{\nu^2} \quad (4.2)$$

where:

$$L_c = A_s/P$$

$$\beta = 1/T_1$$

$$T_{ab} = (T_c + T_1)/2$$

The recommended correlations for the average Nusselt number, Nu for the upper surface and lower surface of hot plate were given in Equation 4.3 and Equation 4.4 respectively [85].

$$Nu = 0.54Ra^{1/4} \quad (10^4 \leq Ra \leq 10^7) \quad (4.3)$$

$$Nu = 0.27Ra^{1/4} \quad (10^5 \leq Ra \leq 10^{10}) \quad (4.4)$$

Finally, based on the previous Nu , the top and bottom heat loss are evaluated as shown in Equation 4.5 and Equation 4.6 respectively.

$$h_{top} = \frac{Nu.k}{L_c} \quad (4.5)$$

$$h_{bottom} = \frac{Nu.k}{L_c} \quad (4.6)$$

The data for thermal analysis of solar collector was obtained from the experimental measurements. The input of the data was based on the results of average no-load experiment. The results of calculated heat transfer are shown in Table 4.10.

Based on the results, the heat transfer at the top collector is two times higher than the bottom collector. The heat transfer highly depended on the location of the collector surface. The area exposed to the heat is higher at the top collector surface than at the bottom part; therefore the heat transfer was higher at the top. The same ratio of heat transfer was obtained by Jilte and Datye [101] in their studies on the design and performance analysis of solar dryer of banana slices.

Table 4.10: The external free convection flows on the upper and bottom surface of solar collector

No.	Attributes	Value
1	Rayleigh number, Ra	1.541×10^6
3	Ratio, Gr/Re^2	$10.35 > 1$ (Natural convection)
4	Average Nu number at the upper surface of hot plate, Nu	19.03
5	Average Nu number at the lower surface of hot plate, Nu	9.51
6	The top heat transfer of the collector, h_{top}	$2.37 \text{ W/m}^2 \cdot \text{K}$
7	The bottom heat transfer of the collector, h_{bottom}	$1.19 \text{ W/m}^2 \cdot \text{K}$

4.7 Analysis of the Performances of Solar Dryer and TBU

Two different types of efficiencies were identified and evaluated including the collector efficiency and the overall dryer efficiencies of the systems. The calculations were based on the experimental measurements. The studies are important in order to analyze the system characteristic. The governing equations are shown accordingly.

4.7.1 The Efficiency of Solar Collector

The efficiency of solar collector, η_c is defined as the ratio of the useful energy gain to the incident solar energy [68] which for air heating collector, may defined as:

$$\eta_c = \frac{\dot{V}c_p \Delta T}{A_c I} \quad (4.7)$$

The collector efficiency, η_c had been calculated based on the average results obtained from no-load experiments. The results are shown in Figure 4.22. Based on the results, it could be observed that the highest collector efficiency is at 1pm which is 1.95%. It is due to the peak hour of temperature rises, where typically, the hour angle is defined to be zero at solar noon and the sun is highest in the sky.

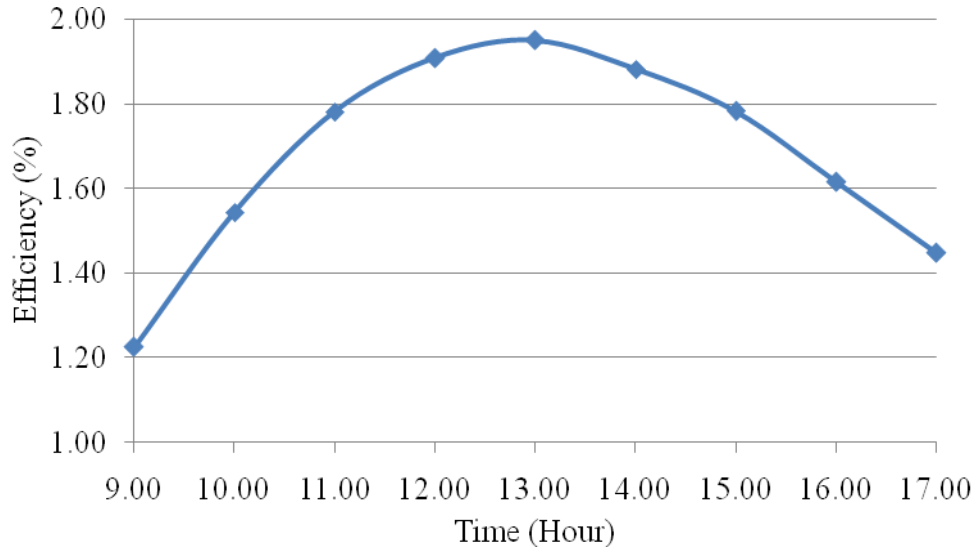


Figure 4.22: Transient behavior of the collector efficiency

The collector efficiency is considerably low which around 1.2% to 1.9%. The reason behind that was due to the large loss to the surroundings and the use of the Perspex as cover material. Using glass will enhance the transmissivity of the solar irradiation and increase the collector efficiency. The other reason is that the inlet of the environmental air to the collector is near the upper surface. The CFD simulation had shown that the hotter air gap is at the bottom surface of the collector. An improvement can be done by changing the location and the size of the inlet air to the bottom side of solar collector.

4.7.2 The Drying Efficiency, η_d

The drying efficiency, η_d was calculated by considering the type of the thermal input whether from solar (s), thermal backup (tb) or hybrid inside the dryer. It is depending on the product mass reduction in drying time as shown in Equation 4.8.

$$\eta_d = \frac{M\lambda}{t[(\Sigma I_c A_c)_s + (\dot{m}c_p \Delta T)_{tb}]} \quad (4.8)$$

where:

$$\Delta T = T_{ib} - T_{chimney}$$

The result of drying efficiency of chillies and EFB based on different operational modes are shown in Figure 4.23. The efficiency increases from open sun to hybrid drying mode.

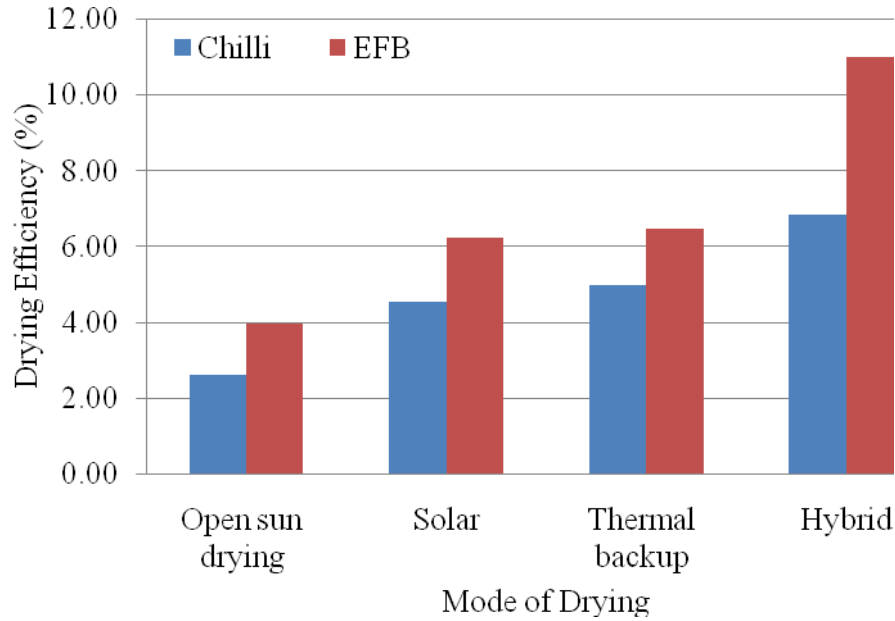


Figure 4.23: Comparison of drying efficiencies at different modes

The lowest efficiencies for both products was in open sun drying and followed by solar mode because the heat received is inconstant and it depends solely on the weather conditions. The drying process took longer time and interrupted especially during the cloudy days and at night. In thermal backup mode, the drying process operates continuously without disruption by the weather condition and hence resulted in higher enhancement index than solar mode. It was observed that the highest efficiencies for both products were in the hybrid mode. The efficiencies of chillies and EFB under hybrid mode were 6.85% and 11% in 5.25 and 4.17 days respectively. The drying process occurred continuously even at night since it was supported with the thermal backup unit. During the day, the heat received was higher than at night since the heat from solar was extended by the thermal backup unit.

To highlight the enhancement gained by using thermal back up, an enhancement index, I_d was introduced in this study and calculated by involving the efficiency and time reduction to observe the best drying mode. The calculation is shown in Equation 4-9.

$$I_d = \frac{\eta_{Drying\ mode} / T_{Drying\ mode}}{\eta_{Opensundring} / T_{Opensundring}} \quad (4.9)$$

The calculated enhancement index drying of chillies and EFB are shown more details in Table 4.11 and Table 4.12. The open sun drying was taken as a reference for comparison. The drying time of both products reduced considerably beginning from open sun, solar, thermal backup and hybrid mode.

Table 4.11: The drying efficiencies and enhancement index of chillies

	Efficiency, η_d (%)	Drying period (days)	Index, I_d
Open sun drying	2.61	7.25	1.00
Solar	4.54	5.25	2.40
Thermal backup	4.96	4.17	3.03
Hybrid	6.85	2.33	8.17

Table 4.12: The drying efficiencies and enhancement index of EFB

	Efficiency, η_d (%)	Drying period (days)	Index, I_d
Open sun drying	3.95	4.21	1.00
Solar	6.22	3.33	1.99
Thermal backup	6.45	2.33	2.94
Hybrid	9.86	1.33	8.80

According to Bena and Fuller [17], the drying performance are hard to compare since most measurement and results reported limited to only one type of crop in a specific particular dryer and in a single climate. The drying efficiencies reported in the literature have been shown to vary widely depending on the loading densities and weather conditions [84], [102], [103]. Besides, it is also influenced by the type of product and its final moisture content level [16-18], [38]. The final moisture in a product generally requires more energy to extract than the initial moisture content, and the preparation of the crops prior to drying affects the thermal efficiency. However, the drying efficiencies achieved in the present study are lower as compared to other reported drying efficiencies since the dryer was fabricated in small scale and it was tested with only small amount of product. Besides, heat obtained on the trays is low due to the shadow of tray arrangement and there were heat losses from inside dryer to the environment.

4.8 Chapter Summary

In this current chapter, the entire experimental results of the thermal backup and solar dryer were discussed. Three types of biomass fuels, rice husk, EFB and wood chips at different feeding rate were burnt in the burner of the TBU in order to study the suitability for food drying. Wood chips with feeding rate of 0.25 kg/hr had been selected as the most suitable biomass fuel rate since it produced stable thermal conditions within the required temperature, easy to ignite, even combustion and produced light smoke. The dried biomass wastes product can also being used as the fuel in next drying operation. In this case, the biomass burner is also known as biomass to biomass or biomass to food dryer.

The solar dryer experiments were conducted under no-load and loading of drying materials with different modes of heating. The no-load experimental results indicated that a combined drying mode of solar with TBU recorded the highest drying temperature inside the dryer. The no-load experimental results were compared with the simulation result to study the heat distribution inside the dryer. The performance of the dryer with loading was tested with drying of chillies and EFB. The loading experiments proved that a combined drying mode resulted in the shortest drying period.

The solar collector efficiencies are totally depending on the orientation of the sun. The highest drying efficiencies and the fastest drying time of chillies and EFB were obtained from solar-thermal hybrid mode. Hence, it was proved that the hybrid mode enhanced the drying process of food and biomass wastes.

CHAPTER 5

NUMERICAL SIMULATION

5.1 Chapter Overview

This chapter discusses the CFD (Computational Fluid Dynamics) method and literature survey done by previous researchers to simulate the solar dryer. The steps of solution are presented in more details beginning from the geometry model completion and the parameter setting of the case study. The results of simulation are presented and discussed. In addition, the comparison between the simulation and experimental results are also presented.

5.2 Overview of Previous attempts on Dryer Simulation

CFD is a tool for solving fluid flow and heat transfer problems in complex geometries. It is typically applied to modeling continuous processes and systems. CFD model eliminates many typical assumptions such as plug flow, averaged quantities and many more. It has successfully replicated the physical domain in the form of computerized prototype and able to solve operating issues in full-scale systems.

Nowadays, it has been widely applied in the industrial and non industrial application area. Among software packages that are available are PHOENICS[®] (Flowsolve, London), CFX[®] (AEA, Harwell, UK), STAR-CD[®] (CD, London) and FLUENT[®]/FIDAP[®] (Lebanon, USA). CFD tool may provide efficient and cost-saving assistance in the development and innovations of thermo-fluid areas. It provides easy visualization of flow and heat parameters that can replace the very costly experiments. However, a disadvantage of CFD model is that it is only suitable for steady-state predictions. The simulation may consume a long computational time to solve in cases of unsteady.

The simulations had been carried out in this project to study the performance of solar dryer performance. FLUENT[®] software had been used where the input was based on the experimental boundary conditions. CFD software had been used in solar drying field to predict air velocities in the drying chamber hence, reducing the difficulties to measure air velocities at various location which in manually will require a lot of sensors. Besides, the CFD may be used as a drying optimization tool to improve the design and to predict the drying time if connected to the thin-film equation [104]. There are no precise references to the literature concerning numerical simulation of air flows and heat transfer in the interior of dryers. The literature review presents on the application of FLUENT[®] software in solving fluid flow conducted in the past by other researchers. However, there were shortages in the literature for the attempts of dryer simulation.

Rigit and Low [105] had studied the heat and mass transfer in a solar dryer with biomass backup burner to obtain the optimum operating temperature. The modeling was performed on an empty chamber without the pepper berries using CFD software, STAR-CD. The simulation had been conducted under natural and forced convection. They had identified that heat and mass transfer by natural convection is more suitable for drying pepper berries with solar irradiation. The simulated result indicates that the thermal heat distribution in drying chamber was uniformly distributed. Solar dryer usually having difficulty to provide uniform hot temperature and air flow which lead to non-uniformity of moisture content over the products being dried.

Dyah et al. [106] had used CFD method to analyze the airflow and heat transfer by varying positions of fan in a solar dryer. The fan was tested by positioning into two different locations, at the bottom inlet and in the middle upper dryer. They had identified that the second position produced more uniform temperature and air flow. The maximum airflow was observed at the inlet and reduced as it approaches outlet. They found that the simulation model described the real condition up to 89%.

Further studies of air movement in dryer had been carried out by Mathioulakis et al. [104]. The dryer which was designed to dry fruits and vegetables, consist of heat exchanger to enhance the heated air supplied from LPG gas burner. Centrifugal fan was located inside the dryer to force the air movement into the drying chamber. Under

different trays location, they found two areas of low air velocity, one was close to the entrance of the air and another one was in the middle of the drying chamber. They had concluded that the air velocities were related very well to the pressures inside the drying chamber. Summary of previous works on simulation studies is given in Table 5.1.

Table 5.1: Summary of simulation studies conducted by previous researchers

Researchers	Scope of Study	Findings
Rigit and Low [105]	Heat and mass transfer in a solar dryer with biomass backup burner	Uniform thermal heat distribution in drying chamber
Dyah et al. [106]	Airflow and heat transfer in a solar dryer	Simulation model described the real condition up to 89%.
Mathioulakis et al. [104]	Movement of air in dryer	The air velocities were related to the pressures inside the drying chamber

The studies that had been conducted by previous researchers have shown that the application of CFD tools is very flexible and wide to solve according to the problem studied even though it may consume a long time to generate result. It is able to generate closer result to the real processes. The simulation results provide practical information by identifying the weakness of the system and consequently assist in design improvement.

5.3 Modeling and Simulation of the Hybrid Dryer

Two analyses techniques had been adopted in the present work, experimental and numerical. The CFD simulation was carried out to investigate the fluid flow and temperature distribution through the solar dryer and it will be validated with the experiment results. These comparisons were made to improve on any problems that occur with the solar dryer model and to ensure the workability and optimum efficiency of the solar dryer.

The CFD analysis technique is a set of numerical analysis where it minimizes the variation calculus to obtain approximate solutions. Finite Volume Analysis (FVA) is one the technique used for CFD analysis by programming mesh to contain the material and structural properties which define how the structure will react to certain

loading conditions. The computational model was carried out by GAMBIT[®] software, which was used to create the geometry of the model and generate the computational grid. Then, the simulation was performed using FLUENT[®] commercial software.

5.3.1 Computational Model

A two dimensional (2-D) geometry model of solar dryer geometry was created using GAMBIT[®] (version 2.2.30). The inlet source for solar and biomass mode were different according to the type of mode. The solar drying mode was design with air inlet located near the collector and at the side wall to enhance the heat flow. In order to maximize the heat received from burner and to minimize the heat escape to the outside, the air inlet was closed in biomass mode. It received heat only from the burner inlet. Label of the model is shown in Figure 5.1.

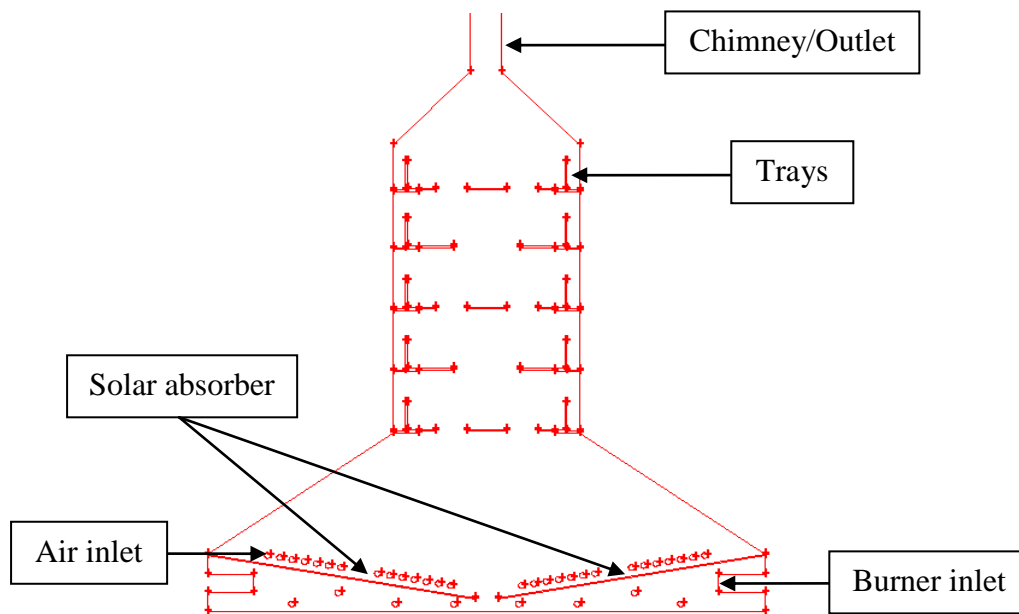


Figure 5.1: Labeled GAMBIT[®] solar dryer model

5.3.2 Computational Grid

The domain was discretized into a finite set of control cells. It was meshed with tri mesh elements and the face meshing type was pave, meaning an unstructured grid of mesh elements was created. The bottom part of the model was meshed with smaller interval size of 1.5 in order to get more accurate results surrounding the solar collector

and biomass burner inlet. The middle and upper part of solar dryer was meshed with larger interval size of 2 and 3 to reduce simulation time. The solar and biomass model had a total of 32394 and 209204 cells respectively. The meshes on solar dryer model are shown in Figure 5.2.

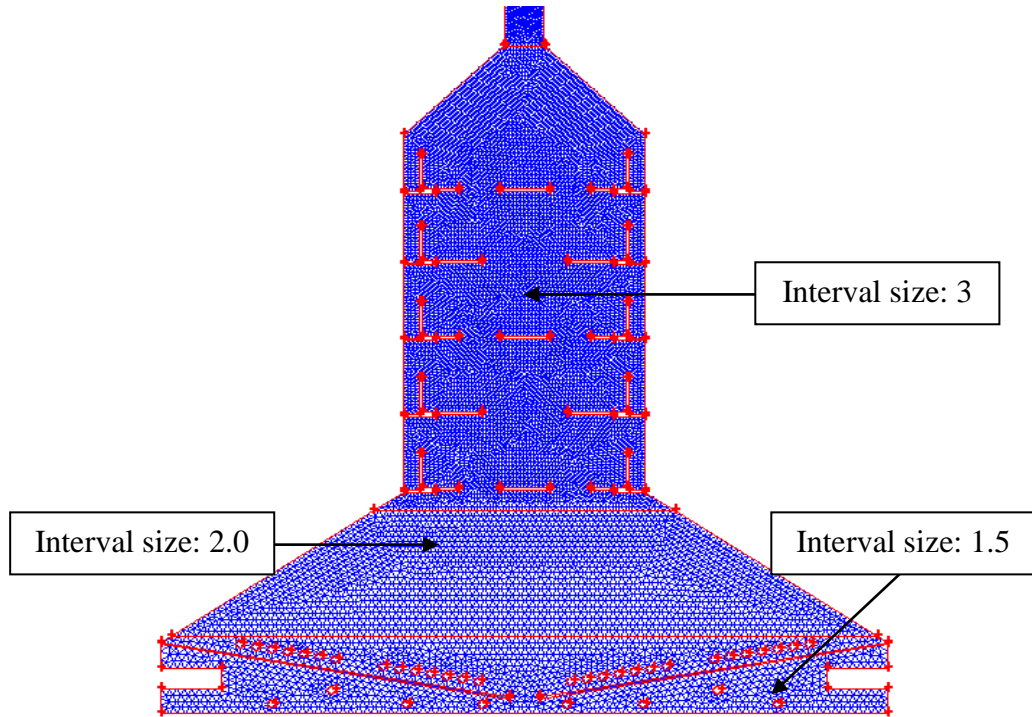


Figure 5.2: Mesh on solar dryer model

5.3.3 Governing Equations of the Thermo Fluid Process

The governing equations for CFD are based on conservation of mass, momentum, and energy. FLUENT[®] uses a finite volume method (FVM) to solve the governing equations. The FVM involves discretization and integration of the governing equation over the control volume. The following is a summary of the theory involved in the FLUENT[®] analysis and is based on the FLUENT[®] User's Manual and CFD studies on solar dryer, Dyah et al. [106].

Several assumptions had been made before modeling the solar dryer as below. Based on the assumption made, the unnecessary equations were removed.

- 2-Dimensional
- Flow in x and y-direction; $u \neq 0$, $v \neq 0$

- Steady state; $\delta/\delta t = 0$
- Compressible; ρ is not constant
- Since the working fluid is gas, the body forces are very small and could be neglected, $g = 0$

5.3.3.1 Continuity Equation

In steady state process, the rate at which mass enters a system is equal to the rate at which mass leaves the system. Properties such as density, pressure, temperature, and velocity are taken to be well-defined at infinitely small points, and are assumed to vary continuously from one point to another. Hence, the change over time can be cancelled, and the continuity equation in two dimensional states [107] becomes:

$$\frac{\cancel{\partial \rho}}{\cancel{\partial t}} + \frac{\partial(\rho u)}{\partial x} + \frac{\partial(\rho v)}{\partial y}$$

$$\frac{\partial(\rho u)}{\partial x} + \frac{\partial(\rho v)}{\partial y} = 0 \quad (5.1)$$

5.3.3.2 Conservation of Momentum Equation

The law of conservation of momentum explains that momentum is neither lost or gained. The two dimensional steady state was divided into two components. Gravity is not taken into consideration in x-component, hence it can be cancelled. The change over time is canceled in both component, x and y.

(i) x-component

$$\rho \left(\frac{\cancel{\partial u}}{\cancel{\partial t}} + u \frac{\partial u}{\partial x} + v \frac{\partial u}{\partial y} \right) = \cancel{\rho g_x} - \frac{\cancel{\partial p}}{\partial x} + \mu \left(\frac{\partial^2 u}{\partial x^2} + \frac{\partial^2 u}{\partial y^2} \right)$$

$$u \frac{\partial(\rho u)}{\partial x} + v \frac{\partial(\rho v)}{\partial y} = \mu \left(\frac{\partial^2 u}{\partial x^2} + \frac{\partial^2 u}{\partial y^2} \right) \quad (5.2)$$

(ii) y-component

$$\rho \left(\frac{\partial v}{\partial t} + u \frac{\partial v}{\partial x} + v \frac{\partial v}{\partial y} \right) = \rho g_y - \frac{\partial p}{\partial y} + \mu \left(\frac{\partial^2 v}{\partial x^2} + \frac{\partial^2 v}{\partial y^2} \right)$$

$$u \frac{\partial(\rho v)}{\partial x} + v \frac{\partial(\rho v)}{\partial y} = \mu \left(\frac{\partial^2 v}{\partial x^2} + \frac{\partial^2 v}{\partial y^2} \right) - \frac{\partial \rho}{\partial y} \quad (5.3)$$

5.3.3.3 Conservation of Energy Equation

The first law of thermodynamics stated that the total energy of conserved [85]. When energy is changed from one form to another in an isolated system, there is no change in the total amount of energy. Same as previous equation, the change over time and gravity on x-component is cancelled.

$$\frac{\partial T}{\partial t} + u \frac{\partial T}{\partial x} + v \frac{\partial T}{\partial y} = \frac{\kappa}{\rho c_p} \left(\frac{\partial^2 T}{\partial x^2} + \frac{\partial^2 T}{\partial y^2} \right) \quad (5.4)$$

$$\left(u \frac{\partial(\rho T)}{\partial x} + v \frac{\partial(\rho T)}{\partial y} \right) = \frac{\kappa}{c_p} \left(\frac{\partial^2 T}{\partial x^2} + \frac{\partial^2 T}{\partial y^2} \right) \quad (5.5)$$

5.3.3.4 State Equation

The state of equation illustrates the dependence between air density and temperature [108]. To close the solution domain, the state equation was considered as:

$$pV = nRT \quad (5.6)$$

5.3.4 Irradiation Model

P-1 irradiation model had been used for heat transfer simulation to study the effect of heating or cooling of surface due to irradiation. The irradiation flux, q_r is given by Equation 5.6.

$$q_r = \frac{1}{3(\alpha + \sigma_s) - C\sigma_s} \nabla G \quad (5.7)$$

Where α is the absorption coefficient, σ_s is the scattering coefficient, G is incident irradiation and C is the linear-anisotropic phase function coefficient. P-1 model assumes that all surfaces are diffuse. This means that the reflection of incident irradiation at the surface is isotropic with respect to the solid angle. The implementation assumes gray irradiation. The P1-irradiation model was applied only with the presence of solar.

P-1 irradiation model was used for heat transfer simulation to study the effect of heating or cooling of surface due to irradiation. P-1 model assumes that all surfaces are diffuse. This means that the reflection of incident irradiation at the surface is isotropic with respect to the solid angle. The implementation assumes gray irradiation. The P1-irradiation model was applied only with the presence of solar.

5.3.5 Turbulence Modelling

The commercial code FLUENT[®] Version 6.2.16 had been used. A "2ddp" option was used to select the 2-dimensional, double-precision solver before setting up boundary condition in FLUENT[®]. Each floating point number in the double-precision solver is represented using 64 bits in contrast to the single-precision solver which uses 32 bits. The extra bits increase not only the precision but also the range of magnitudes that can be represented. The turbulent type of flow inside the dryer was determined by calculating Re numbers. The additional assumptions of the CFD model as described below.

- a. The flow is steady, fully developed and two dimensional.
- b. The thermal conductivity of the solid wall and roughness material does not change with temperature.

A mixing application of flows with $Re \geq 10^4$ can be regarded as fully turbulent. The flow is said to be turbulent when all the transport quantities (mass, momentum

and energy) exhibit periodic, irregular fluctuations in time and space. In this study, a turbulence model of two equation standard k-ε model [109] had been used. The standard k-ε model is a semi-empirical model based on model transport equations for the turbulent kinetic energy (k) and its dissipation rate (ϵ). Flow flows from laminar to turbulent. At turbulent, particles hit each other and lose momentum. This causes fluctuations in velocity at the turbulent part as shown in Figure 5.3.

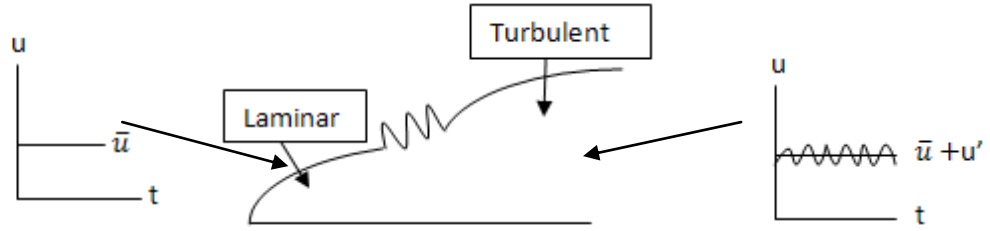


Figure 5.3: Laminar to Turbulent Transition.

Due to fluctuations in velocity, Navier-stokes equations are in the form of $\bar{u} + u'$ and $\bar{v} + v'$. The k-ε model is used to compensate for the fluctuating parts which are u' and v' . Hence, the shear stress in turbulent region, τ is shown in Equation 5.7.

$$\tau = (\mu + \mu_t) \frac{du}{dy} \quad (5.7)$$

Where μ is fluid property and μ_t is turbulent viscosity, obtained as function of shape, Reynolds number, Prandtl number, etc. The “eddy” or turbulent viscosity, μ_t is computed by combining k and ϵ as shown in Equation 5.8.

$$\mu_t = \rho C_\mu \left(\frac{k^2}{\epsilon} \right) \quad (5.8)$$

In addition to the standard k-epsilon, the turbulence model for mode that involves irradiation is modeled using Renormalization Group (RNG). It is based on the two equation models of the Reynolds-Averaged Navier Stokes (RANS) equations. This RNG k-epsilon model is able to produce more accurate results for boundary layer flows than the standard k-epsilon model since it has additional term in its ϵ equation. The turbulence equations being solved using the first order upwind scheme by the

commercial software, FLUENT[®]. The type of turbulence model selection is summarized in Table 5.2.

Table 5.2: Models selection according to drying modes

Modes of Experiment	Irradiation Model	k-ε Model
Solar only	P1	RNG
Indirect heating from burner	-	Standard
Indirect heating from burner with solar	P1	RNG
Direct heating from burner	-	Standard
Direct heating from burner with solar	P1	RNG

5.4 Simulation Procedure

Simulation studies were divided into five drying modes. It had been conducted under no-load experiment to analyze the temperature distribution inside solar dryer. The simulation was done under solar, thermal back up and combination of solar-thermal back up. The thermal back up consists of two heating modes which were fuel gas and hot air. The best drying mode was selected based on the thermal performance comparison of the simulation and experimental results.

5.4.1 Boundary Conditions

The boundary conditions of the model were divided into two categories, which were solar mode and biomass mode. The boundary conditions of both modes consisted of six zones. In solar mode only, the burner was disconnected and the air inlet remained. The working fluid, air is assumed to be compressible, hence the ideal gas state equations was used to estimate the density variation with temperature. The parameters and technical data for the facilities are listed in Table 5.3.

Table 5.3: Parameters used in the numerical simulation

Item:	Solids	Units	Value
Aluminum – absorbing plate		ρ (kg/m ³)	2719
		Cp (J/kg·K)	871
		k (W/m·K)	202.4
Perspex – wall		ρ (kg/m ³)	1150
		Cp (J/kg·K)	1450
		k (W/m·K)	0.25
Polyvinyl chloride (PVC) – chimney		ρ (kg/m ³)	1410
		Cp (J/kg·K)	900
		k (W/m·K)	0.19
Air			
density (function temperature and pressure)		ρ (kg/m ³)	variable
thermal conductivity		k (W/m·K)	0.0242
dynamic viscosity		μ (kg/m·s)	1.7894E-05
specific heat		Cp (J/kg·K)	1006.43
Flue gas			
density		ρ (kg/m ³)	0.522
thermal conductivity		k (W/m·K)	0.0441
dynamic viscosity		μ (kg/m·s)	2.829 E-05
specific heat		Cp (J/kg·K)	1374.091

The thermal condition is depending to the type of model. Thermal conditions with and without P1 model were set as mixed and convection respectively. A mixed thermal condition represent that the heat was received more than one source. The specifications of the boundary conditions for velocity magnitude and temperature were based on the estimated values. The boundary conditions for both models are shown in more details in Table 5.4 and Table 5.5.

Table 5.4: Boundary conditions with P1 model (Involved with Solar mode)

Zone	Boundary Conditions	Specifications
Air inlet	Velocity Inlet	- Velocity Magnitude (m/s): 0.15 - Temperature (K): 310
Outlet	Outflow	-
Solar collector	Radiator	- Loss coefficient: 3 - Heat Transfer Coefficient: 25 W/m ² ·K - Temperature (K): 340
Trays	Wall	- Thermal Conditions: Mixed - Heat Transfer Coefficient: 6 W/m ² ·K - Free Stream Temperature (K): Air temperature surrounds the trays (dryer temperature) - External Irradiation Temperature (K): 318 - Wall Thickness: 0.003 m
Perspex cover	Wall	- Thermal Conditions: Mixed - Heat Transfer Coefficient: 6 W/m ² ·K - Free Stream Temperature (K): Air temperature surround the Perspex cover - External Irradiation Temperature (K): 318 - Wall Thickness: 0.003 m
Chimney	Wall	- Thermal Conditions: Mixed - Heat Transfer Coefficient: 1.1 W/m ² ·K - Free Stream Temperature (K): Air temperature inside chimney - External Irradiation Temperature (K): 318 - Wall Thickness: 0.003 m

Table 5.5: Boundary conditions without P1 model (Biomass mode only)

Zone	Boundary Conditions	Specifications
Burner inlet	Velocity Inlet	- Velocity Magnitude (m/s): 0.27 - Temperature (K): 340
Outlet	Outflow	-
Solar collector	Radiator	- Loss coefficient: 3 - Heat Transfer Coefficient: 25 W/m ² ·K - Temperature (K): 330
Trays	Wall	- Thermal Conditions: Convection - Heat Transfer Coefficient: 6 W/m ² ·K - Free Stream Temperature (K): Air temperature surrounds the trays (dryer temp.) - Wall Thickness: 0.003 m
Perspex cover	Wall	- Thermal Conditions: Convection - Heat Transfer Coefficient: 6 W/m ² ·K - Free Stream Temperature (K): Air temperature surround the Perspex cover - Wall Thickness: 0.003 m
Chimney	Wall	- Thermal Conditions: Convection - Heat Transfer Coefficient: 1.1 W/m ² ·K - Free Stream Temperature (K): 325 - Wall Thickness: 0.003 m

5.4.2 Numerical Solution Procedure

Within this CFD model, the equations for: Flow, Turbulence, Energy and Irradiation (P1) were solved. The discretization and solution schemes used for these equations are: Semi Empirical Pressure (SIMPLE), Standard and First Order Upwind scheme for Momentum, Turbulence Kinetic Energy, Turbulence Dissipation Rate and Energy. The model uses a segregated solution algorithm with implicit formulation as well as absolute velocity formulation. The segregated solver is better for low speed flows while the coupled solver is better for solving transonic or supersonic cases. The segregated solver method also requires less memory than the coupled solver.

The pressure equation was discretized with standard scheme where it interpolates the pressure on the faces using the cell center values. The momentum, energy and P1 equation were solved using the first order upwind scheme to get an approximate solution. The under-relaxation factors were kept at default values and were adjusted only when it was necessary to stabilize the solution by controlling convergence.

Convergence was monitored by checking the information from computed residuals of all equations. Scaled residuals were used. Computations were continued until the values of residuals were progressively reducing by typically five or six orders of magnitude, although in a few cases this could not be achieved. The calculations were considered convergent if the scaled residual for the continuity equation, the energy equation, P-1 irradiation was less than 1×10^{-3} , 1×10^{-8} and 1×10^{-6} respectively.

5.5 Simulation Results and Discussion

The results were focused on the airflow and temperature distribution inside the dryer. It was presented according to the mode of drying from the no-load experimental results. The validation of the simulation result was done by comparison with experimental measurement. The percentage of error was calculated by finding the difference between the experimental and simulated result.

5.5.1 Simulation under Solar Mode

The velocity vectors of air flow inside the solar dryer under solar mode are shown in Figure 5.4. Ambient air flows into the dryer through the side opening holes at the base of the solar dryer and the front holes near the collector. The maximum velocity that can be achieved is 0.26 m/s and it is found to be concentrated at small path in the middle of collector. The air flows to the drying chamber and when it reaches small path of first tray, some of the air flow hits the bottom face of the trays causes a backflow to occur. The velocity increases as it flows through the alternate holes gap of the trays across the drying chamber and finally out at chimney. From simulation results, mean velocity of air escaping from chimney is shown to be 0.17 m/s. The value is approximately same as the velocity obtained through experiments which was 0.19 m/s. Observation of the velocity distribution indicated that the flow velocity in the solar dryer is not uniform. The flow velocity is high mainly at the gaps of the trays.

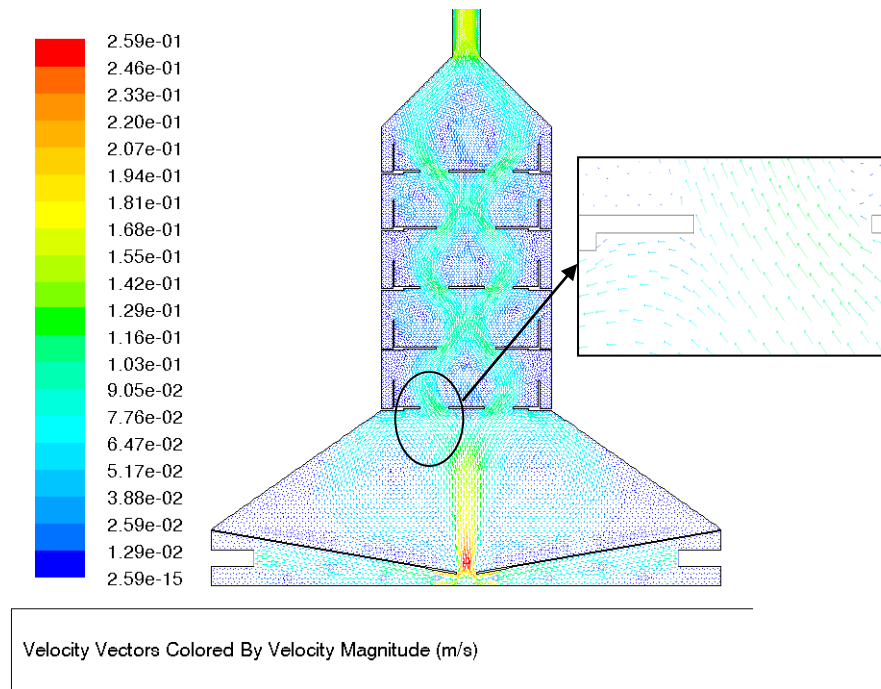


Figure 5.4: Velocity vector of fluid flow under solar mode

The temperature distribution inside the solar dryer is shown in Figure 5.5. It is visible that the highest temperature is concentrated surrounding the solar absorber plate which is around 330K to 341K. The heat has been transferred from bottom to the top part of the dryer by natural convection. The first and second tray recorded the highest temperature around 318K since it was exposed to the high temperature air flow. However, as the location of the tray become farther, the temperature decreases due to the heat losses to the surroundings and to heat up the lower trays. The lowest temperature was spotted below the absorber plate and it represents the ambient air temperature which flow from the side walls of dryer. The simulation results indicated that the heat convection and heat conduction received from the absorber plate and walls respectively maintains the drying chamber at high temperature.

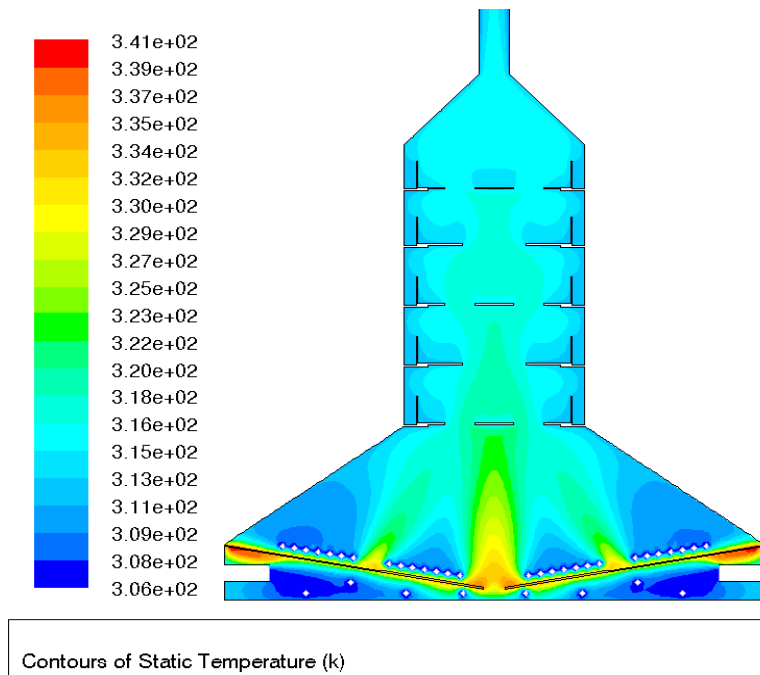


Figure 5.5: Temperature contours under solar mode

The percentage of difference between the simulation and experimental result is shown in Table 5.6. The results show that temperature near the absorber plate is in good agreement since it is around 11%. The value of all data are quite high especially Tray 5. The experimental data is higher than the simulated value due to the presence of solar irradiation. Since it is located at the top of drying chamber, hence it has the largest area exposed to the sun.

Table 5.6: Percentage difference between the experimental and simulation result under solar mode

	Tnear collector (°C)	Tray 1 (°C)	Tray 3 (°C)	Tray 5 (°C)
Experimental	66.5	59.8	53.8	65.8
Simulation	59.0	45.1	43.4	50.0
Percentage difference (%)	11.3	24.6	19.3	24.0

5.5.2 Simulation under Thermal Backup Mode – Hot Air and Flue Mode

A comparison of velocity vectors under hot air and flue thermal backup modes are shown in Figure 5.6. The hot air and flue entered from the side holes at the base of solar dryer and exit from the chimney. The flow is highly concentrated at the small

gap between the two absorber plates with highest velocity, 0.91m/s and 0.85 m/s for hot air and flue thermal backup modes respectively. High velocities are also observed at the alternate holes of the trays for both modes. A backflow occurred at the alternate holes of the trays and the area between solar absorber and Tray 1 because when the flow is concentrated at small path, some particles are not able to flow and hit the wall. The velocity reduces as it flows to the upper part of solar dryer but increases in chimney.

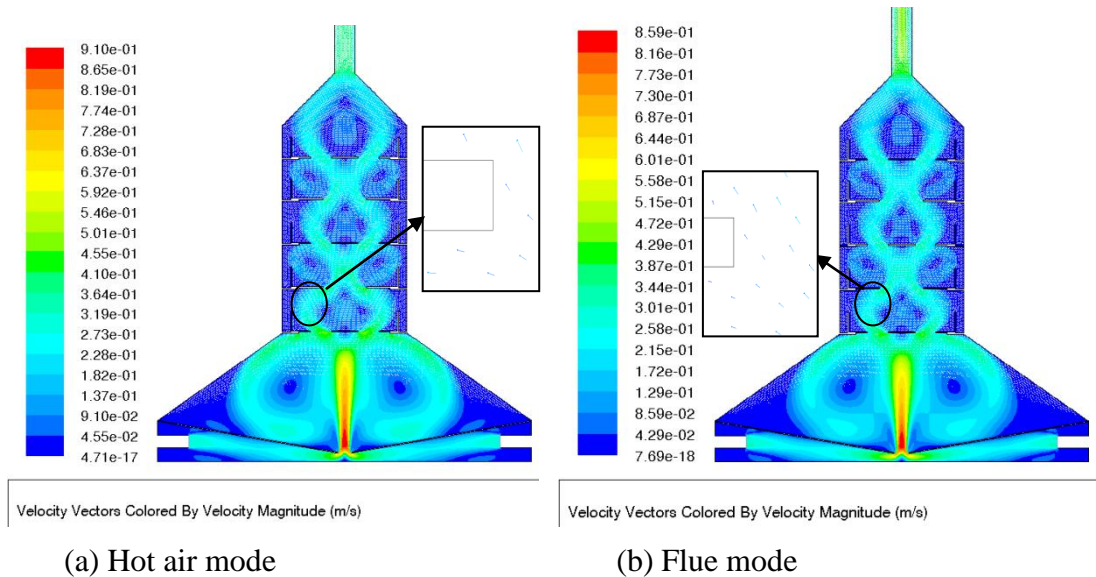
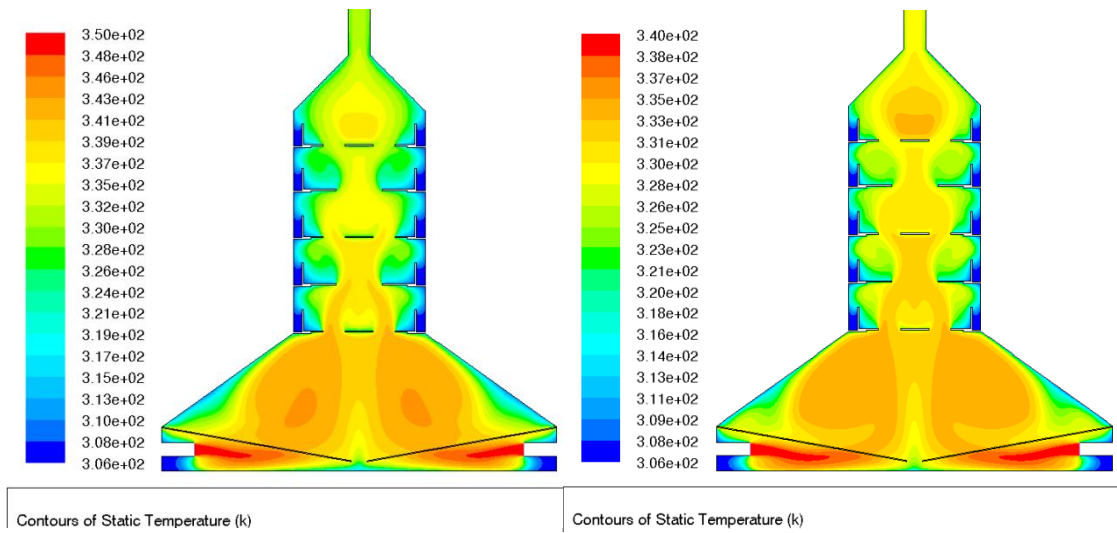


Figure 5.6: Velocity vectors of fluid flow under separated hot air and flue mode

A comparison of solar dryer temperature distribution under hot air and flue modes are shown in Figure 5.7. The heat received by air or within the flue was repeated totally depending on the biomass combustion in the burner of the TBU and it flows from bottom to the top part of the dryer. Both modes indicated that the medium with the highest temperature was concentrated under the absorber plate. The heat was transferred to the absorber plate surface by convection and continuously flows up to the chimney by natural convection. Based on the observation of the simulation results, Tray 1 received the highest amount of heat and the fluid temperature was reduced as it moved to the top part of the drying chamber. The simulation result indicated that the temperature recorded in flue mode was higher than hot air mode since it was the direct product of the fuel combustion. Although the gas temperature was high, the temperature decreased was obviously observed under this mode compared to hot air

mode due to large heat losses to the surroundings. A low temperature spot outside the edge of trays were observed in both cases, as indicated by the blue color in Figure 5.7. This was due to the isolation of these spots from the working fluid which could not penetrate through.



(a) Hot air mode

(b) Flue gas mode

Figure 5.7: Temperature contours under separated hot air and flue mode

The percentage of differences between the experimental and simulation result under hot air and flue gas modes are shown in Table 5.7. Both modes were simulated without irradiation model since the heat source was from the TBU. The table indicates that the simulation results of both modes are higher than the experimental result. In the CFD simulation, it was assumed that the dryer was a fully closed system and the heat losses to the surroundings were not taken into consideration. However the results showed good agreement since they fall below 10%. The percentage difference in hot air mode was larger than the flue mode due to the heat escape from the door and also the wall of dryer.

Table 5.7: Percentage difference comparison between the experimental and simulation result under separated hot air and flue mode

	Hot Air Mode			Flue Mode		
	Exp.	Sim.	% Dif.	Exp.	Sim.	% Dif.
Tnear collector (°C)	54.7	60.1	9.0	65.8	68.2	3.5
Tray 1 (°C)	54.7	58.4	6.4	63.8	66.0	3.2
Tray 3 (°C)	53.9	56.7	5.0	61.7	63.8	3.3
Tray 5 (°C)	52.0	55.0	5.5	59.2	59.4	0.4

5.5.3 Simulation under Hybrid Modes-Hot Air and Flue with Solar Mode

The velocity vectors of hot air with solar mode and flue with solar mode are shown in Figure 5.8. The absorber plate hindered the flowing air and flue, hence causes the flow to be concentrated with high velocities at the small gap between the absorber plates of both modes. The results indicated that a backflow with high velocities as compared to hot air and flue modes occurred at the alternate holes of the trays and the area between solar absorber and Tray 1. The air and flue flow, finally, exit at the chimney with relatively high velocity. It was noticed that the working fluid velocity, comprise hot air from G-to-G HEX and solar absorber, was higher than the fluid velocity comprise flue and solar absorber, in spite of that the flue density is lower than the hot air density. This might be due to larger pressure losses occurred in the flue passage system.

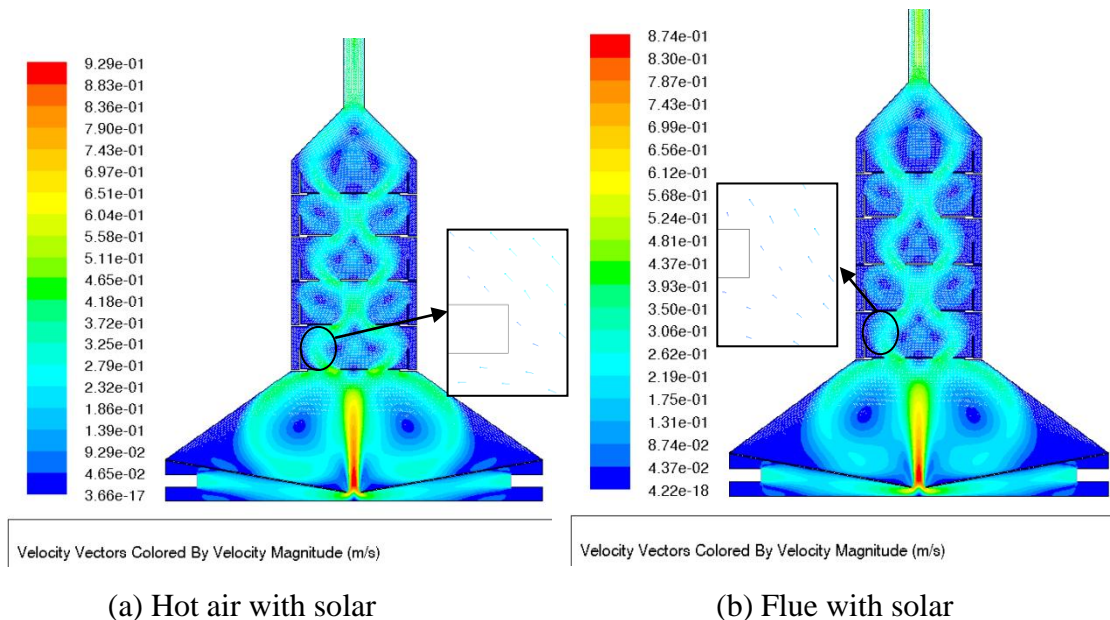


Figure 5.8: Velocity vectors of fluid flow under hybrid mode

The temperature distributions of solar dryer under hybrid modes are shown in Figure 5.9. P1 irradiation model was set across the wall of dryer and the TBU input was connected at the side opening holes near to the base of dryer. The heat flows from bottom to the top part of solar dryer by convection. In addition, the solar absorber also received heat from solar irradiation which indicated by a hot temperature surround the absorber plate. The drying chamber was maintained with high and uniform temperature distribution even though it was much lower than the bottom part due to

heat received from solar irradiation. Based on the results, both modes indicated that temperature inside the dryer was increased with the usage of absorber. It could be seen from the high temperature accumulated between the area of absorber and Tray 1. Flue with solar mode has higher temperature than hot air with solar mode because it received heat directly from the fuel combustion. Same as in the previously discussed mode, a low temperature spot indicated by the blue color was observed outside the edge of trays.

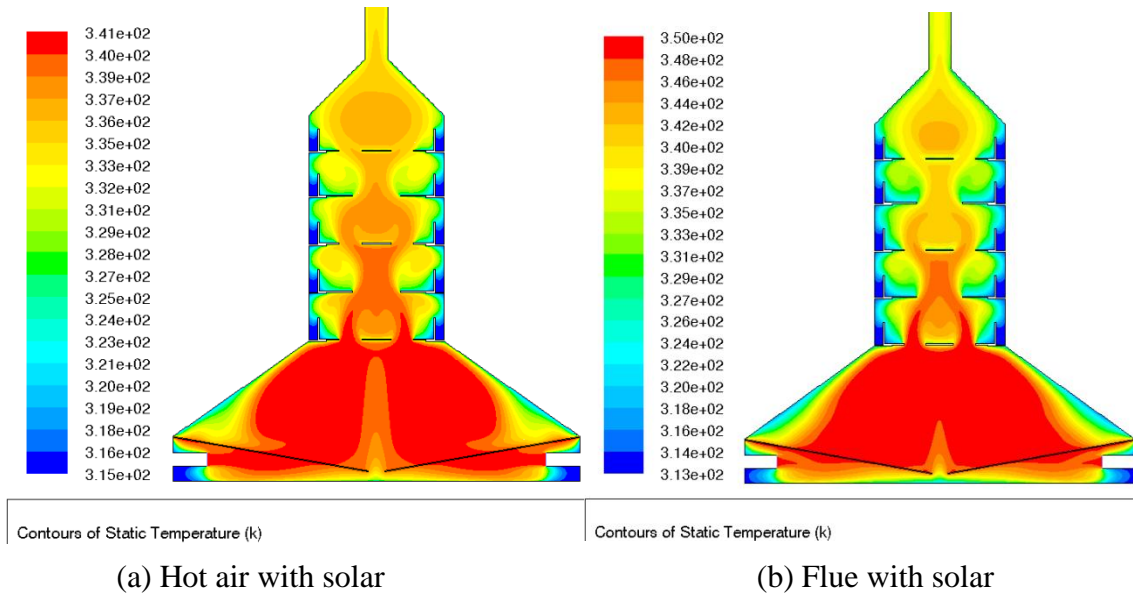


Figure 5.9: Temperature contours under hybrid mode

The percentage difference between the experimental and simulation results under hybrid modes operation had been calculated and shown in Table 5.8. Both modes were simulated with P1 irradiation model to illustrate the presence of solar irradiation. The results indicated that all the data were in good agreement which was below 15%.

Table 5.8: Percentage difference comparison between the experimental and simulation result under indirect with solar and direct with solar mode

	Hot Air with Solar Mode			Flue with Solar Mode		
	Exp.	Sim.	% Dif.	Exp.	Sim.	% Dif.
Tnear collector (°C)	75.1	66.8	11.1	78.3	74.8	4.5
Tray 1 (°C)	64.6	65.5	1.3	75.5	69.2	8.3
Tray 3 (°C)	63.8	62.9	1.5	69.7	67.4	3.3
Tray 5 (°C)	70.1	61.6	12.2	76.5	65.5	14.3

5.6 Chapter Summary

This chapter presented the fluid flow behavior inside the solar dryer by employing CFD tools under solar, thermal backup and hybrid modes. GAMBIT[®] software had been used to model the dryer geometry and generate the computational grid. FLUENT[®] software had been used to solve the governing equation and simulated the velocity and temperature distribution inside the dryer. The simulation results were validated by comparing with the results obtained from experiment measurements. The results indicated that the calculated percentage of errors in thermal backup and hybrid modes were in good agreement. Hybrid mode is the most appropriate mode for drying application since it provides the highest temperature and falls within the required drying temperature range. The low temperature spot was identified and will be assisted in the improvement of dryer design.

CHAPTER 6

CONCLUSIONS AND RECOMMENDATIONS

6.1 Conclusion

This study was aimed to investigate the performance of a portable hybrid solar dryer with thermal backup. The evaluation process composed of mathematical calculation, design, fabrication, experimental measurement and numerical simulation. A mixed mode type solar dryer and biomass burner as backup thermal units were designed and fabricated. First experiment had been conducted on the biomass burner to investigate the best type of biomass fuel which produced within the required thermal heating suitable for drying application. It was tested with different type of fuels, which were rice husk, EFB and woodchip at different feeding rate.

In addition, the principal solar dryer and burner characteristics had been evaluated under five different modes. The experiments were carried out under loading and no-load of drying specimen. The purpose of no-load experiment was to study the flow and temperature distribution inside the dryer. The drying materials, chillies and EFB were selected as samples of food and biomass product. Detailed drying behaviour of the system such as temperature distribution, the uniformity of drying and quality of dried product was studied under different operational modes. The best operational mode was identified from the experimental result.

Numerical simulation was performed in order to analyze the velocity and temperature distribution inside the dryer by CFD method using the commercial code, FLUENT[®] 6.3.26. The simulation results were validated by comparing with the experimental result. The simulation assisted in the improvement of the future system design.

The evaluation involved the systems performance evaluation and then the drying process evaluation. Therefore, the TBU was evaluated by investigating its operation under three different biomass fuels. This investigation leads to select the most suitable type and feeding rate of biomass fuel. Also, the design calculations and the mathematical procedure of the TBU were validated. The evaluation of the solar dryer unit was carried out at different operational modes, namely Solar, Thermal back up and hybrid solar-thermal backup, without loading of drying material. The investigation was carried out experimentally and numerically. The temperature distribution and the flow field in the dryer were investigated.

The following can be concluded from the investigation:

6.1.1 Thermal-Backup Unit

The thermal backup in this work comprise of the burner and the Gas-to-Gas HEX. The investigations to study the fuel performance have shown that:

1. The wood chip with feeding rate of 0.25 kg/h had been selected as the best biomass fuel for the burner. The combustion of this fuel maintained the outlet temperature of hot air within the range of 80°C to 100°C.
2. The TBU was able to produce the required hot air (clean warm air) within the pre-selected design temperature. It was proved that the design of the unit had successfully supplied the required thermal energy to enhance the dryer performance.

6.1.2 No-load Experiment

This was mainly concern the dryer unit performance.

1. A mixed mode solar drying unit alone yields a temperature range within 48°C to 65°C under solar mode. The recorded temperature had shown that the dryer design was capable to be used for drying application but will be interrupted especially during low solar irradiation and at night.
2. A stabilized drying chamber temperature was observed under thermal backup mode. The temperature recorded were within 52 to 56°C under hot air mode and

57°C to 64°C under flue mode. The results indicated that the usage of TBU was proved to be practically efficient in order to compensate the solar drying process continuously during the day and night.

3. Solar with biomass heating mode maintained the drying chamber at high temperature without being disrupted by a low solar irradiation or during the rainy days. The recorded average drying chamber temperature range for solar with hot air and solar with flue modes were 56 to 73°C and 61 to 78°C respectively.
4. Hybrid mode provides an acceptable high temperature for continuous drying which able to increase the productivity considerably.

6.1.3 Loading Experiments

The loading experiment was conducted by drying of chillies and EFB.

1. The drying process of chillies under open sun drying method took 7.25 days to reduce the moisture content from 80% to 5%. The drying period had decreased to 5.25 days under solar mode and 4.17 days in thermal backup mode. Hybrid mode had indicated the fastest chillies drying since it took only 2.33 days. The drying time was 32.14% faster than the traditional open sun drying with good final quality product. This proved the enhancement of drying with hybrid mode.
2. EFB took 4.21 days to complete the drying process from initial moisture content of 75% to 6% under open sun drying. The drying time reduced under solar and thermal backup modes up to 3.33 and 2.33 days respectively. However, the drying time had significantly improved under hybrid mode by taking only 1.33 days to dry, which is 31.6% faster than the open sun drying. Hence, the combination of both, solar and thermal backup had shown to be the excellent to speed up the drying for both food and biomass products.

6.1.4 The Efficiencies of Drying Systems

The efficiency of the system was divided into two, collector and drying efficiencies.

1. The calculated average efficiency of the solar collector was 1.7%. The efficiency increases during the noon time where it received maximum solar radiation.
2. The highest drying efficiencies to reduce moisture content of chillies from 80% to

5% were in hybrid mode which is 6.85%. While under thermal backup mode it was 4.96%, and 4.54% under solar mode.

3. The drying efficiencies to reduce moisture content of EFB from 75% to 6% under solar, thermal backup and hybrid modes were 6.22%, 6.45% and 11% respectively.
4. The highest enhancement index for both products was in hybrid mode followed by thermal backup only, solar only and open sun drying. The drying time was reduced considerably.

6.1.5 Simulation

The fluid flow and temperature contours inside the dryer were studied from simulation. The comparisons between the experimental and simulation results had shown that the calculated percentage of error was less than 15%. Hybrid mode indicates the highest recorded temperature within the required drying temperature inside the drying chamber. The objectives of the research, basically, are achieved and the experimental results were justified by simulation. The simulation results helped in the identification of spot with low temperature distribution which assisted in the design improvement.

6.2 Recommendations

On account of the above conclusions, it appears that the design of the drying systems require further improvement. Accordingly, the following recommendations are suggested to achieve a better drying performance:

6.2.1 Thermal Backup Unit

The thermal backup used in the present work is comprised biomass burner and G-to-G HEX. No like unit has been used previously. However, the following are suggestions to improve the unit.

1. The fuel feeding was done manually. This method is very tedious and not practical since drying process normally took days or weeks to dry its product. An integration of automatic controllable mechanism that able to control the feeding

rate is highly preferred. The installation of this mechanism can ensure the continuity in fuel burning combustion.

2. The fuel was found to be easily stuck along the joining of fuel feeder during the experiment. The fuel feeder might have improper diameter and connections. For improvement, the fuel feeder has to be redesigned by considered increasing diameter and angle of the feeder pipe so that fuel can fall down directly to the combustion bed.
3. The biomass fuel was observed to produce raw ashes at the end of combustion inside the burner. It needs to be removed in order to prevent its accumulation in the combustion bed and cause in low combustion. The best way of removing the ashes is by placing a controllable drain hole with bottom container in the middle of combustion bed. When it got accumulated, the drain hole can be opened to remove all the ashes inside the container before the next burning operation.
4. During the experiment, wood chip was observed to be burn in a fast rate. Hence, a controllable air inlet valve is needed to control the combustion rate. The combustion will be able to sustain with longer time without any fuel feeding and proper monitoring even after being added with excessive fuel.
5. The fuel was hard to ignite at the beginning of experiment. Usually it took more than 15 minutes to ensure that the fuel is completely burnt. Hence, the usage of LPG gas or fire starter is preferable to ignite the fuel easier. The process of fuel ignition was done only once a day since after that the fuel can be refilled with continuous combustion.
6. The smoke from combustion was observed to escape through the ambient inlet holes which are located beneath the combustion bed surrounding the burner body. The installed chimney was not high enough to create the buoyant force. The outlet had been identified to be too small for the flow passage. The diameter is needed to be enlarged for smoother outlet flow.

6.2.2 Mixed Mode Solar Dryer

By mixed mode solar, it meant direct solar on the drying material and indirect solar by absorber.

1. The temperature was observed to be reduced as the working fluid flow from

bottom to the top part of solar dryer. Most of the heat had been absorbed by the trays and wall of dryer. Some heat lost due the leakage. These heat losses can be reduced by changing the trays orientation into horizontal position for uniform heat received on each tray.

2. Based on the simulation result, the heat was mostly trapped under the absorber plate. Hence, the usage of porous solar collector can produce more heated air and enhance the performance. Besides, the location of air, inlet holes should be changed beneath the solar collector to enhance the flow of heat.
3. The simulation result also indicates that the heat was only flow from bottom to the top part of dryer through the meshed holes at each tray. Some area at the outer edge of trays was observed to have low temperature which consequently causes to the non-uniform drying. The problem can be solved by using wire mesh trays material instead of Perspex.

6.2.3 Hybrid Drying System

By hybrid modes, it meant solar and backup by thermal source.

1. Some heat losses were identified especially at the beginning and end part of the flexible hose due to the untied connection, which can be reduced by better insulation. In addition, the burner connection is best to be placed lower than dryer position to increase the buoyant force and better heat flow.

6.2.4 The Efficiencies of Drying Systems

The solar collector and drying efficiencies can be increased by improved.

1. The efficiencies of solar collector obtained was quite low due to the large loss to the surroundings, the use of Perspex as cover material and the location of air inlet. Improvement can be done by using glass material and changing the location of the inlet air to the bottom side of solar collector.
2. The pickup and overall thermal efficiencies can be increased by expanding the area of solar collector, fabricate a rigid closed wall dryer connection to prevent heat loss and changing the orientation the trays from vertical to horizontal position in order to avoid the shadowed area.

6.2.5 Simulation

CFD simulation was found to be a powerful tool to enhance the design of the dryer, where clear visualization of the flow and thermal distribution were gained. The simulation analysis can be extended by considering the drying material as source of vapor.

6.3 Suggestion for Further Studies

Further research work on this study can be continued, and the following are suggested as an extension to the work:

1. Drying of various types of product for example fish and herbs to study the applicability of the system for different agricultural and food products.
2. Development of the CFD simulation by considering the evaporation in the drying process.
3. Improve the design by changing the location of the absorber plate to minimize the shading effect and increase the solar absorption, as shown in Figure 6.1.

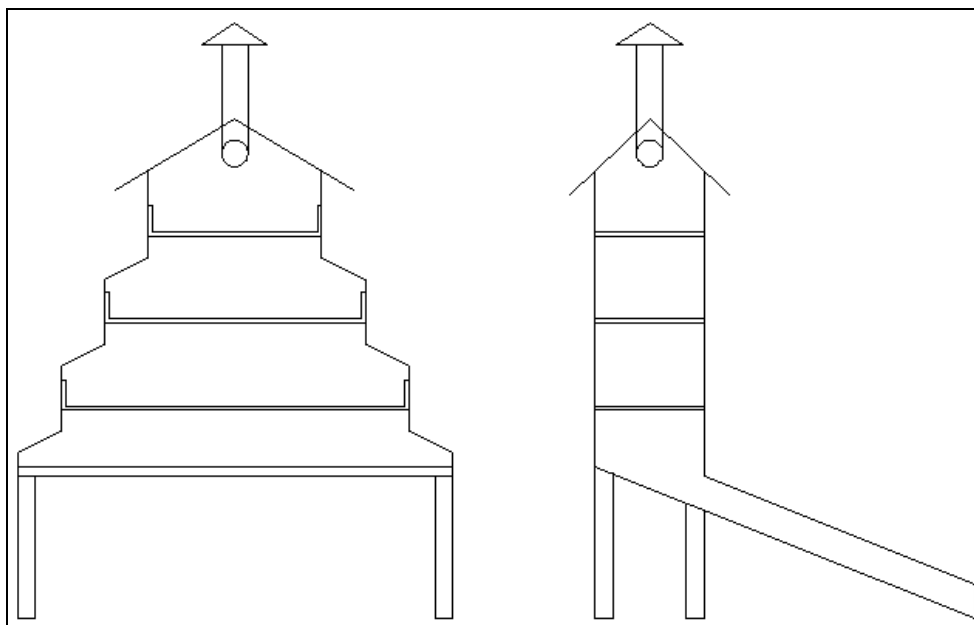


Figure 6.1: Sketch of the proposed design of solar dryer

REFERENCES

- [1] Peter E. Doe, *Fish Drying & Smoking: Production and Quality*. United States of America: CRC PRESS, 1998.
- [2] B. Kerr, *A Review of Solar Food Drying*. The Sustainable Living Center. 3310 Paper Mill Road, Taylor, Arizona 85939 USA, 1999.
- [3] O. V. Ekechukwu, "Experimental studies of integral-type natural-circulation solar-energy tropical crop dryers," *Ph.D. thesis. Cranfield Institute of Technology, United Kingdom*, 1987.
- [4] S. Ahmad, "Drying of Chilli," MARDI, [Interviewed: 05-Mar-2010.]
- [5] Center for Agricultural Policy with Prosperity Initiative, "Chili: Small-scale Review of Chili," Jan-2009. .
- [6] "Energy Information Bureau (EIB) Malaysia." [Online]. Available: <http://eib.org.my/index.php?page=article&item=100,136,143,152>. [Accessed: 22-Apr-2010].
- [7] N. S. Chua, "Optimal utilization of energy sources in a palm oil processing complex," Paper presented at PORIM Seminar on Development in Palm Oil Milling Technology and Environmental Management, Genting Highlands, Malaysia., 1991.
- [8] R. Hasibuan and W. R. W. Daud, "Through drying characteristic of oil palm empty fruit bunch (EFB) fibers using superheated steam," *Asia-Pacific Journal of Chemical Engineering*, vol. 2, no. 1, pp. 35-40, 2007.
- [9] Assoc. Prof. Dr. Md. Abdul Mannan, "Composting EFB - Empty Fruit Bunches of Oil Palm," 22-May-2008. [Online]. Available: <http://www.etawau.com/OilPalm/EFB.htm>. [Accessed: 11-May-2010].
- [10] J. G. Brammer and A. V. Bridgwater, "Drying technologies for an integrated gasification bio-energy plant," *Renewable and Sustainable Energy Reviews*, vol. 3, no. 4, pp. 243-289, Dec. 1999.
- [11] Serafica E. and del Mundo R, "Design and Qualitative Performance of a Hybrid Solar-Biomass Powered Dryer for Fish," presented at the World Renewable Energy Regional Conference, Jakarta, Indonesia, Energy Engineering Program, University of the Philippines Diliman National Engineering Center, Diliman, Quezon City, Philippines 1101, 2005.
- [12] A. Madhlopa and G. Ngwalo, "Solar dryer with thermal storage and biomass-backup heater," *Solar Energy*, vol. 81, no. 4, pp. 449-462, Apr. 2007.
- [13] S.C. Bhattacharya, Tanit Ruangrunghaikul, and H.L. Pham, "Design and Performance of a Hybrid Solar/Biomass Energy Powered Dryer for Fruits and Vegetables," presented at the World Renewable Energy Conference, Brighton, UK, Energy Program, Asian Institute of Technology P.O. Box 4, Klong Luang, Pathumthani 12120, Thailand, 2000.
- [14] J. Prasad, V. Vijay, G. Tiwari, and V. Sorayan, "Study on performance evaluation of hybrid drier for turmeric (*Curcuma longa* L.) drying at village scale," *Renewable Energy*, vol. 30, no. 14, pp. 2097-2109, Nov. 2005.

- [15] T. Thanaraj, D. Dharmasena, and U. Samarajeewa, "Development of a Rotary Solar Hybrid Dryer for Small Scale Copra Processing," *Tropical Agriculture Research*, vol. 16, pp. 305-315, 2004.
- [16] J. Prasad, V. Vijay, G. Tiwari, and V. Sorayan, "Study on performance evaluation of hybrid drier for turmeric (*Curcuma longa* L.) drying at village scale," *Journal of Food Engineering*, vol. 75, no. 4, pp. 497-502, Aug. 2006.
- [17] B. Bena and R. J. Fuller, "Natural convection solar dryer with biomass back-up heater," *Solar Energy*, vol. 72, no. 1, pp. 75-83, Jan. 2002.
- [18] E. Tarigan and P. Tekasakul, "A Mixed-Mode Natural Convection Solar Dryer with Biomass Burner and Heat Storage Back-up Heater," 2005.
- [19] A. G. Mastekbayeva, B. Chandika P., M. L. Augustus, and S. Kumar, "Experimental studies on a hybrid dryer," presented at the ISES 99 Solar World Congress, Israel, Energy Program, Asian Institute of Technology, P. O. Box 4, Klong Luang, Pathumthani 12120, Thailand., 1999.
- [20] P. Prammanee and P. Weerathaworn, "Technologies for Biomass Utilization of agricultural products in Thailand." [Online]. Available: <http://www.biomass-asia-workshop.jp/biomassws/03workshop/material/preecha.pdf>. [Accessed: 18-Nov-2009].
- [21] R. Driscoll, "Food Dehydration," in *Food Processing Principles and Applications*, First Edition., Blackwell Publishing, 2004, pp. 31-44.
- [22] A. S. Mujumdar and A. S. Menon, "Drying of Solids: Principles, Classifications and Selection of Dryers," in *Handbook of Industrial Drying*, Second edition revised and expanded., vol. 1, 1. McGill University, Montreal, Quebec, Canada. 2. Mount Sinai Hospital, Toronto, Ontario, Canada.: Marcel Dekker, Inc., 1995.
- [23] H. Ramaswamy and M. Marcotte, *Food Processing: Principles and Applications*. Taylor & Francis, 2006.
- [24] J. van Brackel, "Mass transfer in convective drying," in *Advances in Drying*, vol. 1, Hemisphere, New York: , 1980, pp. 217-268.
- [25] V. K. Sharma, A. Colangelo, and G. Spagna, "Experimental investigation of different solar dryers suitable for fruit and vegetable drying," *Renewable Energy*, vol. 6, no. 4, pp. 413-424, Jun. 1995.
- [26] Samson A. Sotocinal, "Design and Testing of a Natural Convection Solar Fish Dryer," Master of Science, Macdonald Campus of McGill University, Montreal, Canada, 1992.
- [27] M. R. Murthy, "A review of new technologies, models and experimental investigations of solar driers," *Renewable and Sustainable Energy Reviews*, vol. 13, no. 4, pp. 835-844, May. 2009.
- [28] "El Paso Solar Energy Association." [Online]. Available: <http://www.epsea.org/dry.html>. [Accessed: 11-Aug-2009].
- [29] A. Ayensu, "Dehydration of food crops using a solar dryer with convective heat flow," *Solar Energy*, vol. 59, no. 4, pp. 121-126, 1997.
- [30] A. Fudholi, K. Sopian, M. Ruslan, M. Alghoul, and M. Sulaiman, "Review of solar dryers for agricultural and marine products," *Renewable and Sustainable Energy Reviews*, vol. 14, no. 1, pp. 1-30, Jan. 2010.
- [31] S. Rahim and M. Suffian, "Development of Specialty Particleboard from Oil Palm Fibre," Forest Research Institute Malaysia (FRIM), Kepong, Selangor Darul Ehsan, 2006.

- [32] J. C. Hollick, "Commercial scale solar drying," *Renewable Energy*, vol. 16, no. 1, pp. 714-719, 1999.
- [33] L. B. Rockland, "Food Technol.," no. 23, p. 1241, 1969.
- [34] G. Crapiste, "Simulation of Drying Rates and Quality Changes During the Dehydration of Foodstuffs," in *Food Preservation Technology Series: Trends in Food Engineering*, TECHNOMIC, 2000, pp. 135-147.
- [35] Digdeep, "Dig deep: 3rd April, 2008 (Part 3): Kuala Muda and Taman Robina, mainland Penang." [Online]. Available: <http://digdeep1962.blogspot.com/2008/04/3rd-april-2008-part-3-kuala-muda-and.html>. [Accessed: 09-Aug-2011].
- [36] B. Amer, M. Hossain, and K. Gottschalk, "Design and performance evaluation of a new hybrid solar dryer for banana," *Energy Conversion and Management*, vol. 51, no. 4, pp. 813-820, Apr. 2010.
- [37] G. Mulozoki and U. Svanberg, "Effect of traditional open sun-drying and solar cabinet drying on carotene content and vitamin A activity of green leafy vegetables," *Springer Netherlands*, no. 58, pp. 1-15, Sep. 2003.
- [38] J. Prasad and V. Vijay, "Experimental studies on drying of Zingiber officinale, Curcuma longa l. and Tinospora cordifolia in solar-biomass hybrid drier," *Renewable Energy*, vol. 30, no. 14, pp. 2097-2109, Nov. 2005.
- [39] I. Kurtbas and E. Turgut, "Experimental investigation of solar air heater with free and fixed fin: efficiency and energy loss.," *International Journal of Science and Technology*, vol. 1, no. 1, pp. 75-82, 2006.
- [40] David E. and Whitfield V., "International Conference On Solar Cooking," in *Solar Dryer Systems and the Internet: important resources to improve food preparation*, 2000.
- [41] O. V. Ekechukwu and B. Norton, "Review of solar-energy drying systems II: an overview of solar drying technology," *Energy Conversion and Management*, vol. 40, no. 6, pp. 615-655, Apr. 1999.
- [42] P. Oosthuizen, "A numerical study of the performance of natural convection solar rice dryers," in *In: Drying 1986: Proceedings of Fifth International Symposium on Drying, Cambridge MA, USA.*, pp. 670-7, 1986.
- [43] M. Zaman and B. Bala, "Thin layer solar drying of rough rice," *Solar Energy*, no. 42, pp. 167-171, 1989.
- [44] M. Garba, A. Atiku, and A. Sambo, "Comparative studies of some passive solar dryers," *In: Proceedings of First World Renewable Energy Congress, Reading, UK.*, pp. 927-31, 1990.
- [45] V. Sharma, S. Sharma, R. Ray, and H. Garg, "Design and performance studies of a solar dryer suitable for rural applications," *Energy Conversion and Management*, vol. 26, no. 1, pp. 111-119, 1986.
- [46] D. R. Pangavhane and R. L. Sawhney, "Review of research and development work on solar dryers for grape drying," *Energy Conversion and Management*, vol. 43, no. 1, pp. 45-61, Jan. 2002.
- [47] P. Sharma, K. Sharma, and R. Parashar, "Prospects of raisin production in tribal areas of Himachal Pradesh," *Indian Food Packer*, pp. 16-9, 1992.
- [48] P. Gbaha, H. Yobouet Andoh, J. Kouassi Saraka, B. Kamenan Koua, and S. Toure, "Experimental investigation of a solar dryer with natural convective heat flow," *Renewable Energy*, vol. 32, no. 11, pp. 1817-1829, Sep. 2007.

- [49] B. Ezekoye and O. Enebe, "Development and Performance Evaluation of Modified Integrated Passive Solar Grain Dryer," *The Pacific Journal of Science and Technology*, vol. 7, no. 2, pp. 185-190, Nov. 2006.
- [50] H. Hallak, J. Hilal, F. Hilal, and R. Rahhal, "The staircase solar dryer: design and characteristics.," *Renewable Energy*, vol. 7, no. 2, pp. 177-183, 1996.
- [51] K. Nair and D. Bongirwar, "Solar dryer for agricultural products, A do it yourself solar dryer.," *Indian Chemical Engineering*, vol. 36, no. 3, pp. 103-105, 1994.
- [52] S. Singh, P. P. Singh, and S. S. Dhaliwal, "Multi-shelf portable solar dryer," *Renewable Energy*, vol. 29, no. 5, pp. 753-765, Apr. 2004.
- [53] L. Diamante and P. Munro, "Mathematical modelling of the thin layer solar drying of sweet potato slices," *Solar Energy*, no. 51, pp. 271-276, 1993.
- [54] M. Y. Hj. Othman, "Photovoltaic Thermal System," Presented at World Renewable Energy Congress & WREN Seminar No 73, 26-Nov-2 Dec 2006, Brighton, UK.
- [55] E. Azad, "Design and experimental study of solar agricultural dryer for rural area.," *Livestock Research for Rural Development*, vol. 20, no. 134, 2008.
- [56] W. Eissen, W. Muhlbauer, and H. Kutzbach, "Solar drying of grapes," *Drying Technology*, vol. 3, no. 1, pp. 63-74, 1985.
- [57] A. Dissa, J. Bathiebo, S. Kam, P. Savadogo, H. Desmorieux, and J. Kouliadiati, "Modelling and experimental validation of thin layer indirect solar drying of mango slices," *Renewable Energy*, vol. 34, no. 4, pp. 1000-1008, Apr. 2009.
- [58] A. A. El-Sebaei, S. Aboul-Enein, M. R. I. Ramadan, and H. G. El-Gohary, "Experimental investigation of an indirect type natural convection solar dryer," *Energy Conversion and Management*, vol. 43, no. 16, pp. 2251-2266, Nov. 2002.
- [59] K. E. Al-Juamily, A. J. N. Khalifa, and T. A. Yassen, "Testing of the performance of a fruit and vegetable solar drying system in Iraq," *Desalination*, vol. 209, no. 1, pp. 163-170, Apr. 2007.
- [60] A. Sayigh, *Solar energy engineering*. Academic Press, New York, 1977.
- [61] M. Fisk and H. Anderson, *Introduction to solar technology*, Addison-Wesley publishing Company Inc. 1982.
- [62] Sutainner, "Solar Dryers to Support a Sustainable World: My Solar Dryer." [Online]. Available: <http://solar-dryers.blogspot.com/2007/11/my-solar-dryer.html>. [Accessed: 09-Aug-2011].
- [63] I. N. Simate, "Optimization of mixed-mode and indirect-mode natural convection solar dryers," *Renewable Energy*, vol. 28, no. 3, pp. 435-453, Mar. 2003.
- [64] F. Forson, M. Nazha, and H. Rajakaruna, "Modelling and experimental studies on a mixed-mode natural convection solar crop-dryer," *Solar Energy*, vol. 81, no. 3, pp. 346-357, Mar. 2007.
- [65] Z. Li, H. Zhong, R. Tang, T. Liu, W. Gao, and Y. Zhang, "Experimental investigation on solar drying of salted greengages," *Renewable Energy*, vol. 31, no. 6, pp. 837-847, May. 2006.
- [66] B. O. Bolaji and A. P. Olalusi, "Performance Evaluation of a Mixed-Mode Solar Dryer," pp. AU J.T. 11(4): 225-231, Apr. 2008.
- [67] S. A. Kalogirou, "Solar thermal collectors and applications," *Progress in Energy and Combustion Science*, vol. 30, no. 3, pp. 231-295, 2004.

- [68] J. Duffie and W. Beckman, *Solar engineering of thermal processes*, 2nd ed. New York: Wiley, 1991.
- [69] I.N. Itodo, A. M. Adewole, and S.K. Edemeka, "Development of Active Solar Crop Dryer: Design Analysis and Performance Evaluation," *Nigeria Journal of Renewable Energy*, 10, no. 1, 2002.
- [70] J. Twidell and T. Weir, *Renewable Energy Resources*. E&F N. Span Ltd: London, UK.: , 1986.
- [71] R. Brewer, C. Flood, E. Taylor, J. Koon, and M. White, *Solar Applications in Agriculture*. Auburn, Alabama: , 1979.
- [72] S. Kalogirou, "The potential of solar industrial process heat applications," *Applied Energy*, no. 76, pp. 337-361, 2003.
- [73] A. Saleh and I. Badran, "Modeling and experimental studies on a domestic solar dryer," *Renewable Energy*, vol. 34, no. 10, pp. 2239-2245, Oct. 2009.
- [74] O. V. Ekechukwu and B. Norton, "Review of solar-energy drying systems III: low temperature air-heating solar collectors for crop drying applications," *Energy Conversion and Management*, vol. 40, no. 6, pp. 657-667, Apr. 1999.
- [75] Anil K. Rajvanshi, *Alternative Energy in Agriculture*, D. Yogi Goswami., vol. 2. CRC Press, 1986.
- [76] K. W. Ragland, D. J. Aerts, and A. J. Baker, "Properties of Wood for Combustion Analysis," *Elsevier Science Publishers Ltd, England.*, no. 37, pp. 161-168, 1991.
- [77] R. J. Fuller, Lu Aye, and B. D. Shakya, "Thermal evaluation of a low cost wood burner," in *Life, The Universe and Renewables, Solar 2004*, 2004.
- [78] J. Wang, G. G. Hirs, and P. Rollmann, "The performance of a new gas to gas heat exchanger with strip fin," *Energy Conversion and Management*, vol. 40, no. 15, pp. 1743-1751, Oct. 1999.
- [79] Lei Fang, "A Computational and Experimental Investigation of Clamshell Heat Exchangers in Residential Gas Furnaces," Doctor of Philosophy, Purdue University, 2000.
- [80] T. Tomimura, K. Hamano, Y. Honda, and R. Echigo, "Experimental study on multi-layered type of gas-to-gas heat exchanger using porous media," *International Journal of Heat and Mass Transfer*, vol. 47, no. 21, pp. 4615-4623, Oct. 2004.
- [81] R. Echigo, "Heat Transfer Augmentation in High Temperature Heat Exchangers, High Temperature Equipment," *Hemisphere, Washington, DC*, pp. 41-72, 1986.
- [82] S. Al-Omari, "Experimental investigation on combustion and heat transfer characteristics in a furnace fueled with unconventional biomass fuels (date stones and palm stalks)," *Energy Conversion and Management*, vol. 47, no. 6, pp. 778-790, Apr. 2006.
- [83] M. L. Kevin, "Increasing Heat Exchanger Performance," *Bryan Research & Engineering, Inc.*, 2006.
- [84] F. Forson, M. Nazha, F. Akuffo, and H. Rajakaruna, "Design of mixed-mode natural convection solar crop dryers: Application of principles and rules of thumb," *Renewable Energy*, vol. 32, no. 14, pp. 2306-2319, Nov. 2007.
- [85] Frank P. Incropera, David P. Dewitt, Theodore L. Bergman, and Adrienne S. Lavine, *Introduction to Heat Transfer*, Fifth. John Wiley & Sons, 2007.

- [86] B. Brenndorfer, L. Kennedy, C. Bateman, G. Mrema, and C. Wereko-Brobby, *Solar dryers—their role in post-harvest processing*. London: Commonwealth Science Council, Commonwealth Secretariat Publications, 1985.
- [87] D. Ampratwum, “Design of solar dryer for dates,” *AMA*, no. 29, pp.:59-62.1998
- [88] M. Basunia and T. Abe, “Design and Construction of a Simple Three-Shelf Solar Rough Rice Dryer,” *AMA*, vol. 32, pp. 54-59(2001), 2001.
- [89] El- Amin Omda Mohamed Akoy, Mohamed Ayoub Ismail, El-Fadil Adam Ahmed, and W. Luecke, “Design and Construction of A Solar Dryer for Mango Slices,” *tropentag*, 2006.
- [90] M. Sodha, N. Bansal, A. Kumar, P. Bansal, and M. Malik, “Solar crop drying,” *CPR press, Boca Raton, Florida, USA.*, 1987.
- [91] S. Churchill and H. Chu, *Int. J. Heat Mass Transfer*. 18,1323: , 1975.
- [92] W. Kays and M. Crawford, *Convective Heat and Mass Transfer*, 3rd ed. McGraw Hill, New York, 1993.
- [93] E. Sieder and G. Tate, *Ind. Eng. Chem.* 28, 1429: , 1936.
- [94] A. Bar-Cohen and W. Rohsenow, *J. Heat Transfer*. 106,116: , 1984.
- [95] R. Winterton, *Int. J. Heat Mass Transfer*. 41,809: , 1998.
- [96] T. Kapur, T. C. Kandpal, and H. P. Garg, “Electricity generation from rice husk in Indian rice mills: Potential and financial viability,” *Biomass and Bioenergy*, vol. 10, no. 5, pp. 393-403, 1996.
- [97] S. K. and K. M. N., “Performance analysis of downdraft gasifier for agriwaste biomass materials,” *Indian Journal of Science and Technology*, vol. 3, pp. 58-60, Jan. 2010.
- [98] S. Vijaya, M. Chow, and A. Ma, “Energy Database of the Oil Palm,” in *MPOB Palm Oil Engineering Bulletin*, 2004, pp. 15-22.
- [99] UK Forestry Commission via Forest Research, “Typical calorific values of fuels,” *BIOMASS Energy Centre (BEC)*. [Online]. Available: http://www.biomassenergycentre.org.uk/portal/page?_pageid=75,20041&_dad=portal&_schema=PORTAL. [Accessed: 27-Oct-2010].
- [100] D. Pangavhane, R. Sawhney, and P. Sarsavadia, “Design development and performance testing of a new natural convection solar dryer,” *Energy*, no. 27, pp. 579-590, 2002.
- [101] Prof.R.D.Jilte and Prof.Dr.A.B.Datye, “Design and Performance Analysis of Solar Dryer for Banana slices using Scheffler Dish and its Comparison with Electrical Food Drier,” 2007.
- [102] B. Brenndorfer, L. Kennedy, C. Bateman, G. Mrema, and Wereko-Brobby C, *Solar dryers-their role in post harvest processing*. London: Commonwealth Science Council (Commonwealth Secretariat Publications): , 1987.
- [103] O. V. Ekechukwu, “Natural convection solar crop dryers,” PhD thesis, Cranfield University, England, 1987.
- [104] E. Mathioulakis, V. T. Karathanos, and V. G. Belessiotis, “Simulation of air movement in a dryer by computational fluid dynamics: Application for the drying of fruits,” *Journal of Food Engineering*, vol. 36, no. 2, pp. 183-200, May. 1998.
- [105] A. R. Rigit and P. T. Low, “Heat and Mass Transfer in a Solar Dryer with Biomass Backup Burner,” *World Academy of Science, Engineering and Technology*, pp. 115-118, 2010.

- [106] W. Dyah, L. O. Nelwan, A. Kamaruddin, and S. A. Indra, "Analysis of Temperature and Air Flow Distribution in Solar Dryer Using CFD," *IPB (Bogor Agricultural University)*, vol. 17, no. 1, Apr. 2003.
- [107] R. Bird, W. Stewart, and E. Lightfoot, *Transport Phenomena*. New York: John Wiley & Sons, Inc.
- [108] C. M. VEST, *Holographic interferometry*. New York: John William&Sons, 1979.
- [109] B. Launder and D. Spalding, "The numerical computation of turbulent flows.," *Computer Methods in Applied Mechanics and Engineering*, no. 3, pp. 269-289, 1974.

LIST OF PUBLICATIONS & ACHIEVEMENTS

- [1] Y. M. Yunus, H. H. Al-Kayiem and K. A. K. Albaharin
Design of a Biomass Burner/Gas-to-Gas Heat Exchanger for Thermal Backup of a Solar Dryer.
International Conference on Plant Equipment and Reliability, ICPER2010.
15-17 June, Kuala Lumpur Convention Center, Malaysia.

- [2] Y. M. Yunus, H. H. Al-Kayiem and K. A. K. Albaharin
Design of a Biomass Burner/Gas-to-Gas Heat Exchanger for Thermal Backup of a Solar Dryer
Journal of Applied Science (available online)

- [3] Y. M. Yunus and Hussain H. Al-Kayiem
A Hybrid Dryer to Dry Solid Waste
World Engineering Congress, WEC2010, 2nd -5th August, Kuching, Sarawak, Malaysia.

- [4] International Invention, Innovation & Technology Exhibition, ITEX2009
15th – 17th May, Kuala Lumpur, Malaysia.

- [5] Patent Application No. : PI 20100014

Appendix A

Moisture contents of solar drying of various agricultural produces [30]

Product	Moisture content		Max. allowable temp. (°C)	Drying time (h)
	Initial (%)	Final (%)		
Onions	85	6	55	48
Onion flakes	80	10	55	24
Onion rings	80	10	55	
Tomatoes	95	7	60	36
Green peas	80	5	60	8–10
Grapes	80	15–20		32–40
Apples	82	11–14	65–70	24–26
Figs	70	20	70	32
Bananas	80	15	70	15
Cassava	62	17		
Copra	30	5		
Tobacco	90	10		96
Coffee	65	11		288
Garlic flakes	80	4		48
Chillies	80	5		48
Ginger	80	10		168
Cabbage	80	4	65	48
Tea	80	3		96
Pepper	71	13		48
Turmeric	80	10		120
Potato chips	75	13	70	72
Paddy, raw	22–24	11	50	
Paddy, parboiled	30–35	13	50	
Maize	35	15	60	
Wheat	20	16	45	
Millet	21	4		
Corn	24	14	–	
Rice	24	11	50	
Cauliflower	80	6	65	
Carrots	70	5	75	
Green beans	70	5	75	
Garlic	80	4	55	
Cabbage	80	4	55	
Sweet potato	75	7	55	
Red lauan	90	20		
Potatoes	75	13	75	
Spinach	80	10		
Prunes	85	15	55	
Apricots	85	18	65	
Peaches	85	18	65	
Guavas	80	7	65	
Mulberries	80	10	65	
Okra	80	20	65	
Pineapple	80	10	65	
Yams	80	10	65	
Nutmeg	80	20	65	
Sorrel	80	20	65	
Coffee	50	11	–	
Coffee beans	55	12	–	
Cocoa beans	50	7	–	
Cotton	50	9	75	
Cotton seed	50	8	75	
French bean	70	5	75	
Groundnuts	40	9	–	

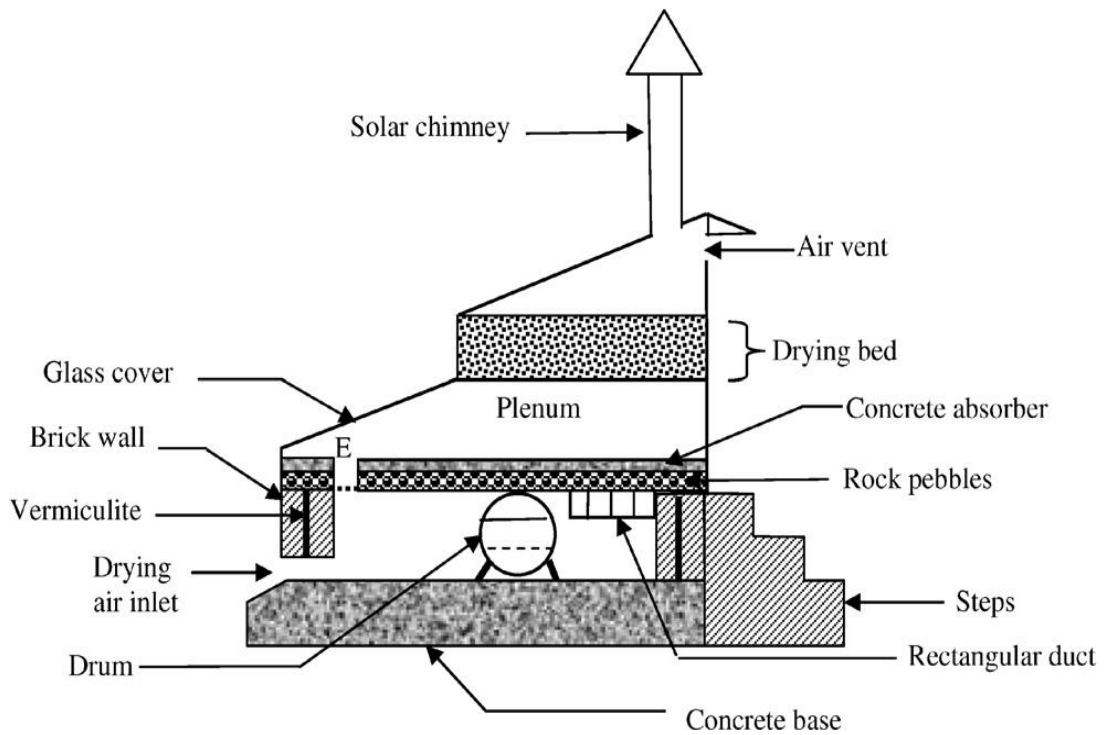
Appendix B

Properties of plastic films and other cover materials [74]

Material	Thickness available (mm)	Transmittance of visible light ^a	Transmittance of infrared radiation	Weatherability ^b	Ultimate tensile strength (N mm ⁻²)	Propagating tear strength (N mm ⁻¹)	Maximum width (mm)
Commonly available plastic films							
Polyethylene (PE) (u.v.- inhibited)	0.01 upwards	0.86	0.77	Poor	10–30	20–115	12.2
Polypropylene (PP)	0.01–0.25	0.92	No data	Fair	30–275	1–230	3.0
Polyvinyl chloride (PVC)	0.015–0.75	0.90	0.12	Poor	10–70	2–380	2.1
Polyethylene terephthalate (polyester) (PET) e.g. Mylar TM	0.002–0.35	0.88	0.24	Very good	140–275	19–115	3.0
Polyvinyl fluoride (PVF) e.g. Tedlar TM	0.01–0.1	0.86–0.92	0.33	Very good	50–125	45–390	3.5
Ethylene/tetra-fluoro-ethylene Copolymer (ETFE) e.g. Teflon TM	0.05–0.2	0.95	0.20	Very good	50–55	230–350	1.2
Less common films							
Cellulose acetate	0.02–0.75	0.93	0.03	Fair	50–110	1.5–3.9	1.5
Cellulose triacetate	0.05–0.5	0.93	0.11	Good	62–110	1.5–11	1.2
Cellulose acetate butyrate	0.28–0.75	0.93	—	Good	35–60	1.9–3.9	2.5
Ethylene/vinyl acetate copolymer (EVA)	0.02 upwards	—	—	Poor	6–24	20–115	12.2
Ethylene chlorotrifluoro-ethylene (ECTFE)	0.01–2.2	—	—	Very good	55–70	350–500	1.4
Fluoroethylene propylene (FEP)	0.01–0.75	0.93	—	Very good	17–20	50	1.2
Perfluoro-alkoxy (PFA)	0.01–0.75	—	—	Very good	27–50	15–27	1.2
Polychlorotrifluoro-ethylene (PCTFE)	0.02–0.25	—	—	Very good	34–70	1–15	1.2
Polycarbonate (PC)	0.006–0.35	0.87–0.92	—	Good	55–80	7.5–10	1.4
Polymethyl methacrylate (acrylic) (PMMA) e.g. Plexiglass TM	0.05–0.25	0.87	0.01	Good	55–60	No data	2.7
Polystyrene (PS)	0.006–0.5	0.87–0.92	0.35	Fair	55–80	2	1.9
Vinyl chloride/acetate copolymers	0.02–0.75	—	—	Fair	17–55	4–540	2.1
Other materials							
Horticultural glass	3.0	0.90	0.01	Very good	—	—	—
PVC-coated polyester cloth	—	0.10	—	Very good	150	—	—

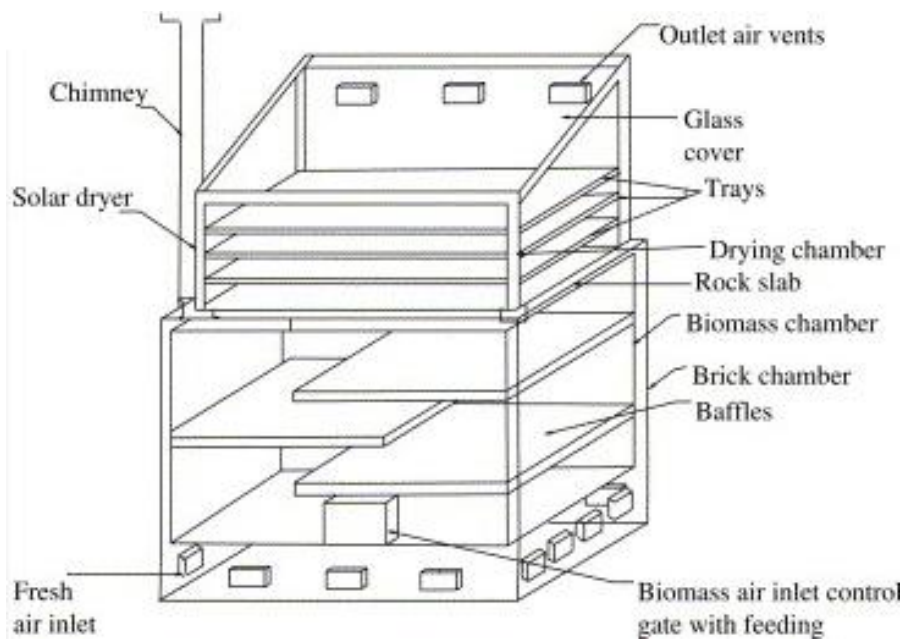
Appendix C

Solar dryer with thermal storage and biomass=backup heater [12]



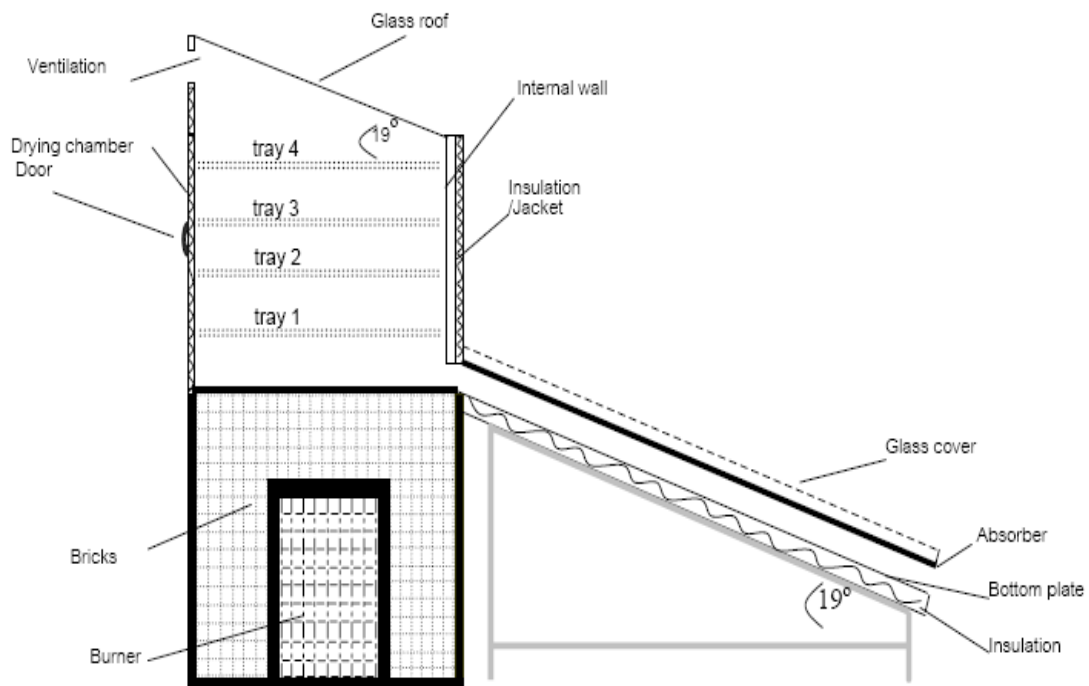
Appendix D

Solar-biomass hybrid dryer [38]



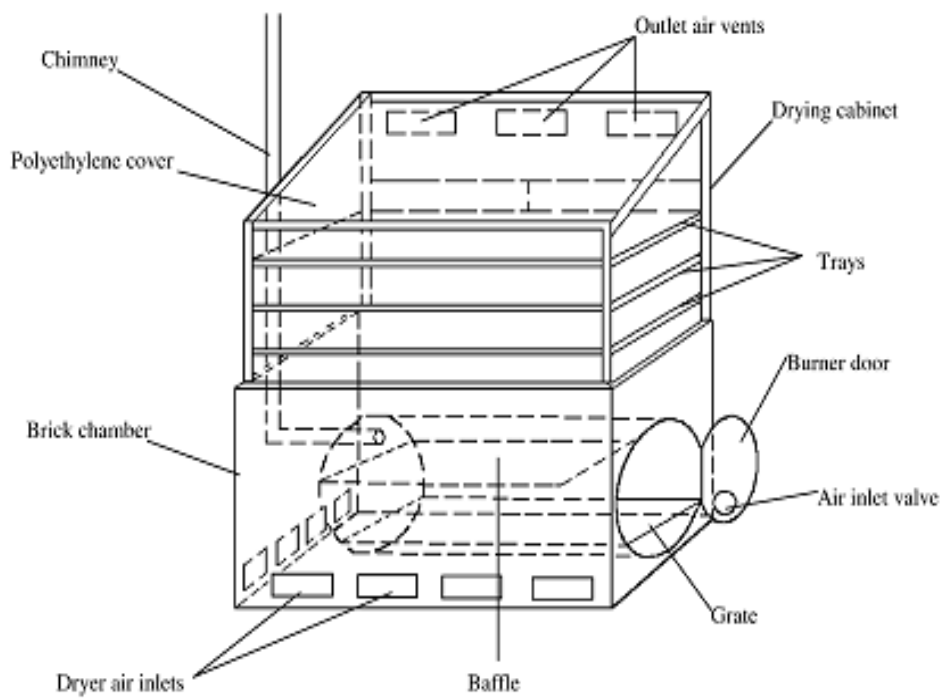
Appendix E

Mixed-mode natural convection solar dryer with biomass burner and heat storage back-up heater [18]



Appendix F

Natural solar dryer with biomass back-up heater [17]



Appendix G
Solar-biomass hybrid dryer [19]

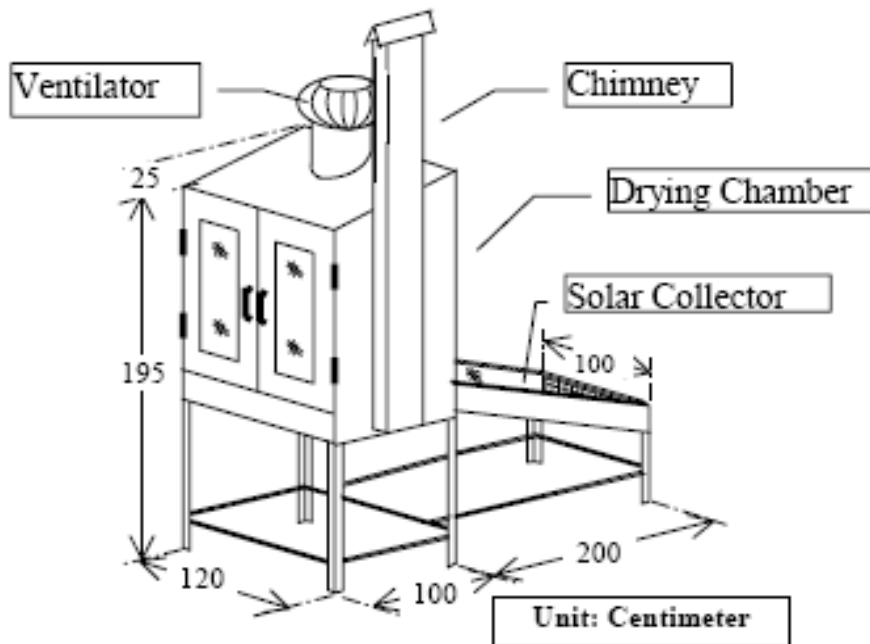


Appendix H
Cross-draft biomass gasifier of hybrid dryer [11]



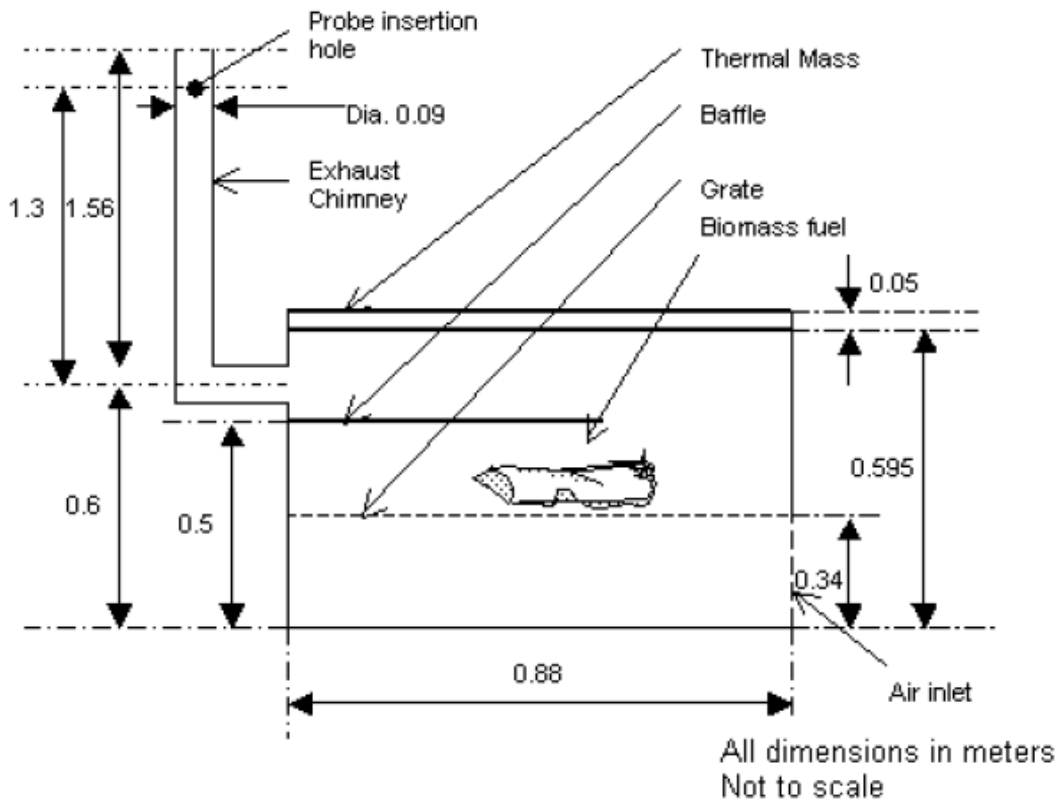
Appendix I

Hybrid solar/biomass energy powered dryer for fruits and vegetables [13]

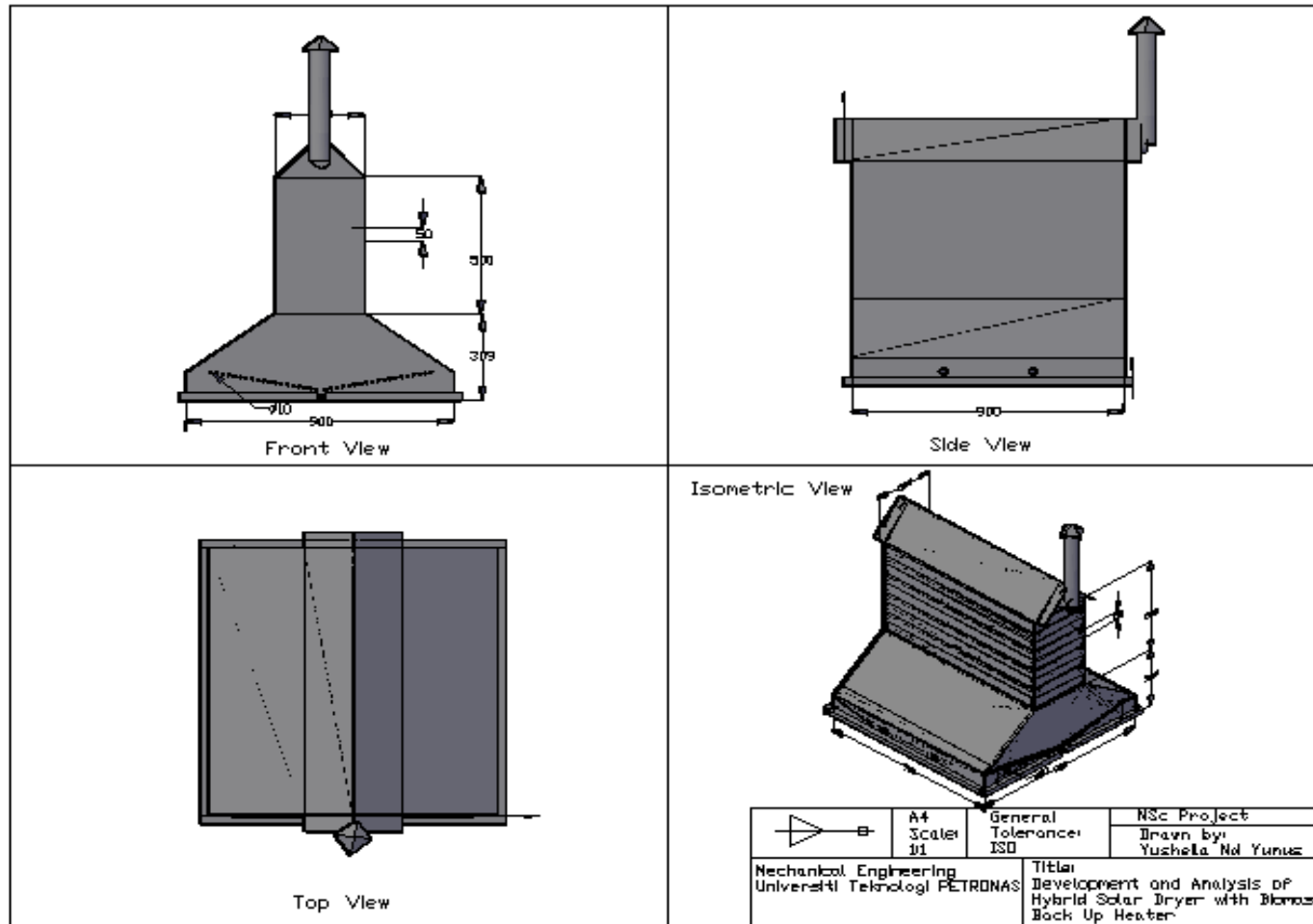


Appendix J

Longitudinal cross-section through the burner [77]

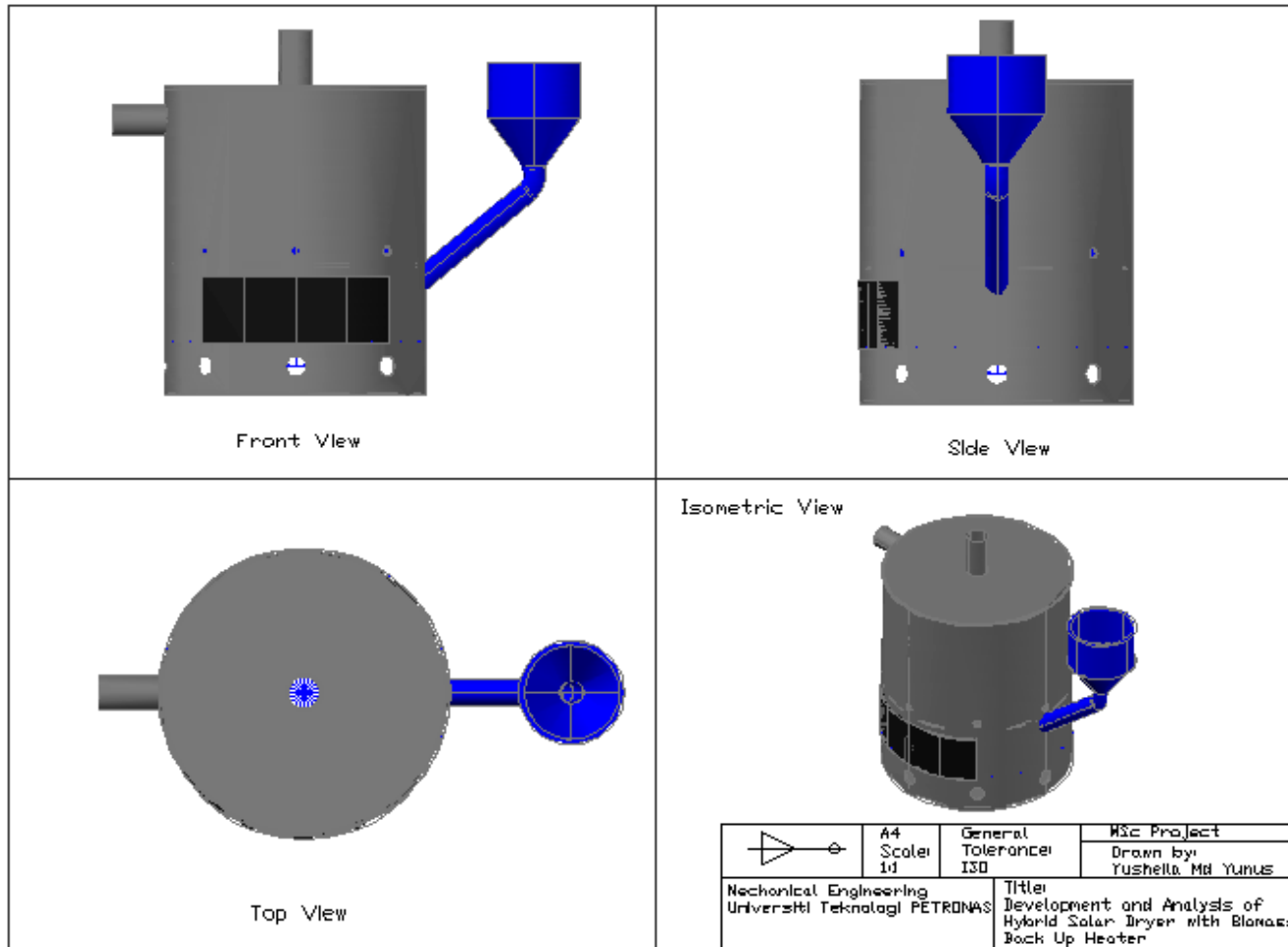


Appendix K
 Outlines of the solar dryer



Appendix L

Outlines of the thermal backup unit



Appendix M

Sample of no-load experimental measurement data

TIME	Tambient (°C)				Tcollector (°C)				T1 near collector (°C)				Toutlet (°C)	
	Temp.	Dry Bulb	Wet Bulb	RH (%)	T1	T2	T3	T4	Temp.	Dry Bulb	Wet Bulb	RH (%)	Amb Temp	Vel. (m/s)
9am	26.5	26.1	28.0	53.4	49.8	50.1	32.5	34.9	48.7	27.9	31.7	38.1	34.5	0.13
10am	28.6	27.5	28.8	52.1	51.2	54.6	38.9	40.2	53.8	26.8	32.8	20.9	36.0	0.14
11am	30.4	25.4	26.2	76.5	53.5	60.3	40.4	42.9	59.8	24.7	33.9	15.3	36.3	0.17
12pm	31.4	26.0	27.9	53.8	65.9	67.8	49.8	51.5	61.5	21.4	37.4	13.3	38.4	0.21
1pm	31.6	24.2	28.3	44.8	70.7	67.2	58.7	60.6	66.5	20.1	39.8	12.7	42.2	0.19
2pm	32.8	24.4	28.9	34.0	71.0	68.5	54.1	55.8	67.3	21.4	36.2	7.6	39.9	0.18
3pm	31.5	24.5	29.0	36.3	69.8	69.1	57.9	59.3	67.1	21.9	39.6	12.1	41.3	0.18
4pm	29.3	26.1	31.8	30.0	69.7	68.9	56.3	57.5	62.5	23.5	32.8	12.9	39.5	0.14
5pm	28.4	24.1	29.1	28.9	66.4	67.5	51.9	53.0	60.2	21.5	35.6	12.5	30.3	0.11

TIME	Tchamber - BOTTOM SIDE (°C)				Tchamber - MIDDLE SIDE (°C)				Tchamber - TOP SIDE (°C)				Solar irradiation (W/m2)		
	Temp.	Dry Bulb	Wet Bulb	RH (%)	Temp.	Dry Bulb	Wet Bulb	RH (%)	Temp.	Dry Bulb	Wet Bulb	RH (%)	OPEN SPACE	LEFT	RIGHT
9am	47.1	27.4	31.8	32.3	46.1	26.4	32.9	33.0	47.9	28.3	31.1	31.1	321	332	328
10am	49.3	26.9	32.1	30.4	48.8	26.8	31.7	29.1	49.6	27.9	31.6	30.5	397	401	395
11am	51.4	26.3	32.5	25.8	50.2	26.1	32.3	22.9	54.3	27.2	32.8	29.1	483	487	439
12pm	54.9	22.3	37.6	24.9	52.6	23.0	35.1	20.1	61.0	25.1	34.1	15.0	587	407	503
1pm	59.8	22.5	36.1	19.4	53.8	23.8	38.6	19.9	65.8	23.3	35.3	10.2	650	640	644
2pm	60.1	29.1	32.8	20.3	56.0	22.4	34.9	15.5	65.5	22.7	34.8	10.6	640	620	616
3pm	61.3	29.2	28.7	10.6	59.2	21.2	35.7	13.4	65.1	21.9	34.5	10.3	623	630	657
4pm	56.6	24.1	32.9	23.2	55.4	22.4	32.5	17.6	59.7	24.0	32.7	18.0	526	531	483
5pm	55.4	22.7	36.3	24.4	52.8	22.6	37.2	19.8	58.0	22.2	32.5	14.7	440	442	558

Appendix N

Sample of loading experimental measurement data

Time	Mass reduction (g)						Tambient (°C)			
	Open sun drying	Tray 1	Tray 2	Tray 3	Tray 4	Tray 5	Temp	Dry Bulb	Wet Bulb	RH %
9am	965	879	875	883	877	882	41.9	27.3	30.2	44.6
11am	957	852	852	863	855	861	38.8	24.4	28.1	43.7
1pm	944	826	828	843	832	832	40.3	25.4	28.7	43.5
3pm	926	804	808	825	812	798	43.2	26.7	30.8	41.2
5pm	908	778	784	803	788	770	25.4	23.9	74.5	80.1

Time	T1 near collector (°C)				Tchamber-Top Side (°C)				Tcollector (°C)	
	Temp.	Dry Bulb	Wet Bulb	RH %	Temp.	Dry Bulb	Wet Bulb	RH %	Left	Right
9am	48.6	29.3	32.8	38.1	49.5	31.5	35.2	38.7	53.9	56.7
11am	61.5	23.5	33.6	34.6	53.9	25.8	31.6	28.5	66.4	65.9
1pm	67.0	26.3	35.2	33.1	58.9	29.4	35.9	21.3	70.7	70.6
3pm	60.1	24.1	34.6	35.7	56.6	30.1	35.8	25.2	69.3	68.1
5pm	44.0	21.6	73.4	76.2	24.5	20.9	73.8	77.8	21.4	22.6

Time	Chimney		Solar irradiation (W/m ²)
	Tchimney (°C)	Vel. (m/s)	
9am	32.3	0.10	340
11am	35.8	0.13	453
1pm	38.5	0.19	642
3pm	37.2	0.20	582
5pm	35.0	0.15	410